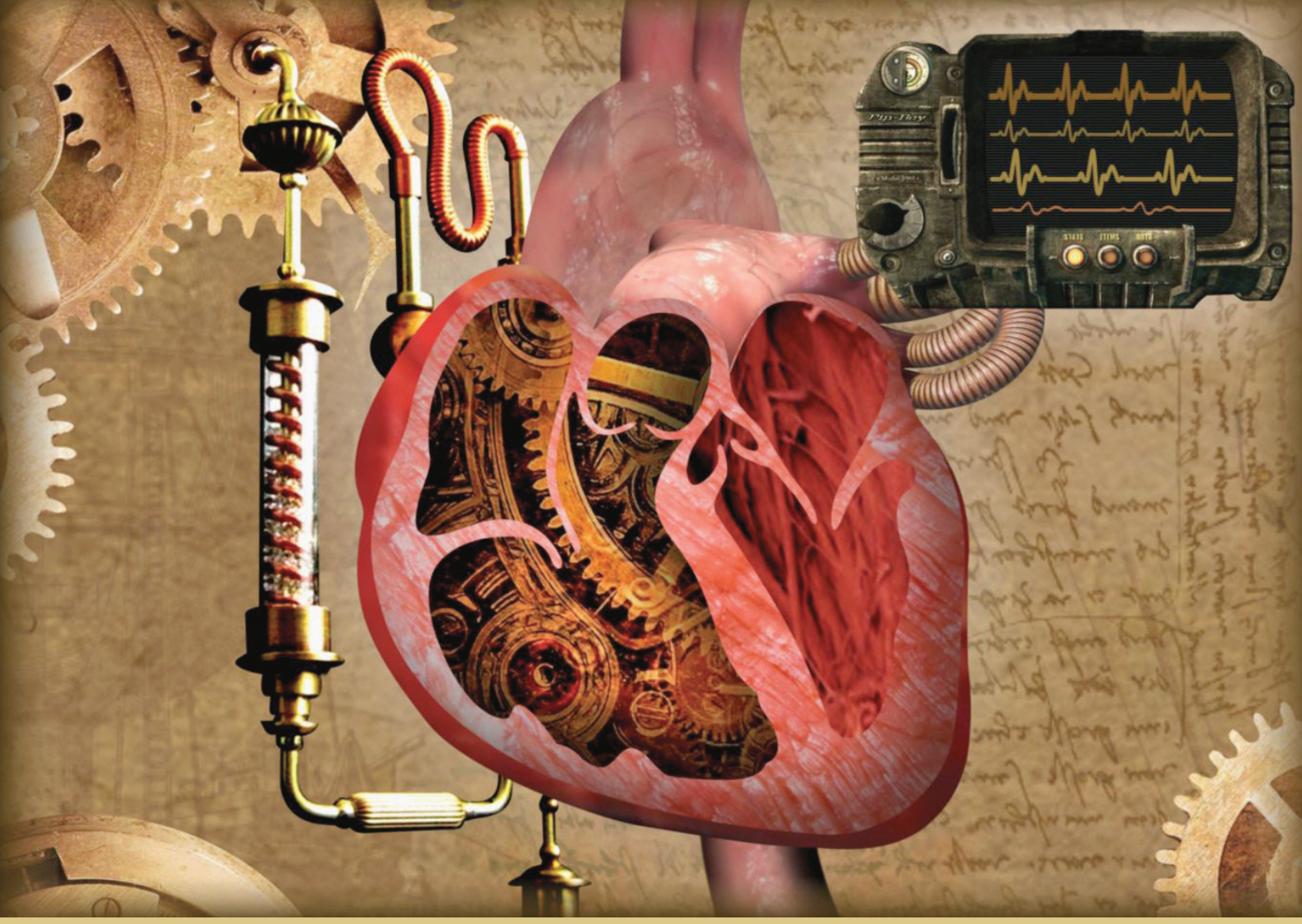

Pedro José Azeredo de São Bento Gouveia

Cardiac Tissue Constructs for Drug Screening

Tese de doutoramento em Biologia Experimental e Biomedicina, ramo de Biotecnologia e Saúde, sob orientação científica do Doutor Lino Ferreira e do Doutor Ricardo Neves, e apresentada ao Instituto de Investigação Interdisciplinar da Universidade de Coimbra

Novembro de 2015

· U C ·

Universidade de Coimbra

INSTITUTE FOR INTERDISCIPLINARY RESEARCH

UNIVERSITY OF COIMBRA

Cardiac tissue constructs for drug screening

PhD thesis in Experimental Biology and Biomedicine,
in the area of Biotechnology and Health

Pedro José Azeredo de São Bento Gouveia

November 2015

Cover by Sónia Pereira

Thesis presented to the Institute for Interdisciplinary Research of the University of Coimbra for PhD evaluation in Experimental Biology and Biomedicine, in the area of Biotechnology and Health. This study was performed at the Center for Neuroscience and Cell Biology (CNC) of the University of Coimbra and at Biocant Park (UC Biotech), under the supervision of Dr. Lino Ferreira and of Dr. Ricardo Neves. The studies were performed with the financial support from a PhD scholarship provided under the PhD programme in Experimental Biology and Biomedicine of the CNC, University of Coimbra, provided by the Foundation for Science and Technology and COMPETE (PTDC/SAU-ENB/113696/2009, FRH/BD/51197/2010, UID/NEU/04539/2013)

"The only constant in the Universe is change,
(therefore) life is flux."

Heraclitus of Ephesos (c. 500 BCE)

Acknowledgements

To my supervisors Dr. Lino Ferreira and Dr. Ricardo Neves, for believing in me and providing the opportunity to fulfil a key step towards my dream. Thank you both for the patience you had and the guidance you provided for this endeavour of mine. Above all, thank you for the respect and trust placed in me and on my every so often risky ideas.

To Susana Rosa, whose help and guidance was crucial for my work. Thank for the enormous amount of patience to teach this rookie the 101 of Science (which sometimes I know was a Herculean task). Thank you for your constant support, for the countess discussions, critical suggestions, your kindness and understanding. All of this was invaluable beyond measure and helped me grow as a researcher. From the bottom of my heart, thank you my "Scientific Mother" for everything. I will cherish forever all you taught me, and I will try to make you proud.

To Leonardo Ricotti, whose help was important to define the core of my work and polish the little details that gave it its proper shape Thank you for your thoughtful opinions and for always having time for my doubts. Thank you for your friendship and for giving me the inspiration to pursue new challenges.

To the research groups "Laboratory of Synapse Biology", "Growth Factor Signalling and Brain Ischemia" and "Glutamatergic Synapses" at the Center for Neuroscience and Cell Biology, for so kindly offering invaluable biological material used to perform the work presented here. A particular thanks for the help given by Elisabete Lopes, Joana Fernandes, Marta Vieira, Mariline Silva, Susana Sampaio, Sandra Santos and Tatiana Catarino.

To all my colleagues at the Biomaterials group, for shining light into dark days and giving me a smile when I was grumpy (or hungry). Thank you for the support in difficult times, the laughs, the advices and all the funny moments (always at the right time). From each of you I have different memories that I will cherish, and because of these I am glad to call many of you friends.

To the friends from before the PhD, Nuno Fonseca and Isabel Onofre, thank you for the inspiration. I have always been running to catch you both and I can only hope

one day make you proud, as a researcher and as a friend. Your invaluable friendship always helped me and I hope to keep it by my side.

To the friends that the PhD brought me, the following individuals are of particular notice since they had to face "me jolly self" more frequently than other people: Joana Vindeirinho, paradoxically, a person I know for a long long time but that destiny only brought together during the PhD, thank you for all the good disposition, geeky, funny, amazing moments (Game!); Rui Benfeitas, the nice guy who plays a mean guitar, thank you for listening my rants, for the awesome music and rocking parties; Gabriel Costa, the film buff that is always good to talk to before/after a movie, thank you for the amazing help when I was headbutting ImageJ/Matlab, and for all the fun moments around and about cinema and gaming (especially those picking on poor Nuno); to Jorge Nunes, the fellow McGuiver, thank you for your help on the early versions of what probably will be a Doomsday machine; Angela Valério e Ana Gregório, for helping in the "Bureaucratic Revolution" of 2014.

To the remainder friends, thank you for all the support, laughs, good disposition, kindness, funny moments, understanding, party times, and so much more that I cannot put all into text. Each small chat, each cheer, each happy moment that you, my friends, shared with me has helped me to reach the place I am now.

To my parents, thank you for all your love and support. Thank you so much for believing in my dream and cheering me on at the darkest hours. There is no gratitude large enough to thank you for helping me grow to be the person I am.

To Sónia, my companion and soul mate, who walked by my side during all the challenging path of my PhD, always offering me unconditional support and understanding, always reaching a hand and a smile to help me rise above all difficulties. Thank you so much for believing in my dreams and helping me catch them.

To "Hypericum" and related friends, who helped me escape from stressful moments and made me relax.

To Big Bang/God/Inevitable-Moment-of-Creation, which without it for sure this work would not have happened.

Publications and communications

Publications

P.J. José Gouveia, S. Rosa, L. Ricotti, J. Nunes, F. Sofia Carvalho, S. Luchkin, A.L. Kholkin, P. Jorge Oliveira, R. Carvalho, A. Menciassi, R. Pires das Neves, L. Silva Ferreira. *Flexible nanofilms coated with aligned piezoelectric microfibres preserve the long-term contractility of cardiomyocytes*. ACS Nano, (Submitted August, 2015, currently under revision)

S. Rosa, P. José Gouveia, L. Ricotti, A. Menciassi, L. Silva Ferreira. *Combining induced pluripotent stem cells and nanofilms to generate human arterial and venous endothelial patches.* (Work in progress)

Oral presentations

P.J. Gouveia, S. Rosa, L. Ricotti, R. Pires das Neves, A. Menciassi, L. Ferreira. *Towards an in vitro cardiac tissue: developments in the extracellular matrix and iPSC-derived cells*. Santa Marta 8th Lisbon Summer Meeting, 2015, July 2-3rd, Lisbon (POR)

Poster presentations

P.J. Gouveia, S. Rosa, L. Ricotti, R. Pires das Neves, A. Menciassi, L. Ferreira*. Flexible nanofilms coated with aligned piezoelectric microfibres preserve the long-term contractility of cardiomyocytes*. 9th International Meeting of the Portuguese Society for Stem Cells and Cellular Therapy (SPCE-TC), 2015 October 15-16th, Oeiras (POR)

P.J. Gouveia, S. Rosa, L. Ricotti, R. Pires das Neves, A. Menciassi, L. Ferreira. *Flexible nanofilms coated with aligned piezoelectric microfibres preserve the long-term contractility of cardiomyocytes*. XVIII Congress of the Portuguese Biochemical Society, 2014, December 17-19th, Coimbra (POR).

P.J. Gouveia, S. Rosa, L. Ricotti, R. Pires das Neves, A. Menciassi, L. Ferreira. *Cardiokit: a system for cardiac tissue engineering and toxicity assessment*. TERMIS (Tissue Engineering and Regenerative Medicine International Society) Conference, 2014, December 13-16th, Washington D.C. (USA). Published in: Tissue Eng: Part A. 20: S124-S124; 2014.

P.J. Gouveia, S. Rosa, L. Ricotti, R. Pires das Neves, A. Menciassi, L. Ferreira. *Flexible nanofilms coated with aligned piezoelectric microfibres preserve the long-term contractility of cardiomyocytes*. HEART WITH(OUT)BORDERS – International conference on cardiovascular development, disease & repair, 2014, November 28-29th, Porto (POR).

P.J. Gouveia, S. Rosa, L. Ricotti, R. Pires das Neves, A. Menciassi, L. Ferreira. *Cardiokit: human cardiac engineered tissue for toxicity assessment*. Center for Neuroscience and Cell Biology Annual Meeting, 2013, December 17-18th, Cantanhede (POR).

Table of contents

Abbreviations

AFM – Atomic force microscopy

AV – Atrio-ventricular node

CF – Cardiac fibroblasts

CM – Cardiomyocytes

CSQ2 – Calsequestrin

CTC - Cardiac tissue construct

CTFC – Corrected Total Cell Fluorescence

cTnI – Cardiac troponin I

cTnT – Cardiac troponin T

Cx – Connexin

EC – Endothelial cells

ECM – Extracellular matrix

ESCs – Embryonic stem cells

FACS – Fluorescence-activated cell sorting

FEM – Finite Elemental Model

hERG – Human Ether-à-go-go Related ion channel

iPSC – Induced pluripotent stem cells

LTCC - L-type calcium channels

MEA – Micro- electrode arrays

MHC – Myosin heavy chain

MLC – Myosin light chain

MNF – Magnetic nanofilm

NCX - Na,Ca-exchanger

NKA - Na^+,K^+-pump

NMR – Nuclear magnetic resonance

P(VDF–TrFE) – Poly(vinylidene fluoride–trifluoroethylene)

PCL – Poly(caprolactone)

PEG – Poly(ethylene glycol)

PLA – Poly(lactic acid)

PS – Poly(styrene)

PSC-CM – Pluripotent stem cell-derived cardiomyocytes

qRT-PCR- Quantitive Real-Time Polimerase Chain Reaction

RyR - Ryanodine Receptors

SA – Sinoatrial node

SEM - Scanning electron microscopy

SERCA – Sarcoplasmic Reticulum Ca^{2+}-ATPase

SMC – Smooth muscle cells

SR - Sarcoplasmic Reticulum

α-cd - Cardiac α-actin

α-sk - Skeletal α-actin

Abbreviations

AFM – Atomic force microscopy

AV – Atrio-ventricular node

CF – Cardiac fibroblasts

CM – Cardiomyocytes

CSQ2 – Calsequestrin

CTC - Cardiac tissue construct

CTFC – Corrected Total Cell Fluorescence

cTnI – Cardiac troponin I

cTnT – Cardiac troponin T

Cx – Connexin

EC – Endothelial cells

ECM – Extracellular matrix

ESCs – Embryonic stem cells

FACS – Fluorescence-activated cell sorting

FEM – Finite Elemental Model

hERG – Human Ether-à-go-go Related ion channel

iPSC – Induced pluripotent stem cells

LTCC - L-type calcium channels

MEA – Micro- electrode arrays

MHC – Myosin heavy chain

MLC – Myosin light chain

MNF – Magnetic nanofilm

NCX - Na,Ca-exchanger

NKA - Na^+,K^+-pump

NMR – Nuclear magnetic resonance

P(VDF–TrFE) – Poly(vinylidene fluoride–trifluoroethylene)

PCL – Poly(caprolactone)

PEG – Poly(ethylene glycol)

PLA – Poly(lactic acid)

PS – Poly(styrene)

PSC-CM – Pluripotent stem cell-derived cardiomyocytes

qRT-PCR- Quantitive Real-Time Polimerase Chain Reaction

RyR - Ryanodine Receptors

SA – Sinoatrial node

SEM - Scanning electron microscopy

SERCA – Sarcoplasmic Reticulum Ca^{2+}-ATPase

SMC – Smooth muscle cells

SR - Sarcoplasmic Reticulum

α-cd - Cardiac α-actin

α-sk - Skeletal α-actin

Abstract

Few examples have reported the successful use of engineered cardiac tissue for drug screening/toxicology assessment. This issue is of paramount importance since cardiac toxicity has been implicated in 28% of drug withdrawals over the last 30 years (Gwathmey et al., 2009). The development of tissue engineered cardiac tissue for drug screening requires the development of scaffolds that can be easily produced, flexible, small, and preserve the long-term contractility of cardiomyocytes, ideally in the absence of complex external electrical stimulation apparatus. Here we developed a flexible scaffold relatively easy to prepare that reproduces aspects of cardiac ECM, and can preserve the contractility of fetal rat cardiomyocytes for high-throughput drug screening applications. The scaffold is formed by a nanofilm of poly(caprolactone) (NF) coated by piezoelectric microfibers (PIEZO) composed of poly(vinylidene fluoride–trifluoroethylene) (PVDF-TrFE). When a mechanical force is applied to a piezoelectric material a shift or rotation of the constitutive dipole crystals occurs resulting in the generation of an electric charge. Therefore, PIEZO fibres may act as Purkinje cells, which in the native heart tissue are responsible for initiating and synchronizing cardiac beatings.

To evaluate whether NF+PIEZO scaffolds preserve CM contractility, the number of spontaneous synchronous beatings per minute was monitored at day 1 and 12 after seeding the cells. While the average rate of beats in cells cultured in poly(styrene) and NF scaffolds maintained constant from day 1 to day 12, a significant increase in beats/minute of the cells cultured on NF+PIEZO scaffolds was observed (from 18 to 106 beats/min). This indicates that, for at least 12 days, NF+PIEZO scaffold provided a better environment to preserve the spontaneous contractility of CMs. Alongside, cells cultured in NF+PIEZO scaffold displayed higher levels of functional connexin 43 and waveform-like electrochemical signalling. These observations denote the stimulation of proper cell-cell communication and action potential conduction. When compared to tissue culture poly(styrene), the piezoelectric scaffold promoted transmembrane transients of Ca^{2+}. This was confirmed by a high concentration of intracellular Ca^{2+} and a higher expression of important ion channels, namely sub-units of L-type Ca^{2+} channels and human Ether-à-go-go-Related ion channels. These observations were accompanied

by clear morphological changes when compared to poly(styrene), including a 3-fold increase in CM alignment, more organized sarcomeric structures and a higher CM surface area. In addition, a main component of the contractile machinery (α-cardiac actin) was up-regulated, while its fetal counterpart (α-skeletal actin) maintained in the piezo scaffold.

To evaluate the usefulness of the engineered cardiac construct for drug screening, the cell construct was tested with norepinephrine. The results showed an adequate chronotropic response denoted by the rise of intracellular Ca^{2+} concentration which was accompanied by an increase in beating rates. Finally, metabolic studies based on glucose consumption and lactate production demonstrated that CMs cultured in NF+PIEZO had more efficient aerobic metabolism. This profile is inverted in the presence of doxorubicin, a cardiotoxic drug, which forces CMs to a glycolytic (anaerobic) metabolism and induces cell death. Overall, the results present in this thesis highlight the advantages of a piezoelectric-based scaffold to develop cardiac constructs for cardiotoxicity assessment.

Resumo

Poucos estudos reportam a utilização bem-sucedida de tecido cardíaco criado *in vitro* na análise de efeitos farmacológicos e toxicológicos de medicamentos. Esta falha é de extrema importância, visto que toxicidade cardíaca tem sido implicada em cerca de 28% das remoções de medicamentos do mercado nos últimos 30 anos (Gwathmey et al., 2009). O desenvolvimento de tecido cardíaco *in vitro* para *screening* de medicamentos requer o desenvolvimento de matrizes que sejam facilmente produzidas, flexíveis, de pequena dimensão e preservem a contractilidade a longo termo de cardiomiócitos, idealmente na ausência de sistemas complexos de estimulação eléctrica. Aqui é descrito o desenvolvimento de uma matriz flexível para *screening* de medicamentos que é de fácil produção, reproduz aspectos da matriz extracelular cardíaca e permite a preservação da contractilidade de cardiomiócitos fetais de rato. A matriz é constituída por um nanofilme de poli(caprolactona) (NF) revestido por microfibras piezoeléctricas (PIEZO) de poli(vinilideno-trifluoroetileno) (P(VDF-TrFE)). Quando uma força mecânica é aplicada sobre o material piezoeléctrico ocorre uma alteração ou rotação nos dipolos cristalinos constitutivos, resultando na geração de uma carga eléctrica. Assim, fibras piezoeléctricas podem actuar como células de Purkinje, que no tecido cardíaco nativo são responsáveis por iniciarem e sincronizarem os batimentos cardíacos.

Para avaliar se a matriz de NF+PIEZO preservaria a contractilidade de cardiomiócitos, o número de batimentos sincronizados por minutos foi monitorizado ao 1º e 12º dia após semear as células. Enquanto que a média de batimentos nas células cultivadas em poli(estireno) e em NFs foi semelhante no 1º e 12º dia, um aumento significativo foi observado (de 18 para 106 batimentos/min) nas células cultivadas nas matrizes de NF+PIEZO. Isto indica que, pelo menos até 12 dias, a matriz de NF+PIEZO oferece um microambiente melhor para a preservação da contracção espontânea de cardiomiócitos. Paralelamente, as células cultivadas nas matrizes de NF+PIEZO apresentaram níveis superiores de conexina 43 funcional e uma sinalização electroquímica em forma de onda. Estas observações denotam o desenvolvimento adequado da comunicação intercelular e do potencial de acção. Quando comparado com tecido cultivado em poli(estireno), a matriz piezoeléctrica promoveu o desenvolvimento

de transientes de Ca^{2+}, como foi confirmado pelos níveis elevados de Ca^{2+}intracelular e pela elevada expressão de canais iónicos relevantes, nomeadamente sub-unidades de canais de Ca^{2+} tipo-L e canais *Ether-à-go-go-Related.* Estes resultados foram acompanhados por claras alterações morfológicas que incluíram um aumento de 3 vezes no alinhamento de cardiomiócitos, a presença de estruturas sarcoméricas alinhadas, e uma área de superfície de cardiomiócitos superior do que na condição controlo. Adicionalmente, a expressão de um dos componentes da maquinaria contráctil (α-actinina cardíaca) foi aumentada, enquanto que o respectivo homologo fetal (α-actinina esquelética) não aumentou significativamente na matriz piezoeléctrica.

De forma a avaliar a utilidade do tecido cardíaco criado *in vitro* no *screening* medicamentos, o tecido celular construído foi testado com noradrenalina. Os resultados demonstram uma resposta cronotrópica adequada, evidenciada pelo aumento da concentração intracelular de Ca^{2+} acompanhado por um incremento no ritmo de batimento. Para finalizar, estudos metabólicos baseados no consumo de glucose e na produção de lactato demonstraram que os cardiomiócitos cultivados nas matrizes de NF+PIEZO apresentam um metabolismo aeróbico mais eficiente. Este perfil é invertido na presença de doxorrubicina, um agente farmacológico cardiotóxico que força cardiomiócitos a adquirirem um metabolismo glicolítico (anaeróbico) e induz morte celular. Em suma, o conjunto de resultados apresentados nesta tese evidenciam as vantagens que uma matriz baseada num material piezoeléctrico apresenta no desenvolvimento de tecidos *in vitro* para a análise de efeitos cardiotóxicos.

Chapter 1

Introduction

1.1 - Physiology of the heart

1.1.1 - Macrophysiology of the heart

The heart is composed of four chambers divided into two separate pumps positioned side-by-side, which work in synchrony to maintain the constant flow of blood in the body (Figure 1). These two pumps are composed of an atrium and a ventricle. The top-sided atria collects the blood that returns to the heart and facilitates the filling of the ventricle, which in turn pumps blood from the heart to the rest of the body. The left side of the ventricle keeps flow in the systemic circulation, whereas the right side maintains the pulmonary circulation. Due to the high load of the systemic circulation, the left ventricle has a thicker wall than the right ventricle.

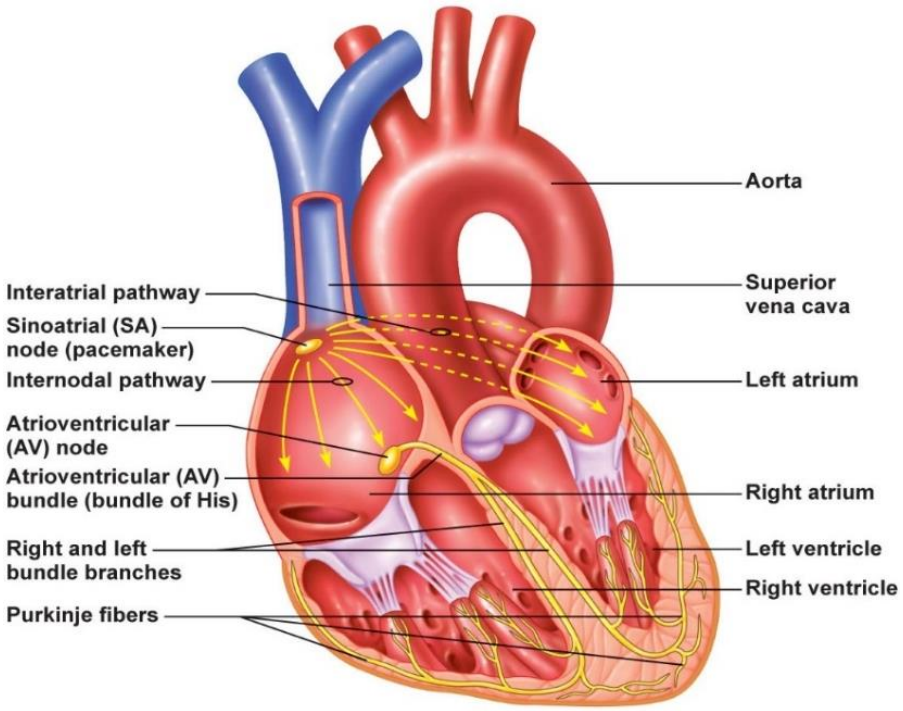

Figure 1 – **Cross-section of the adult heart**. Shows the main cardiac cavities, the conduction nodes and related conduction fibres, which are responsible for the conduction contraction signal. Adapted from Seeley's Anatomy and Physiology 6th ed.

The muscle wall of the heart, also named as myocardium, is composed of three layers: i) the visceral epicardium on the outside, ii) the contractile myocardium in the middle, which forms the bulk of the heart tissue, and iii) the endocardium, an endothelial layer covering the inside surface of the heart chambers. A normal human

heart weights on average 300 g, contracts approximately 100,000 times a day and 3×10^9 times in a lifetime (Li et al., 2009). The cyclic work-load requested by the vascular system requires that the heart structure to be flexible, strong and resilient. Simultaneously, it has to be able to cope with events related, directly or not, to growth, aging, physical activity and diseases. On a beating cycle, load volumes in the left ventricle range from 40 to 130 mL, while pressure loads vary between 10 and 120 mmHg. Studies have described that while relaxed, the values of elastic modulus in the human ventricle range between 0.2 and 0.5 MPa (Jawad et al., 2008). Local myofibre stress loads range between 5 and 50 kPa, with strains representing an area deformation between -10% at contraction and 15% at passive elongation (Bouten et al., 2011).

Although the contraction process is an independent mechanism, the heart possesses autonomic and sympathetic nerve fibres extending to and through the myocardium. The autonomic nerves can modify the contraction rhythm of the heart according to the needs of the body, whereas the sympathetic nerves participate in the maintenance of the proper synchronous contraction of all myofibres. The control of heart contractions is almost entirely self-contained. Groups of specialized cells, usually referred as pacemaker cells, are located in the sinoatrial node (Figure 1), from where they generate electrical stimuli that propagates along the myocardium, thus driving to the periodic contractions of the heart (Boyett et al., 2000). In general, the synchronous contraction results from the propagation of the electrical excitation through the tissue, which is conducted by ion currents occurring between the extracellular and intracellular spaces of cardiac cells (Boyett et al., 2000, Aronsen et al., 2013).

The unidirectional flow in the heart is controlled by valves. At the outlet of the atria to the ventricles are situated the mitral and tricuspid valves, whereas at the outlet from ventricles to the systemic and pulmonary circulation, are the aortic and pulmonary valves (Figure 2). Structurally, the semilunar valves consist of flexible tissue leaflets, sinuses and an artery root. The individual leaflets are attached to the artery root in a semilunar fashion, from where it ascends to the area where the leaflet attachments run parallel (commissures), and descends to the basal attachment of each leaflet. Due

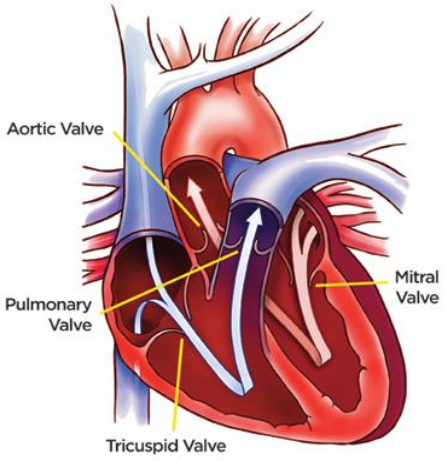

Figure 2 – Directional flow of blood inside the heart. Adapted from SSM Health.

to this attachment, the leaflets form cusps that closely fit together during valve closure. Both the mechanical forces exerted by the contraction of the heart and the dynamics of the blood flow cause the opening and closing of the valves.

1.1.2 - Microphysiology of the heart

1.1.2.1- Cardiac cell population

The myocardium is composed by four major cell types: i) cardiac myocytes (CM), ii) fibroblasts (CF), iii) vascular cells and iv) neuronal cells. The particular spatial organization of these components determines the metabolic, electrical and mechanical performance of the heart. Cellular organization in the heart is structured by arranged sheets of CM which are kept together by the extracellular matrix (ECM). CFs are dispersed throughout the ECM which surrounds the CMs, allowing intercellular force actuation as well as biochemical-based signalling. Endothelial cells (EC) and smooth muscle cells (SMC) are confined to the vasculature (Figure 3).

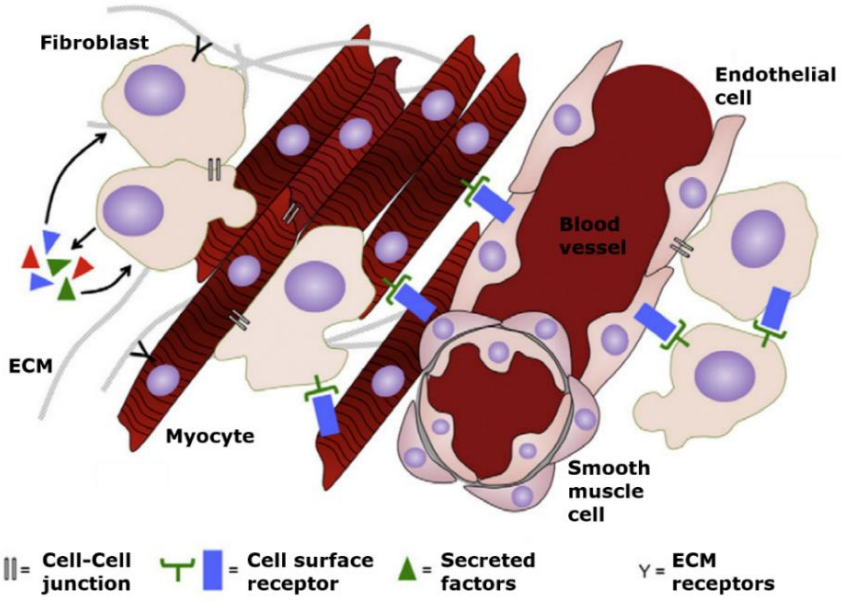

Figure 3 – **Cardiac cell environment**. CMs, CF and ECs take a particular spatial distribution and can interact between them and the ECM in multiple ways. Through these different interactions diverse changes in cell function can be induced. Adapted from Howard and Baudino, 2014.

The myocardium has a very tightly packed structure with an average cell density of $5x10^8$ cells/cm^3 in the native rat myocardium (Gerecht-Nir et al., 2006). CMs and CFs comprise the majority of cells in the heart, and their relative numbers not only change considerably during development and throughout life, but also vary from species to species (Table 1). During fetal development, the numbers of CMs and CFs increase in parallel until birth. However, when CM proliferation ceases, CFs continue to proliferate.

Although CMs account for the vast majority of the cardiac volume (75%), they represent in average only 30% of the total adult heart cell population (Banerjee et al., 2007, Jugdutt, 2003).

Species	Cardiac Fibroblast	Cardiac Myocytes	Non-CF/Non-CM
Mouse neo-natal	10%	60%	30%
Rat neo-natal	30%	60%	10%
Mouse adult	25%	55%	20%
Rat adult	60%	30%	10%

Table 1 – Cardiac cell population ratios during development on mouse and rats (Jugdutt, 2003, Gerecht-Nir et al., 2006, Dolnikov et al., 2006).

CFs main function is the production and maintenance of ECM components. These cells can be identified by their flat, spindle-shaped morphology with multiple filopodia originating from the main cell body. The distinctive characteristics of the CFs include an extensive Golgi apparatus and a relatively large endoplasmic reticulum (Howard and Baudino, 2014). These features emphasize the fibroblast's role in synthesizing and secreting proteins destined for roles outside of the cell itself. Structurally, the CFs form a network of cells that are connected to the ECM. Additionally, they share heterotypic cell–cell contacts with myocytes and endothelial cells, and homotypic cell–cell contacts with each other (Howard and Baudino, 2014). Some of these contacts involve connexins (Cx), such as connexin 43 (Cx43), present in the association of fibroblasts with myocytes, and connexin 45 (Cx45) present between fibroblasts.

Since CFs are responsible for the production, organization and turnover of the ECM, they regulate much of the mechanotransduction phenomena on the heart (Brown et al., 2005, Curtis and Russell, 2011, Goldsmith et al., 2014). Research has shown that application of a defined mechanical stimuli to cultured CF has been associated with ECM gene expression, growth-factor production and/or bioactivity. As example, dynamic stretching caused the β1-integrin dependent activation of ERK and JNK pathway, as well as the expression of collagen III, fibronectin and TGF-β1 (MacKenna et al., 1998). Therefore, CFs are recognised to transmit to CMs a stretch-induced response, through autocrine or paracrine signalling and ECM remodelling.

CMs are the motor unit of the contracting heart. These cells form myofibres which are then arranged into muscle bundles with helicoid and spiral conformations. The CM form a three-dimensional syncytium with electrical conductive properties, which enable propagation of electrical signals across specialized intracellular junctions. This process allows the generation of coordinated contractions, the mechanical force that pumps blood throughout the body. Morphologically, intact CMs have an elongated, rod-shaped appearance. Their contractile apparatus consists of sarcomeres arranged in parallel (Severs, 2000), being its metabolic requirements supported by a dense mitochondrial network. CM signal propagation is provided by specialized intercellular connections denominated as gap junctions (Severs, 2000, Yang et al., 2014a).

CF-CM communication can occur through gap-junction and tight junctions. It is currently known that CMs can induce CF excitation trough gap junction-based communication. Consequently, CFs facilitate the communication between CMs that are not directly connected (Kamkin et al., 2005, Kohl et al., 2005). On the other hand, there are indications that tight cell junctions are involved in the exchange of intracellular material between CFs and CMs, however the precise composition of this material is not yet known (Howard and Baudino, 2014).

1.1.2.2- Heart ECM

The development and physiological function of the heart is greatly determined by the interaction between cells and the composition of the ECM. Some of its most important molecular components include structural and adhesive proteins that form a mesh, surrounding myocardial constitutive cells. This intricate biomaterial provides a template for mechanical support (guiding and transmitting the mechanical forces) while retaining the shape of the tissue (Figure 4).

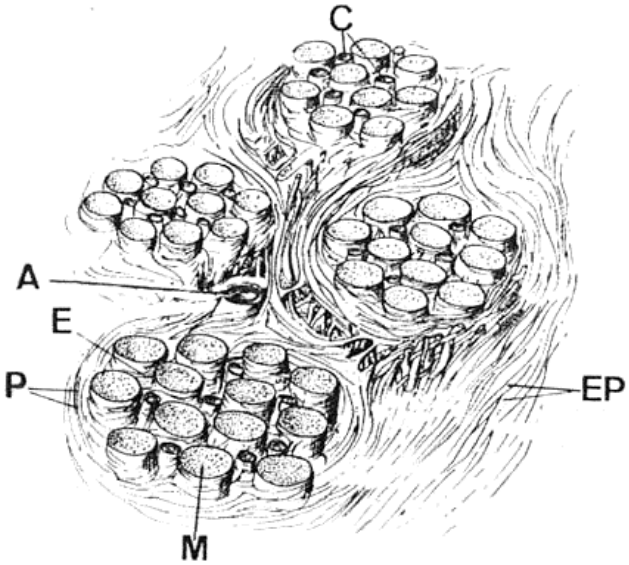

Figure 4 - **A schematic representation of the myocardial ECM network**. EP – epimysium; P – perimysium; E – endomysium; M – cardiac myocyte; A – arteriole; C – capillaries. It is important to note that ECM provides support to the aligned configuration of the muscle bundles. Adapted from Brilla et al.,1993.

The molecular components of the ECM include: i) structural proteins, such as collagen; ii) adhesive proteins, including

fibronectin and laminin; iii) anti-adhesive proteins, as osteopontin; and iv) proteoglycans, such as hyaroluranan (Hsueh et al., 1998, Corda et al., 2000, Lockhart et al., 2011). It is important to note that the synthesis of these molecules differs among cardiac cells. CFs and SMCs secrete type I and III collagens and fibronectin, while CMs and ECs secrete type IV collagen. In addition, laminin is produced by SMCs, CMs and ECs (Corda et al., 2000).

The most abundant structural proteins of the ECM are collagens (de Souza, 2002). These include a family of proteins characterized by a fibrous structure, with slow synthesis, accumulation and turnover. Until now, five collagen types (I, III, IV, V, VI) have been identified in the adult heart (Corda et al., 2000, Lockhart et al., 2011). Among them, two categories of collagen are the most important in the cardiovascular system: i) collagen I and III, which represent more than 90% of total collagen of the heart, and ii) type IV and VI collagen, as components of the vascular basal lamina (Weber et al., 1988, de Souza, 2002). Collagen type I forms strong, thick fibres (average diameter of 75 nm) that play an essential role in providing structural stability to the tissues. On the other hand, collagen type III forms thin fibres (average diameter of 45 nm) which are assembled in a fine reticular network (Debessa et al., 2001). Thus, collagen type I provides high tensile strength and stiffness to tissues, whereas collagen type III allows high compliance to tissues (Kwak, 2013). A high ratio collagen type III: collagen type I indicates a more compliant tissue, while a low ratio corresponds to a stiffer, less compliant tissue.

Besides structural proteins, adhesive proteins, anti-adhesive proteins and proteoglycans form the cardiac ECM. Adhesive proteins are extracellular glycoproteins closely associated to the cell membrane. Among them, fibronectin, a multi-domain ECM protein, interacts with multiple integrins, proteoglycans, collagens, and fibrins to mediate cellular behaviours (Pankov and Yamada, 2002). This protein is found in an insoluble form and is secreted to the extracellular compartment of the heart associated to other ECM components (Schwarzbauer, 1991). Laminin is another glycoprotein of the basal lamina, which includes different functional domains that bind to constitutive elements such as collagen IV, proteoglycans and transmembrane cell receptors (Aumailley, 2012). Among the non-adhesive components of the ECM, osteopontin is synthesized by SMC and fibroblasts. This ECM component participates in cell adhesion and controls cellular growth and migration. This calcium binding protein forms complexes with collagens and integrins and induces the synthesis of ECM proteins by

fibroblasts (Hsueh, 1998). Finally, proteoglycans are composed of a core protein associated to glycosaminoglycan sidechains, being hyaroluranan one of the most common in the heart (Lockhart et al., 2011). Proteoglycans contribute to the architecture of the ECM network, bind growth factors that participate in the paracrine signalling, and promote tissue remodelling and cell migration (Ruoslahti and Yamaguchi, 1991).

The bulk properties of the cardiac tissue change during tissue growth. During rat heart development, a shift of the local elasticity of tissue occurs from ~7 kPa on neonatal pups to ~30 kPa on the adult animal (Engler et al., 2008, Bhana et al., 2010, You et al., 2011). This results from local structural changes, such as ECM crosslinking density, tissue composition, and cell-ECM interactions (Jacot et al., 2010, Williams and Black, 2015). Therefore, the composition and architecture of the ECM acts in concert to provide environmental cues that regulate tissue morphogenesis and function (Figure 5). The sensors and effectors of this process are the cells, which consequently respond by changing their own morphology and function accordingly.

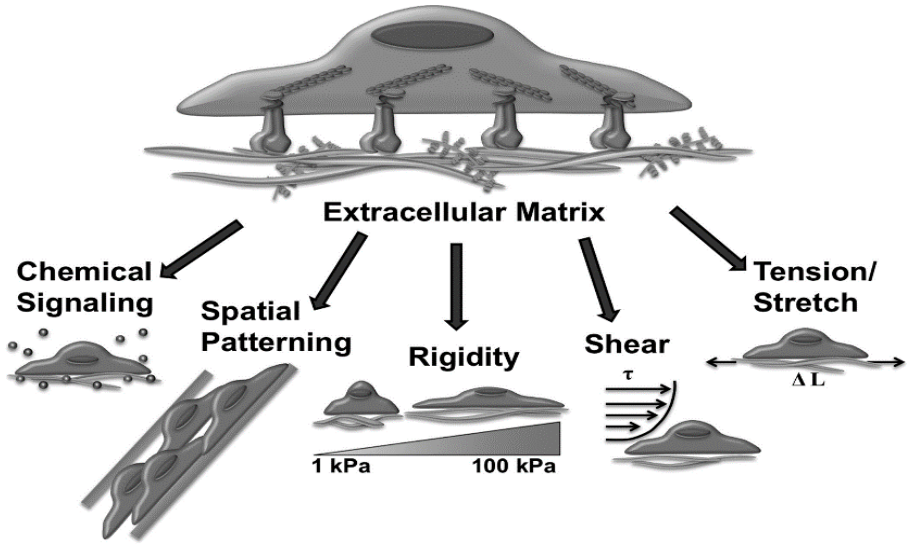

Figure 5 – **Microenvironmental modulation of cell morphology and fate**. The chemical, physical, and mechanical properties of the ECM influence cell shape and behaviour. Adapted from (Nakayama et al., 2014).

The ECM can modulate cell activity by the process of mechanotransduction. The cell senses the mechanical properties of the ECM by a complex process involving actin and microfilaments which can act directly in the cell nucleus (Lin and Worman, 1993). It is particularly relevant to note that mechanical signals are transferred to the nucleus much faster than diffusion-based molecular signalling (approximately 5 μs to 5 s), resulting in a more efficient transduction of the surface forces through the cell

(Nakayama et al., 2014). In fact, due to mechanical-based processes, cells can modify their secretory activity and modulate ECM composition, a process referred as matrix remodelling (Hsueh et al., 1998, Manso et al., 2006, Howard and Baudino, 2014). The main extracellular mediators of this process are matrix metalloproteinases and the tissue inhibitor of metalloproteinases. The coordinated activity of both elements determines matrix degradation rate. Consequently, this will regulate the release rate of several biomolecules, which otherwise would be confined within the ECM.

The electromechanical function of heart muscle is critically dependent on adequate cell–cell adhesion and communication. Several studies confirm that an active interplay occurs between cell-ECM adhesions and cell-cell interactions (Kléber and Rudy, 2004, McCain et al., 2012). In early stages of development, cell-ECM connections are more predominant, however as the tissue develops, cell–cell adhesion is then favoured, particularly at longitudinal myocyte borders (Figure 6).

The active role of ECM on modulating cell behaviour can be also observed in artificial conditions. Simulation of a supra-physiological stiff environment can be achieved through biocompatible substrates or scaffolds. On these conditions, several parameters have been detected: i) increased integrin expression (Terracio et al., 1991) and cell-cell uncoupling (Kostin et al., 2003); ii) disruption of contraction cycle dynamics; iii) metabolic and structural remodelling at the cellular level (McCain et al., 2012). These observations imply that the arrangement of cellular adhesions and cell-cell connections obey to a defined hierarchy, which shifts according to the stiffness of the microenvironment.

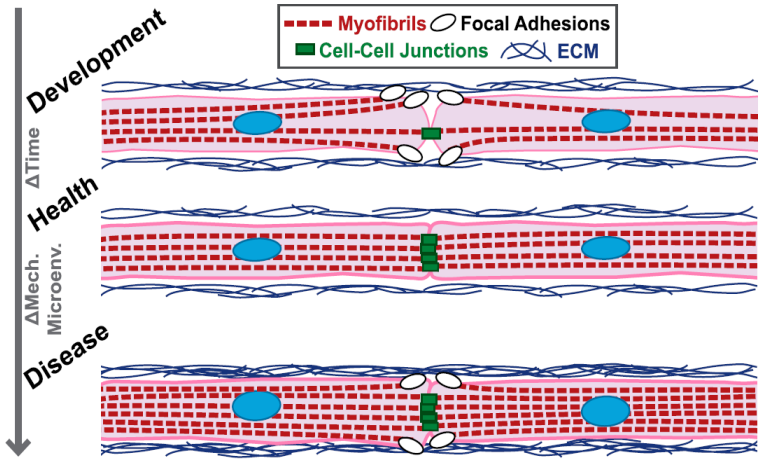

Figure 6- Interplay between CM-ECM and CM-CM during development and disease. During development, focal adhesions guide migration and cell–cell junctions assembling. In health, cell–cell junctions dominate over focal adhesions near the cell–cell interface and forces are transmitted intercellularly. When the micro-environment is stiff, for example due to pathologies, focal adhesions are re-organized to near the cell–cell interface to stabilize excessively loaded cell–cell junctions. Adapted from (McCain et al., 2012).

1.2 - Heart function

1.2.1 - Cardiac action potential and electrochemical-based contraction

Cardiac function results from the excitation of individual CMs through a variation of the cell's membrane electrochemical potential, a process known as action potential. Electrochemical variations and cell-cell coupling are the underlying mechanisms that link electrical conduction and depolarization of the muscle cells during contraction (Olson, 2004, Aronsen et al., 2013). The membrane potential of a CM (V_m) is defined by the ionic current (I_{ion}) and membrane capacitance (Cm), as a function of time (Kléber and Rudy, 2004): $\frac{dV_m}{dt} = -\frac{I_{ion}}{Cm}$. The action potential is then dependent of the total flux of ions, which occurs via the coordinated activity of various ion channels (e.g. sodium, potassium, calcium, chloride), and transporters in the membrane (Figure 7).

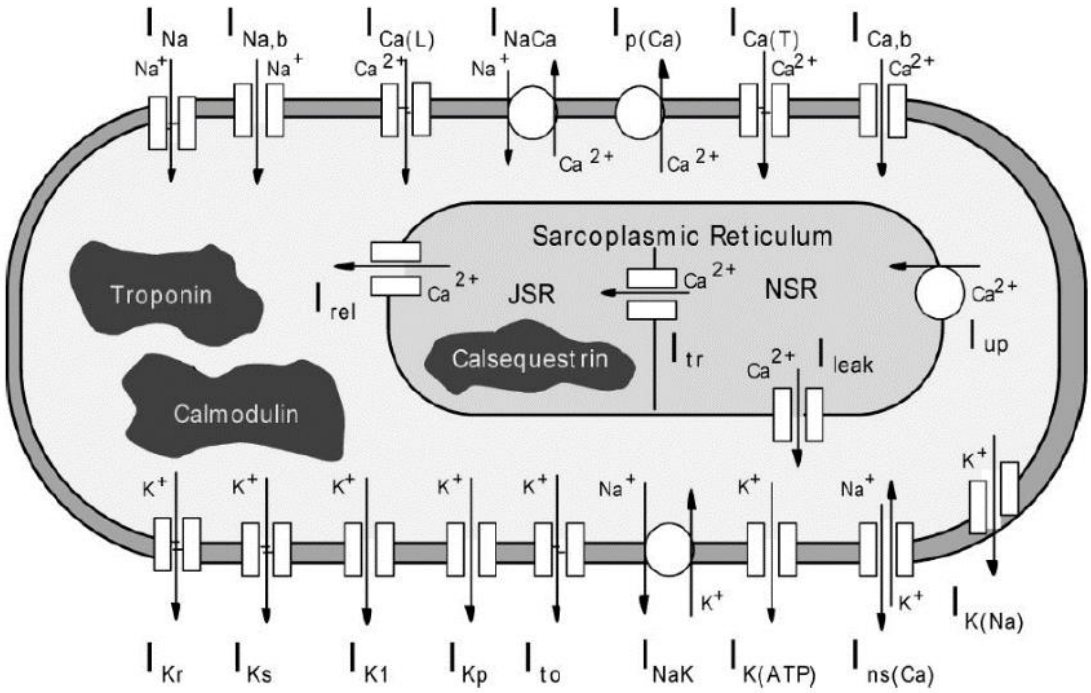

Figure 7 - **Diagram of the dynamic Luo-Rudy ventricular cell model.** I_{Na}, fast sodium current; $I_{Ca(L)}$, calcium current through L-type calcium channels; $I_{Ca(T)}$, calcium current through T-type calcium channels; I_{Kr}, rapid delayed rectifier potassium current; I_{Ks}, slow delayed rectifier potassium current; I_{to}, transient outward current; I_{K1}, inward rectifier potassium current; $I_{K(ATP)}$, ATP-sensitive potassium current; I_{Kp}, plateau potassium current; $I_{K(Na)}$, sodium-activated potassium current (activated under conditions of sodium overload); $I_{ns(Ca)}$, nonspecific calcium-activated current (activated under conditions of calcium overload); $I_{Na,b}$, sodium background current; $I_{Ca,b}$, calcium background current; I_{NaK}, sodium-potassium pump current; I_{NaCa}, sodium-calcium exchange current; $I_{P(Ca)}$, sarcolemnal calcium pump; I_{up}, calcium uptake from the myoplasm to the sarcoplasmic reticulum (SR); I_{rel}, calcium release from SR; I_{leak}, calcium leakage from network sarcoplasmic reticulum (NSR) to the myoplasm; I_{tr}, calcium translocation from NSR to junctional sarcoplasmic reticulum (JSR). Calmodulin and troponin are calcium buffers in the myoplasm. Calsequestrin is a calcium buffer in the JSR. Adapted from (Kléber and Rudy, 2004).

The action potential consists in a sequence of events occurring between the intracellular and extracellular environment, comprising five phases (Figure 8). When the membrane potential of a myocardial cell reaches the threshold for action potential generation, it initiates the depolarization of the cellular membrane with the opening of voltage gated sodium channels (I_{Na}). As a result, Na^+ influx occurs, which in a feed-forward manner, further depolarizes the membrane (Phase 0). As sodium channels inactivate, the outward potassium current (I_{to}) quickly activates during Phase 1 to create a small spike at the action potential peak. Voltage gated L-type calcium channels (LTCCs) subsequently open (Phase 2) to allow Ca^{2+} influx from the extracellular environment ($I_{Ca,L}$). Calcium ions entering the cytosol bind to and open ryanodine receptors (RyR) in the membrane of the sarcoplasmic reticulum (SR), leading to a feed-forward amplification of the free intracellular calcium concentration to approximately tenfold, a mechanism called Ca^{2+}-induced Ca^{2+} release. As the L-type Ca^{2+}-mediated current is inactivated, outward potassium currents I_{Ks}, I_{Kr}, and I_{K1} induce the fast repolarization of the cellular membrane (Phase 3), bringing the CM to the resting potential (Phase 4), which is maintained primarily by the inward rectifier potassium current (I_{K1}). At this phase, subsequent initiation of depolarization can occur through the pacemaker current, which is typically mediated by spontaneously active cardiac cells from the sinoatrial node (SA) and atrio-ventricular node (AV), and the Purkinje fibres (Figure 1).

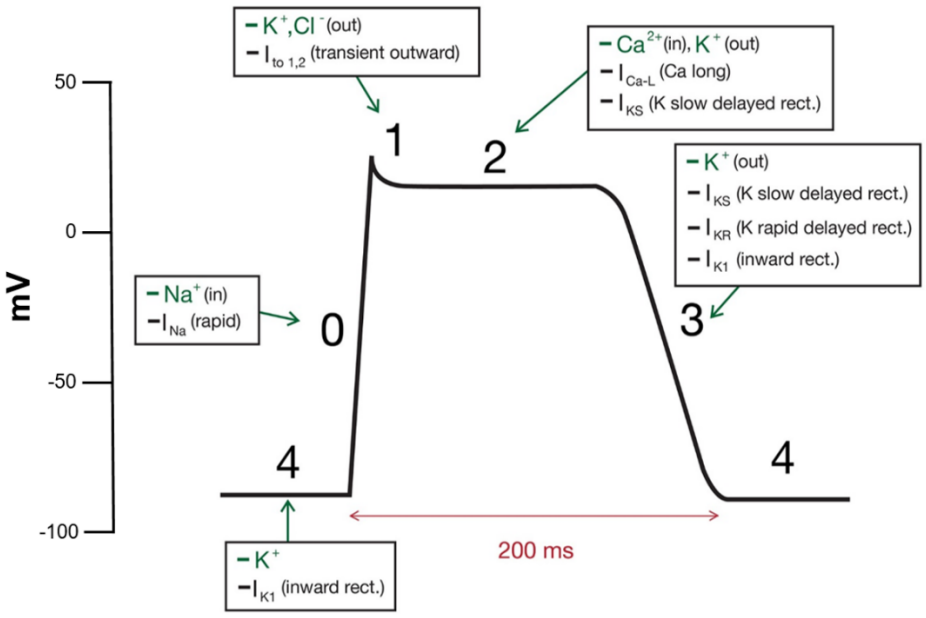

Figure 8 - **Phases of the action potential.** The phases of the cardiac action potential: from rest (4) to upstroke (0), notch (1), plateau (2), repolarization (3), and back to rest (4).

Muscle contraction, referred as systole, is initiated in the CMs with the binding of Ca^{2+} to Troponin C of the myofilaments, inducing a conformational change which allows cross-bridges to form between myosin and actin. At greater Ca^{2+} transients more cross-bridges are activated, therefore inducing stronger contractions. For the relaxation of the muscle, named as diastole, Ca^{2+} must be removed from the cytosol. This removal is done through an outward transportation of Ca^{2+} via Na,Ca-exchanger (NCX), and by the re-uptake into the SR, which is mediated by SR Ca^{2+}-ATPase (SERCA).

The intracellular Na^+ levels in CMs is regulated by the equilibrium between its influx and efflux. The Na^+,K^+-pump (NKA) is the only Na^+ efflux mechanism, requiring ATP consumption to pump Na^+ against its electrochemical gradient. This makes the NKA crucial for the control of the intracellular Na^+ concentration and consequently, of the cardiac electric coupling. In contrast, several transport proteins mediate Na^+-influx. Voltage gated Na^+-channels, NCX, Na^+,H^+-exchanger, HCO^--cotransporter and Na^+,K^+,$2Cl^-$-cotransporter can all contribute to the Na^+ influx, though it is mainly mediated by voltage gated Na^+-channels and NCX in the beating CM. Transportation of Na^+ and Ca^{2+} between the cytosol and mitochondrial compartment can also occur, since the mitochondrial membrane also contains NCX and Na^+,H^+-exchanger. The overall intracellular Na^+ concentration is determined by the ratio of leak and pump rates, and the relative contribution of the various Na^+ transport proteins varies in different situations.

1.2.2 - Action potential propagation

Propagation of the action potential signal in cells occurs mainly through the flow of ions between intercellular compartments and extracellular space. In single cells, the velocity of the signal propagation is proportional to the inward sodium current. Conversely, in the cardiac tissue multiple variables and factors define the velocity of action potential propagation (Spach and Kootsey, 1985): ion channel conductance, cell geometry, cell interconnections and tissue boundaries. As previously described, intercellular connectivity in a multicellular context is mediated by gap junctions, which include protein complexes composed by connexins (Bukauskas, 2014). These structures provide a direct pathway for electrochemical and metabolic signalling between cells. Therefore, gap junction-based communication is crucial in the conduction of the action potential, in the cardiac muscle.

Gap junctions are composed by protein complexes, known as hemichannels or connexons, which result from the combination of six connexins. Intercellular pores are formed by docking with a hemichannel counterpart in the adjacent cell membrane (van Veen et al., 2001). Gap junctions can be organized through homotypic (same Cx isotype in both hemichannels), heterotypic (2 Cx isotypes form gap junction channels, but each hemichannel is assembled from 1 isotype) and heteromeric (different Cx isotypes at least in one of the hemichannels) channels that vary in conductance, selective permeability, and gating properties (Moreno, 2004). Cx43, Cx45, and Cx40, mCx30.2 are the main cardiac isoforms and they differ in their open channel conductance and distribution within the heart (Figure 9) (Kléber, 2014). Among these, Cx43 is the predominant form of connexins in the heart, being mainly present in atria, ventricles, and distal conduction system. Cx40 is primarily expressed in atrial CMs, the atrioventricular node, and the conduction system, while mCx30.2 and Cx45 are expressed throughout the conduction system and in the sinoatrial node (van Veen et al., 2005, Kléber, 2014). The distribution of gap junction in the CM's membrane is a dynamic process which changes according the developmental stage and in the diseased state. As an example, gap junction distribution shifts from uniformly spaced around the entire cell perimeter in neonatal cells to primarily at cell ends in adult myocytes (Gourdie et al., 1992, Hoyt et al., 1989, McCain et al., 2012)

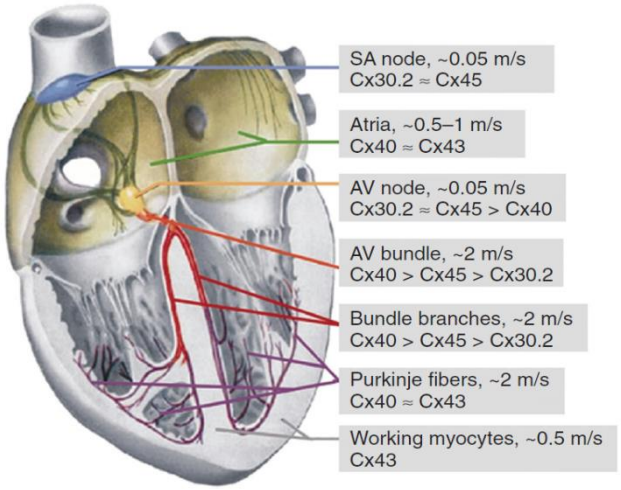

Figure 9 – Distribution of Cx expression and their respective conduction velocities in different regions of the heart. Adapted from "Cardiac Electrophysiology: From Cell to Bedside, 6th Ed., 2013".

An additional fact that must be considered in the action potential propagation is its velocity. In the multicellular context of the native heart tissue, the maximum upstroke velocity is not directly proportional to the peak of sodium current, as it happens in a single cell situation. A fraction of the electrochemical differential generated during the depolarization phase is diverted from a CM's surface and partially stimulates neighbouring cells. This phenomenon leads to a reduction in the magnitude of stimulation necessary to drive the membrane potential rise. Consequently, the stimulation of CM's contraction on a multicellular context occurs before the peak of

sodium current when a CM is in a single cell context (Fast and Kléber, 1995, Spach and Kootsey, 1985). Directly related to this is the particular geometry and cellular components of CMs. In a model of action potential with a continuous propagation, it would be expected a lower upstroke velocity associated with slower conduction, due to signal dispersion. However, by taking in consideration the particular aligned nature of cardiac tissue architecture and the presence of specialized intercellular connection, this association does not occur. In reality, maximum upstroke velocity increases while conduction velocity decreases due to lateral Cx uncoupling (Shaw and Rudy, 1997, McCain et al., 2012). With this mechanism, the action potential signal is contained in the aligned cell and signal dispersion is reduced, thus maximizing forward signal conduction.

Another factor to be taken in consideration in cardiac tissue's signal propagation is the degree of cell membrane excitability. This process is mainly dependent on the activity of Na^+ channel. The impairment of this channel can reduce or stop action potential conduction (Shaw and Rudy, 1997, Rohr et al., 1998). When Na^+ fluxes are severely impaired, L-type Ca^{2+} current may support conduction at lower rates (Shaw and Rudy, 1997). In addition, reduced conduction velocities can also be sustained by L-type Ca^{2+} current in conditions where cell-to-cell coupling is hampered.

1.2.3 - Cardiomyocyte ultrastructure

The CM is an elongated cell, typically 100 to 150 μm in length and 20 to 35 μm in width (Severs, 2000) (Figure 10). The internal basic unit of contraction in CMs is the sarcomere. This structure is composed by long contractile myofilaments (actin and myosin) that are packed together to form the striated myofibril tubules that fill most of the cell. Contraction and relaxation of the muscle tissue results from actin and myosin sliding past each other (VanPutte et al., 2015).

Sarcomeres are repeating units, delimited by the Z-lines/bands along the length of the myofibril. Each of these lines are composed of a filamentous network of proteins to which actin filaments dock (Figure 10). Between the Z-lines, the myofilaments have a particular arrangement that gives the myofibril a banded or striated appearance. The isotropic band (I-band) occupies each side of the Z-line and consists only of actin myofilaments. The anisotropic band (A-band) extends to the length of the myosin filaments and includes an area where actin and myosin myofilaments overlap. The H-

zone is placed at the centre of the A-band and encompasses a zone with only myosin myofilaments. The M-line is in the centre of the H-zone, and it holds the myosin my

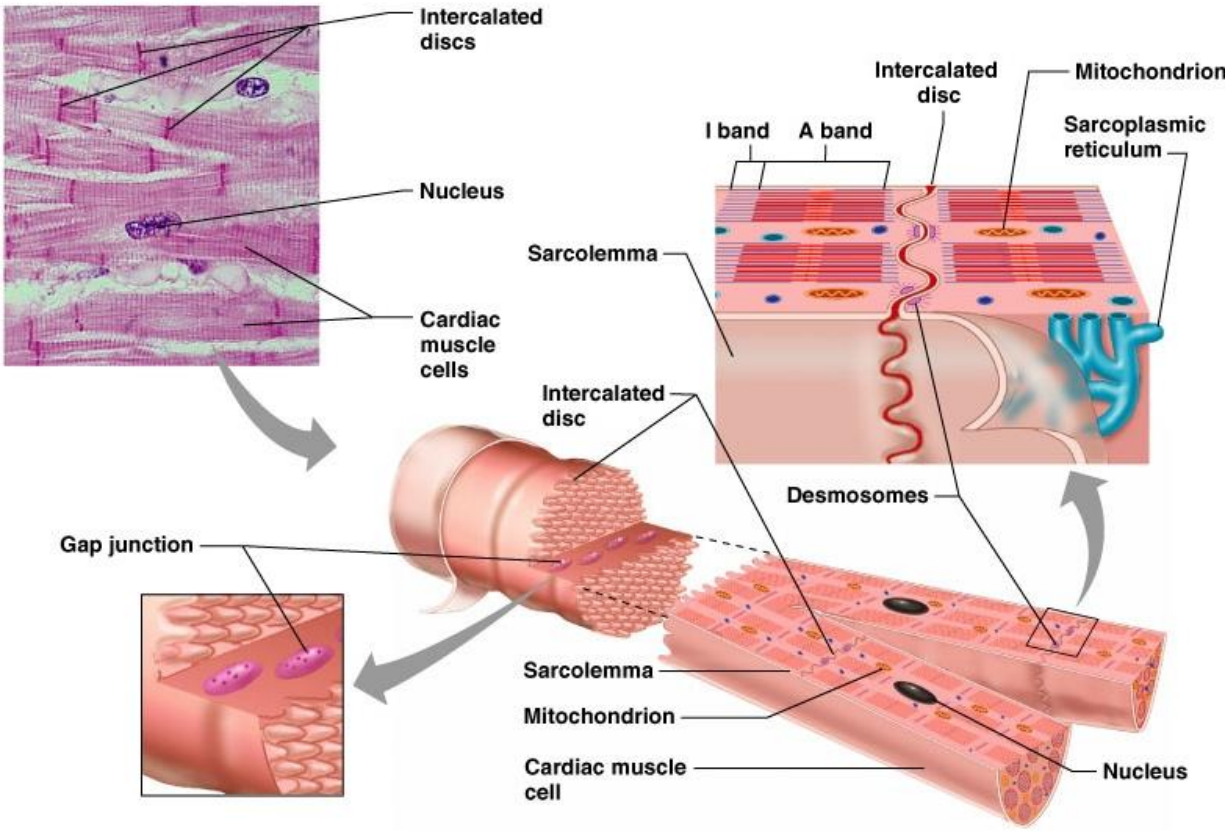

Figure 10 - **Cardiomyocyte's ultrastructure**. Adapted from Seeley's Anatomy and Physiology 6th Ed.

Actin myofilaments (thin filaments) are primarily composed of fibrous actin and a series of tropomyosin and troponin molecules. Myosin myofilaments (thick myofilaments) are composed of several myosin molecules, which form a long, fibrous tail and a globular head, referred as myosin heads. These myosin heads can bind to actin and to ATP, which is the energy source for the contraction phenomena. However, this can only occur when its binding sites are exposed to Ca^{2+} ions. During contraction, actin myofilaments slide over the myosin myofilaments thus shortening the length of the sarcomeres, consequently myofibrils, muscle fibres, muscle bundles and the overall muscle also shorten. During relaxation the myofilaments slide back and the sarcomere lengthen.

The cell membrane in CMs, also called sarcolemma, is characterized by many invaginations, the transverse tubules (T-tubules), establishing a network mainly centred at the Z-lines (Figure 11). The main function of the T-tubules is to accelerate the events

that lead to cell contraction. This is justified by the fact that not only Na^+ transport proteins tend to be clustered in the T-tubules, but also these structures provide proximity between the LTCCs in the cell membrane and RyRs in the SR membrane (Aronsen et al., 2013). The Ca^{2+} release from one RyR cluster is known as a Ca^{2+} spark, and as membrane depolarization rapidly spreads through the T-tubules during an action potential, a large amount of Ca^{2+}-sparks from different RyR clusters lead to the Ca^{2+} induced Ca^{2+} release, thus initiating contraction.

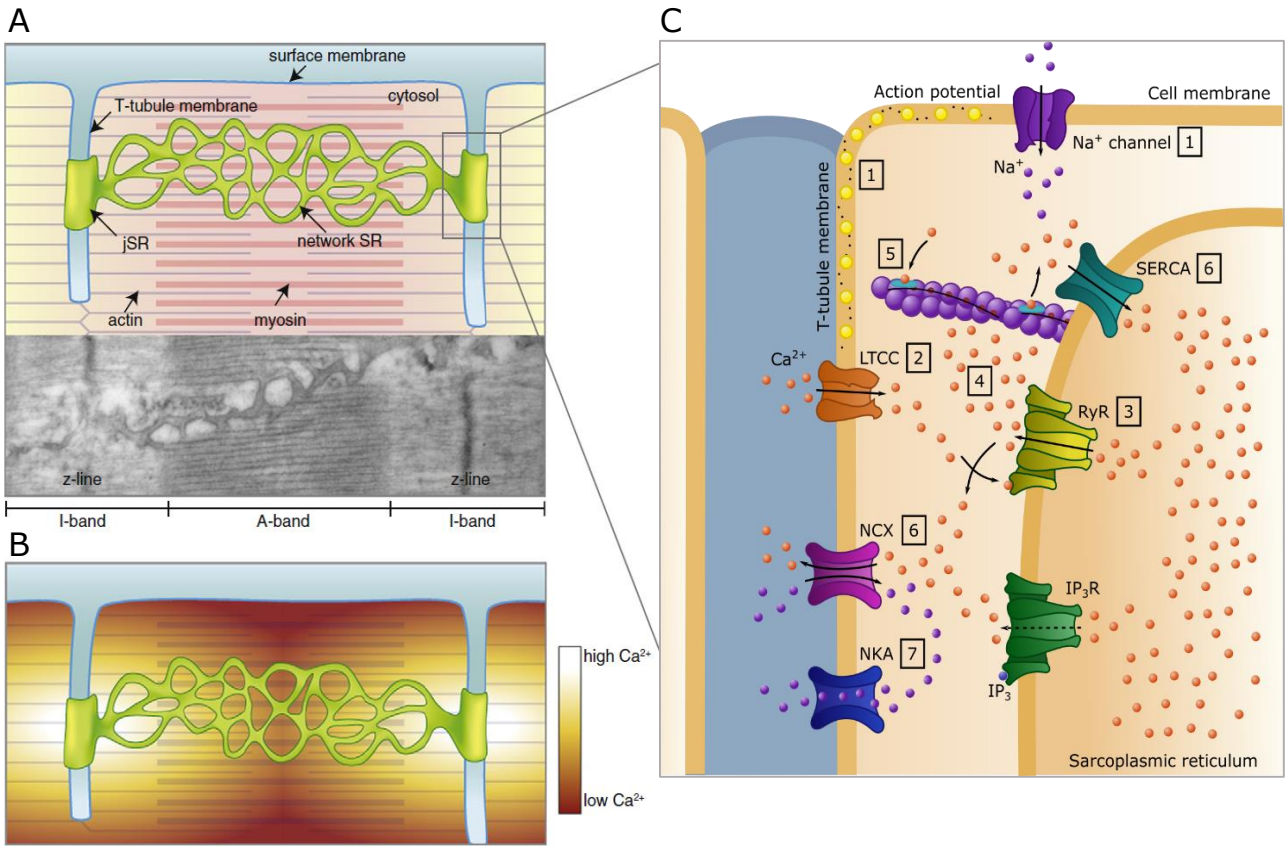

Figure 11 - **Structural basis for cell coupling in ventricular CMs. A)** T-tubules allow close interaction between the SR and the sarcolemma. **B)** The concentration gradient of Ca^{2+} rapidly increases the local Ca^{2+} concentration in the dyad (bright colour), leading to Ca^{2+} diffusion out of the dyadic cleft to increase the global Ca^{2+} levels in the cell (dark colour), which triggers contraction. Adapted from Aronsen et al 2013. **C)** Contraction generated by action potential. *1)* The action potential spreads rapidly in the cell membrane. The rapid depolarization phase is due to the opening of Na^+ channels. *2)* The depolarization opens LTCCs in the T-tubule membrane so that a small amount of Ca^{2+} is released into the cytosol. *3)* Ca^{2+} then binds to the Ca^{2+} RyR in the SR. *4)* The activation of Ca^{2+} RyR leads to the release a larger quantity of Ca^{2+} to the cytoplasm. *5)* The released Ca^{2+} binds to the contractile proteins. *6)* In the relaxation phase, while some of the Ca^{2+} is pumped back to the SR by SERCA, some is transported outward through the cell membrane by the NCX. *7)* NCX and NKA coordinate the regulation of Ca^{2+} and Na^+ at the cell membrane.

1.3 - Cardiac tissue engineering

The term "tissue engineering" was introduced in the late 80´s as: "Application of principles and methods of engineering and life sciences toward fundamental

understanding of structure-function relationship in normal and pathological mammalian tissues and the development of biological substitutes to restore, maintain, or improve functions" (Eschenhagen and Zimmermann, 2005). Cardiac tissue engineering thus combines knowledge of biology, engineering and medicine to re-create functional cardiac tissue.

One of the first studies in cardiac tissue engineering was reported by Moscona (Moscona, 1959). In this study, cardiac spheroid aggregates were generated from embryonic chick heart cells. Later on, it was found that these 3D spheroid tissues were functionally more similar to intact heart tissue than standard 2D-monolayer cultures (McDonald et al., 1972). These studies confirmed that embryonic cardiac cells had the capacity to give rise to heart-like tissues under specific cell culture conditions while retaining some of its functional capacity (McDonald et al., 1972).

Tissue growth is controlled *in vivo* by multiple factors acting in concert according to specific spatial and temporal queues. Thus, cardiac tissue engineering has the contribution of different disciplines, such as developmental biology, cardiac muscle cell biology, and material science, to better understand the cellular environment of the growing heart. The study of heart's biology and development was of particular importance since it provided several insights regarding the particular needs for "building" this specific tissue. Some of these biological factors are crucial components to be considered while developing strategies for growth of cardiac tissue *in vitro*.

Over the years, the collective work of several groups established the necessary components for engineering a heart tissue: i) cells that can be selected, expanded, and transfected to express the intended cellular function; ii) biomaterial scaffolds that serve as a structural template and whose mechanical properties match those of the native tissue; and iii) bioreactors that maintain the physiological milieu of the cell (pH, temperature, biochemical factors and nutrients).

1.3.1 - Source of cardiac cells

The adult human left ventricle contains nearly 5 thousand million CMs (Beltrami et al., 1994), meaning that the creation of a small patch of cardiac tissue requires an enormous amount of CMs. Therefore, obtaining cardiac cells from reliable and efficient sources remains one of the major limitations in cardiac tissue engineering.

Although cardiac development and basic principles of function are conserved between species, there are still significant differences between human and non-human cells (Doggrell and Brown, 1998). These differences reduce the value of non-human cells when trying to model the human heart. Nevertheless, non-human cells are still a good starting point to engineer cardiac tissue for small proof-of-concept studies.

Human embryonic stem cells (hESCs), derived from the inner cell mass of blastocysts (Thomson et al., 1998), have broad potential to differentiate into cells from all three embryonic germ layers, including CMs (Caspi and Gepstein, 2004). However, ethical issues in the use of hESCs shifted research to the exploration of alternative cell sources. Induced pluripotent stem cells (iPSCs) may be also an important source of human cardiac cells. Yamanaka and colleagues demonstrated that the exogenous expression of four proteins in somatic cells (c-Myc, Klf4, Oct4, and Sox2) was sufficient to induce pluripotency in the cells (Takahashi and Yamanaka, 2006). Autologous adult cells can then be converted into pluripotent cells, by inducing expression of embryonic genes, which can then be differentiated into CMs (Batalov and Feinberg, 2015). Results indicate that hESC-derived and iPSC-derived CMs have a similar phenotype, expressing early cardiac transcription factors, as well as the expected sarcomeric proteins, ion channels, connexins and calcium-handling proteins (Yamashita, 2010). They exhibit functional properties similar to those reported for CMs in the developing heart, and they undergo comparable mechanisms of excitation-contraction coupling and neuro-hormonal signalling (Zwi et al., 2009, Zhang et al., 2009a). Importantly, CMs derived from pluripotent stem cells are immature and so they lack the expression profile, morphology and function of adult ventricular myocytes.

1.3.2 - Cell density and cardiac cell sub-populations

The native myocardium is composed of non-proliferating CMs (20%–30% in human heart, 50% in mouse heart, and 30% in rat heart) (Jugdutt, 2003, Banerjee et al., 2007), and proliferating non-CMs, such as fibroblasts, endothelial and smooth muscle cells (Gerecht-Nir et al., 2006). Having in mind that cell coupling is needed for proper cell-cell signalling, and CMs have limited capacity to proliferate, an engineered cardiac construct must have the right ratio of cardiac cell subpopulations.

Several experimental evidences support the importance of co-plating CMs with other cardiac cells for generating a functional engineered construct. Tissue constructs produced from a non-purified heart cell mixture had higher contraction forces than those

made from purified CMs (Naito et al., 2006). In addition, poly(glycerol sebacate) constructs seeded consecutively with CFs and CMs had better tissue structure and lower activation threshold than those cultured with pure CMs (Radisic et al., 2008). Moreover, the addition of fibroblasts to a pure, genetically selected CM population from mouse and hPSC showed improved function and morphology while comparing to a pure CM population (Kensah et al., 2013). Finally, cardiac tissue obtained from human derived CMs co-cultured with endothelial and stromal cells had improved structure and function than the one obtained by culturing CMs alone (Caspi et al., 2007, Marsano et al., 2010, Stevens et al., 2009, Tulloch et al., 2011).

1.3.3 - Tissue construct size

Adult beating CMs have a very high metabolic activity and therefore oxygen and nutrients are supplied by diffusion from a high-density network of capillaries that are spaced approximately 20 μm apart (Rakusan and Korecky, 1982, Rakusan et al., 1992). A central problem in cardiac tissue engineering is the limitation in size of the engineered tissue. Typically engineered cardiac tissues have a thickness of no more than 100 μm to avoid nutrient and oxygen diffusion limitations (Shimizu et al., 2002, Carrier et al., 2002a, Radisic et al., 2003). Some strategies have been described in the last years to enhance oxygen and nutrient diffusion such as the ones using bioreactors, increasing ambient oxygen concentrations (Carrier et al., 2002b) and/or by supplementing the culture medium with synthetic oxygen carriers, such as perfluorocarbons (Radisic et al., 2005). Perfusion of cardiac tissue constructs has been shown to improve their functional properties (Radisic et al., 2004b).

1.3.4 - Cellular coupling

The orientation and elongation of CMs observed in the native tissue favours inter-cellular communication, as previously mentioned. Therefore, some studies aimed to assess the impact of patterned substrates that guide the growth of cardiac tissue into an aligned conformation. Several combinations of materials and design patterns have been tested revealing a positive correlation between topography and cell coupling (Lee et al., 2008, Kim et al., 2013). Stiffness modulation is also another factor that has demonstrated to affect the coordination of cell-cell interactions (McCain et al., 2012).

Studies with hydrogel-based cardiac tissue constructs (CTCs) have shown that mechanical stimulation of the construct leads to CM alignment and maturation. In these

cases a static (Eschenhagen et al., 1997, Zimmermann et al., 2002, Baar et al., 2005, Black et al., 2009, de Lange et al., 2011) or a dynamic tension (Leychenko et al., 2011, Salameh et al., 2010b, Dhein et al., 2014) has been applied. Improved cardiac tissue structure and higher contraction force have been observed when the tissue constructs were exposed to phasic stretch of 10% to 15% by a stretching device (Fink et al., 2000) or performed work against elastic anchoring points (Zimmermann et al., 2006b, Hansen et al., 2010). These observations confirm that it is beneficial to subject engineered cardiac tissues to a mechanical tension similar to the one occurring in the native tissue.

Direct application of electrical stimulation on tissue constructs during cultivation, has also been shown to enhance the excitation-contraction coupling and improved the properties of engineered myocardium at cell's ultrastructure level (Radisic et al., 2004a, Feng et al., 2005, Tandon et al., 2009, Nunes et al., 2013). It is important to note that, although electrical fields enhanced CM elongation and orientation, topographical cues that mimic the natural physical environment of the ECM are stronger determinants of cell elongation than electrical stimulation (Au et al., 2007).

1.4 - Scaffolds

The scaffolds for cardiac tissue engineering should meet certain requisites. First and foremost, the biomaterial substrate should provide adequate mechanical support to the cells. In addition, its composition should allow their physiological growth and maturation. Consequently, and to reproduce the role of the native ECM, topographic queues should be present in order to drive an adequate cellular organization. This property should be either a constitutive part of the biomaterial or a result from a fabrication process (Curtis and Russell, 2011, Moraes et al., 2011). Next, to maximize CM contractile function, the scaffold's elastic properties must allow compliance under deformation forces, preferentially mimicking the elasticity of the native tissue (McDevitt et al., 2003). In parallel, additional features or properties of the biomaterial should facilitate generation and propagation of the contraction wave-front signal (Dvir et al., 2011, Shin et al., 2013).

Natural and synthetic polymers have been suggested for cardiac tissue engineering (Nair and Laurencin, 2006). The biochemical motifs present in the structure of natural polymers have been shown to facilitate cell adhesion and proliferation. Some examples

of these biopolymers include collagen (Eschenhagen et al., 1997), Matrigel® (Zimmermann et al., 2000), hyaluronic acid (Young and Engler, 2011) and gelatin (Li et al., 2000) (Akhyari et al., 2002). Nonetheless, these biopolymers are not suited to serve as solid templates for cell seeding due to their weak mechanical properties. On other hand, synthetic polymers offer easy control in scaffold properties such as elasticity, shape and rate of degradation, just by changing their copolymer ratio (Giraud et al., 2007). One of the major classes of biopolymers used in tissue engineering are aliphatic polyesters, which comprise examples such as poly(caprolactone) (PCL), poly(lactic acid) (PLA), poly(glycolic acid) and their copolymers (Gunatillake et al., 2006, Liu et al., 2012b, Kim et al., 2014).

Unlike natural polymers, synthetic polymers have the key advantage of allowing precise control of their chemical and mechanical properties. Nevertheless, they do not possess the biological cues of natural polymers. In an attempt to overcome the singular downsides of some biomaterials, compositions of two or more materials have been tested (Pok and Jacot, 2011, Ravichandran et al., 2011). As an example, neonatal rat CMs have been cultured on electrospun PCL nanofibrous meshes coated with collagen type I (Shin et al., 2004). These scaffolds have nanoscale topographic cues similar to that of the ECM and natural cell adhesion cues. In another strategy, materials with known conductive properties were incorporated into the scaffold to overcome the reduced capacity of most of the biomaterials in conducting electric signals. Examples include scaffolds of alginate with dispersed gold nanowires (Dvir et al., 2011), and methacrylated gelatin embedded with carbon-nanotubes (Shin et al., 2013).

Elastomeric polymers, that can be natural or synthetic, represent an important class of materials in cardiac tissue engineering. They offer a wide variety of elastic properties that can closely resemble the elasticity of the native tissue. In addition, these polymers are also able to withstand strong deformation forces and return to their original size upon removal of the stress, therefore are well suited to move in synchrony with each contraction/relaxation motion. This class comprises polymers and respective co-polymers such as poly(urethane) (McDevitt et al., 2003), 1,3-trimethylene carbonate (Pego et al., 2003), poly(glycerol sebacate) (Radisic et al., 2008, Chen et al., 2008), poly(N-isopropylacrylamide) (Fujimoto et al., 2009, Wang et al., 2009a, Wang et al., 2009b, Wall et al., 2010), and poly(ethylene glycol) (PEG) (Iyer et al., 2009) (Jiang et al., 2009, Kraehenbuehl et al., 2011, Wu et al., 2011).

1.4.1 - Piezoelectric materials

Newer approaches for cardiac tissue engineering sought to use materials with active properties to provide an adequate electric environment to cardiac cells. Piezoelectric materials are one such example. Piezoelectricity, from the Greek word *piezein* (press), was first reported by Jacques and Pierre Curie at 1880. The most common way to describe the piezoelectric effect is by the so-called direct effect that concerns the conversion of the mechanical energy into electrical energy. In opposition, the inverse piezoelectric effect, describes the conversion of electrical energy into the mechanical energy. The piezoelectric effect can be described by four piezoelectric coefficients d_{ij}, e_{ij}, g_{ij}, h_{ij} (Kochervinskii, 2003):

$$d_{ij} = \left(\frac{\partial D_i}{\partial X_j}\right)^E = \left(\frac{\partial x_i}{\partial E_j}\right)^X \qquad e_{ij} = \left(\frac{\partial D_i}{\partial x_j}\right)^E = -\left(\frac{\partial X_i}{\partial E_j}\right)^X$$

$$g_{ij} = \left(\frac{\partial E_i}{\partial X_j}\right)^D = \left(\frac{\partial x_i}{\partial D_j}\right)^X \qquad h_{ij} = \left(\frac{\partial E_i}{\partial x_j}\right)^E = \left(\frac{\partial X_i}{\partial D_j}\right)^X$$

The piezoelectric coefficients are given by the correlation between electrical variables "D" (electric induction) and "E" (electric field strength) and mechanical parameters, "X" (mechanical stress) and "x" (strain). In these four relationships, the first terms relate to the direct piezoelectric effect and the second terms correspond to the inverse piezoelectric effect.

The piezo effect is highly dependent on the crystallographic properties of the material, mainly the molecular anisotropy of the structure. Denoting this, for some synthetic polymers with an isotropic noncrystalline or semicrystalline structure it is necessary a procedure (e.g. mechanical stretching or corona poling) to achieve a dipole-crystal structure which provides permanent piezoelectric properties (Figure 12) (Furukawa, 1989, Kholkin et al., 2008). This class of polymer includes poly(aniline), poly(pyrrole), PLA, vinylidene fluoride (VDF) and poly(vinylidene fluoride) (PVDF) and its respective copolymers (Ribeiro et al., 2015). Among these polymers, PVDF and VDF copolymers, are synthetic, semi-crystalline polymers with the highest electroactive features, including piezoelectric, pyroelectric and ferroelectric properties (Nalwa, 1995, Serrado Nunes et al., 2009).

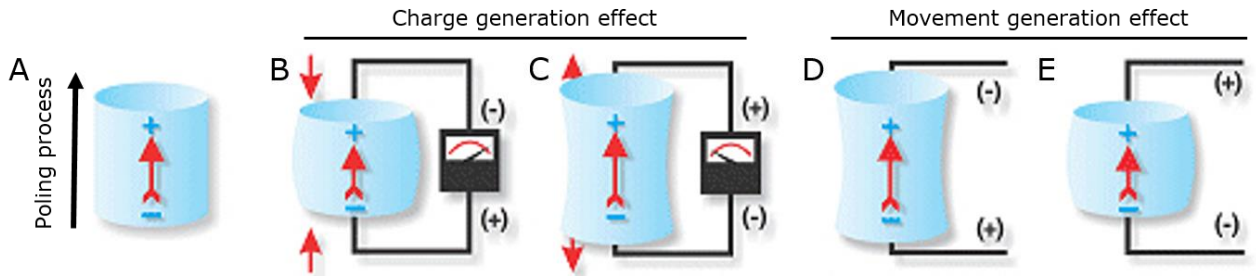

Figure 12 – **Schematic representation exemplifying the relative piezo effects after previous activation by a poling process. A**) Poling of the material by voltage aplication; **B**) Compression of the material: voltage generated has the same polarity as the poling voltage; **C**) Stretching of the material: voltage has opposite polarity to that of the poling voltage; **D**) Applying voltage as same polarity as poling voltage: material lengthens; **E**) Applying voltage as polarity opposite of the poling voltage: material shortens.

Piezoelectric electromechanical properties have been widely used in electronics, including sensor technologies, actuator applications and energy harvesting (Tressler et al., 1998, Chopra, 2002, Steven and Henry, 2007, Dong et al., 2011). Piezoelectricity has been also described in the human body (Fukada and Yasuda, 1957, Marino and Becker, 1970, Ribeiro et al., 2015). Only recently piezoelectric materials have been explored in the context of tissue engineering (Ribeiro et al., 2015). These materials have been fabricated as films and fibres meshes and have been tested in the culture of mesenchymal stem cells (Damaraju et al., 2013), neurons (Lee et al., 2011), fibroblasts (Weber et al., 2010b) and C2C12 myoblasts (Martins et al., 2013). Unfortunately, the effect of the electrical stimulus resulting from a piezoelectric response in the cells or tissues is largely unknown from a mechanistic point of view.

PVDF and its co-polymers are the most used polymers in cell/tissue related applications. The high piezoelectric properties of these polymers make them ideal for electromechanical transduction (Damaraju et al., 2013). For example, mesenchymal stem cells cultured on PVDF fibres showed higher alkaline phosphatase activity and early mineralization relatively to the control. In addition, osteoblasts cultured in PVDF films showed higher bone formation, increased metabolic activity and bone gene expression as compared with the control (Frias et al., 2010). PVDF films were also tested for bone tissue response under static and dynamic conditions (Ribeiro et al., 2012). For the dynamic condition, mechanical stimulation was applied by placing the culture plate on a vertical vibration module at a frequency of 1 Hz and an amplitude of ~1 mm. It was then observed that the surface charge under mechanical stimulation improved the osteoblast growth. PVDF has demonstrated to have impact in neuronal tissue culture. Neurons seeded directly on PVDF films showed enhanced nerve fibre outgrowth (Valenti,

1993). The piezoelectric effect has been also investigated for wound healing applications (Guo et al., 2012). In this study, polyurethane/PVDF (PU/PVDF) fibre scaffolds were subjected to intermittent deformation of 8% at a frequency of 0.5 Hz for 24 h. The results indicated that piezoelectric-excitation enhanced cellular migration, adhesion and secretion, leading to more rapid wound healing. *In vivo* assays were also performed with the implantation of these scaffolds in rats. The piezoelectric stimulation resulting from the mechanical deformation of the scaffolds caused by the animal's movements, induced higher fibrosis at the wound area.

The use of piezoelectric materials in cardiac tissue engineering is relatively new. Fibronectin-coated PVDF nanofibers electrospun with an anisotropic or isotropic arrangement have been used to grow ventricular CMs (Liu et al., 2014). CMs were plated on the aligned nanofibres showed synchronized actuation and developed an anisotropic cell pattern. Until now, this study is the only work reporting the direct seeding of CMs in a fibrous piezoelectric scaffold. More recently, a piezoelectric material has been successfully combined with a flexible nanofilm in order to create a system for harvesting electrical energy (Xia et al., 2014). In this bio-hybrid micro generator, neonatal rat CMs were seeded in a film substrate composed by a top layer of PDMS and a bottom layer of piezoelectric PVDF. In order to maximize mechanical actuation CMs were uniaxially aligned thanks to 2D patterns produced by microcontact printing of fibronectin lines. By coupling the layered film with an electrode, it was possible to collect the power generated from the PVDF resulting from the mechanical strain performed by the contraction of CMs. They also reported in this study that continuously synchronous contraction was stable for up to one month and that peak output voltage reached 92.3 mV. Future application for this system can include powering implanted micro/nano devices or use as a sensor that can reflect the mechanical performance of CMs.

1.4.2 - Thin films

For engineering cardiac tissue one must consider the degree of freedom provided by the substrate for cellular contraction. Intrinsically, the stiffness of a material will dictate the resistance that it will offer towards contraction. This means that the higher the elastic modulus, the higher will be the force necessary to deform the material (Jacot et al., 2010). Freedom for contraction can also be provided by the extrinsic design of the substrate. An example includes the use of free-standing films produced by single layer (Feinberg et al., 2007, Greco et al., 2011) or layer-by-layer spin-coating (Ricotti

et al., 2011, Van Tassel, 2013). In this strategy, the films are released from the template thanks to the dissolution of a hydrophilic sacrificial layer (Taccola et al., 2011). Once floating the only resistance to cell deformation/contraction results from the bulk properties of the film (e.g. thickness and area). It is also important to note, that without the 2D planar restriction, contraction on free-floating films can occur in 3D, thus adding dimension to contraction (Figure 13) (Feinberg et al., 2007, Shim et al., 2012).

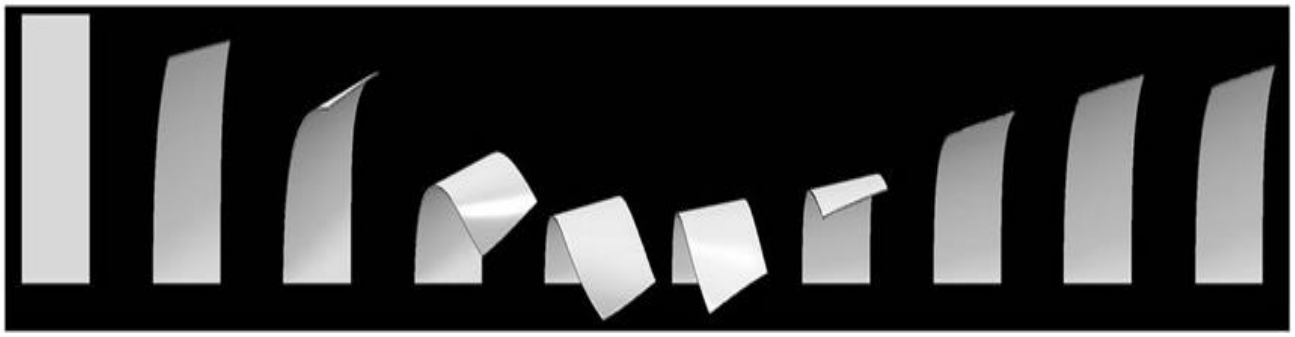

Figure 13 – Modelling of the contractile behaviour of CMs with diagonal cell alignment seeded on a PDMS free standing film (thickness of 14:5 mm). Adapted from (Shim et al., 2012).

Studies have analysed the passive tension forces provided by a free-floating film system with anisotropic surface patterns (Feinberg et al., 2007, Alford et al., 2010). While the topographical cues lead to the alignment of cell bodies of neonatal ventricular CMs, the loose conformation of the film allowed deflection on a 3D manner (Figure 14). With this design, variations on the thickness of the PDMS thin-film dictate the degree of resistance offered by the substrate towards CM contraction. In addition, it was showed that contractions resulted in deformations along the axis of the surface patterns, therefore demonstrating a correlation between uniaxial sarcomere alignment and contraction.

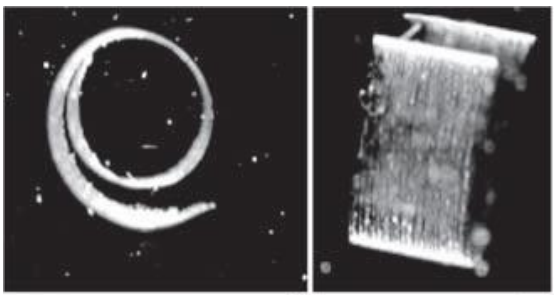

Figure 14 – A coiled free-floating film with anisotropic cardiac cells (on the concave surface) that cyclically contracted from an uncoiled to coiled state. Adapted from Feinberg et al., 2007.

More complex designs can be created with suspended film substrates in order to test structure-function relationships in tissue engineering-based strategies. This is the case of a study demonstrating the creation of a medusoid tissue structure (Nawroth et al., 2012). To simulate the propelling mechanism seen in jellyfish, neonatal rat CMs were assembled into a micro-patterned, jellyfish-shaped, PDMS thin film. While the aligned topography controlled the 2D tissue architecture, the overall medusoid shape

provided an adequate muscle stress and the necessary substrate compliance upon CM contraction (Figure 15). This last feature is of particular interest since with a homogeneous disc shape, the film would be incompressible and could not be turned into a bell without wrinkling, buckling or cracking. Likewise, the elastomeric properties of PDMS were tuned in order to allow an adequate compliance during the power stroke, and facilitate the restoration of the original shape through elastic recoil during the recovery stroke.

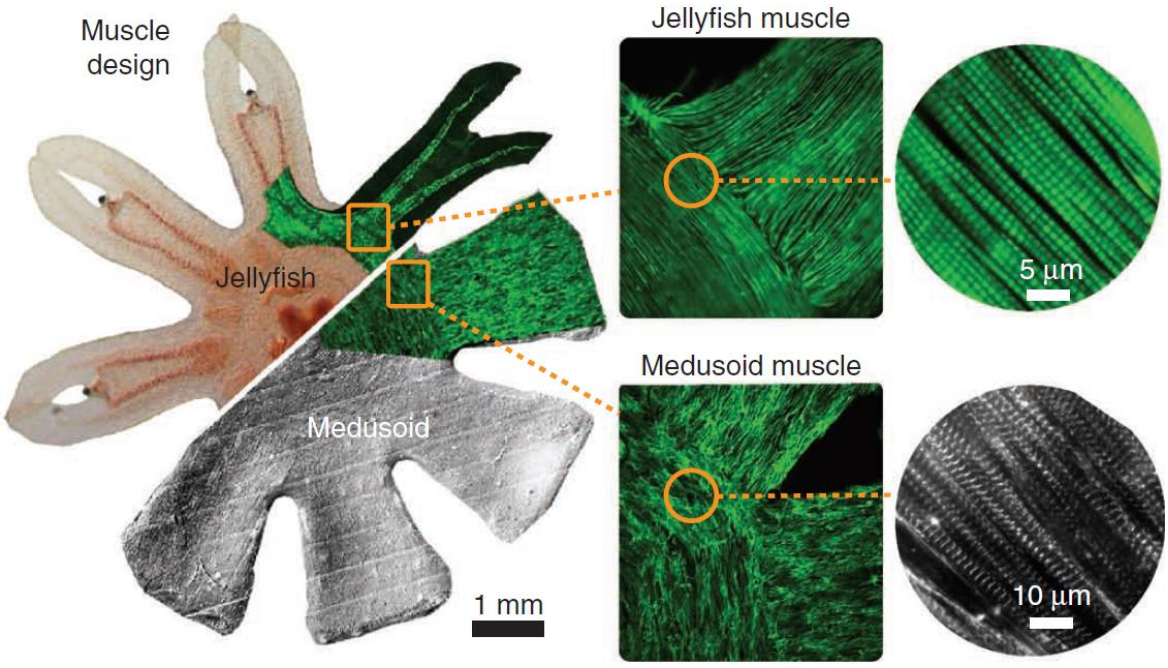

Figure 15 - **Jellyfish 2D muscle architecture (top) was reverse-engineered into medusoids (bottom).** Left: Composite brightfield image overlaid with F-actin stain (green) of muscle cell monolayer. Square inset: Close-up on muscle organization at lobe-body junction; F-actin stain (green). Circular inset: microstructure of single myofibril layer; F-actin stain (green), sarcomeric α-actinin (gray). Adapted from Nawroth et al., 2012.

1.5 - Cardiomyocyte maturation

1.5.1 - Morphology

During heart development, the adult phenotype results from a complex series of phenotypic and structural changes that occur to cardiac cells. As mentioned previously, cardiac tissue growth at embryonic/fetal stages occurs via CM proliferation. After birth, tissue growth occurs through cellular hypertrophy, as CM body enlargement can be up to 30–40 fold (Laflamme and Murry, 2011). Direct comparison of cell surface area has shown that hESC-CMs have a significantly smaller area than adult CMs, which in

prolonged cell cultures show a characteristic long rod-shaped cell body. Cell surface area is crucial to membrane capacitance and both parameters are directly proportional. As an example, the capacitance of the hESC-CMs has been reported to be around 18 pF (Zhu et al., 2010), while in adult human ventricular CMs is approximately 150 pF (Drouin et al., 1995). Therefore, CM size can influence functional processes such as impulse propagation, maximum rate of action potential depolarization, and total contractile force (Spach et al., 2004b).

In addition to CM size, cell shape is another morphological parameter with relevant functional implications. In the adult cardiac tissue, CMs have elongated anisotropic shapes with a length to width ratio of 7 to 9.5 (Gerdes et al., 1992). *In vivo*, immature and adult CMs share the same morphological rod-shape configuration, however, when cultured *in vitro*, immature cells start to flatten and spread in all directions, contrary to the adult cells which maintain their cylindrical morphology (Bird et al., 2003, Louch et al., 2011).

T-tubules are one of the structural components that has a major impact in excitation-contraction coupling. In adult mammalian ventricular CMs, these membrane invaginations have a regular spacing of around 2 μm, matching the Z-line regions (VanPutte et al., 2015). This particular pattern facilitates the initiation of a rapid electrochemical excitation and the synchronous triggering of SR calcium release. Since T-tubules enable the coordinated contraction throughout the cell body, T-tubule presence is a hallmark of CM maturation (Lundy et al., 2013). During fetal development, rat CMs do not have T-tubules. At the end of the first postnatal week, the first T-tubule-like structures are generated. Only at one month of age the T-tubule system reaches full maturation, showing the characteristic striated pattern of the adult CM.

At early stages of development, gap junction protein Cx43 and the adherens junction protein N-cadherin exhibit a homogeneous distribution around the cell periphery. As tissue maturation progresses, these proteins start to concentrate at the ends of the cells, coinciding with the intercalated disks (Angst et al., 1997) (McCain et al., 2012). In the case of pluripotent stem cell-derived CMs (PSC-CM) cultured in 2D cultures, Cx43 and N-cadherin are circumferentially distributed, therefore confirming their immature phenotype (Zwi et al., 2009). Nevertheless, pluripotent stem cell-derived CMs cultured over prolonged periods of time showed increased levels of Cx43

transcripts, when compared to early stages of culture time, indicating some degree of maturation of cell-cell connections (Lundy et al., 2013).

In embryonic stages, CMs display a robust capacity to proliferate, however this capacity reduces overtime as the heart develops. Before entering in cell cycle arrest, CMs commonly display binucleation and, in some cases, extensive polyploidy (Laflamme and Murry, 2011). Polyploidy as seen in the mature CMs results from DNA replication without nuclear division or cytokinesis and, in human cells, ploidy can reach 8N in healthy hearts (Brodsky et al., 1992). Studies have reported that in developing CM, DNA synthesis occurs in two distinct phases: the early fetal phase, which relates to greater cell division, and a second phase, which results in binucleation (Clubb and Bishop, 1984, Li et al., 1996a). It is important to note that the degree of binucleation differs between species, as rodent, dog and pig CMs exhibit multinucleation in all stages of postnatal life, whereas in humans the majority of these cells are mononucleated (Olivetti et al., 1996).

1.5.2 - Contractile activity

Adult CMs do not display spontaneous beatings when cultured *in vitro*, confirming that, in the adult tissue, initiation of contraction is strictly dependent of pacemaker cell stimulation. In contrast, more immature CMs show spontaneous beatings, suggesting lower excitation potentials (Keung et al., 2014).

Sarcomeres are central in CM contraction, therefore the analysis of sarcomere genes and proteins provides a good strategy to evaluate the level of CM maturation. The most relevant sarcomeric proteins include cardiac troponin I (cTnI), cardiac troponin T (cTnT), α-cardiac actinin, α-myosin heavy chain (MHC) and β-MHC (Lundy et al., 2013, Yang et al., 2014b). It is important to note, that since immature CMs also express these proteins, the distinction between immature and mature state relies in shifts of expression levels. For example, in the developing heart, the slow skeletal-troponin I is the predominant form, whereas, as the organ grows, a shift occurs to the fast isoform cTnI. A similar situation is observed between the embryonic skeletal α-actin and the mature cardiac α-actin (McDonough and Glembotski, 1992, Tiburcy et al., 2011). In rodents, a shift occurs from the pre-natal slow isoform, β-MHC, to the post-natal fast isoform, α-MHC (Tiburcy et al., 2011). Contrasting, in humans, the predominant isoform at all stages of heart development is β-MHC, however, more α-MHC can be detected in fetal hearts than adult ones (Xu et al., 2009).

Ultrastructural analysis is a fundamental tool to assess the degree of sarcomeric organization, since transcript expression levels do not translate to active protein presence and their respective organization (Zimmermann et al., 2002). As the CM matures, sarcomeric length increases in order to generate greater contraction forces. Also, sarcomeric organization becomes more defined, reaching a characteristic striped appearance, as seen by electron microscopy. As an example, relaxed immature hPSC-CMs shown a sarcomere length of approximately 1.65 μm (Lundy et al., 2013), while an adult human CM has been reported to display a sarcomere with a length of about 2.2 μm (Bird et al., 2003).

Force of contraction is a parameter directly correlated to CM maturation. In tissue samples of human and rat myocardium it has been described peak twitch tensions of approximately 44 mN/mm^2 and 56 mN/mm^2, respectively (Hasenfuss et al., 1991). In contrast, hPSC-CMs in collagen constructs showed an average force of 0.08 mN/mm^2, which is nearly 500-fold less than what is detected in the adult tissue (Tulloch et al., 2011). Regarding rat samples, neonatal CMs on a collagen based construct displayed twitch forces between 0.4 to 0.8 mN, and resting tension forces of 0.1 to 0.3 mN (Zimmermann et al., 2002). These studies confirm that force generation of engineered human or rat myocardium is much lower than the respective adult cardiac muscle.

1.5.3 - Metabolism

Mitochondria from *ex vivo* samples of immature CMs display a network-like shape, which is distributed throughout the cytoplasm, occupying a small fraction of the total cell volume (Lopaschuk and Jaswal, 2010, Kolwicz et al., 2013, Gaspar et al., 2014). Ultrastructural analysis further revealed that the inner mitochondrial membrane does not have well-defined cristae (Figure 16) (Shepard et al., 1998). During tissue growth and maturation, mitochondria start to develop more cristae which are regularly distributed among the mitochondrial matrix. At the adult stage, the mitochondria occupies in average 30% of the CM cell volume, and is distributed in highly ordered crystal-like structures, tightly packed along myofibrils or beneath the sarcolemma (Piquereau et al., 2013).

As development proceeds, the structural changes are accompanied by an increasing mitochondrial oxidative capacity, which can be appreciated by a switch in the preferred metabolic substrate. At early developmental stages, nearly 80% of the energy demands are covered by glycolysis. During maturation, mitochondrial oxidative capacity

progressively increases to the point where the major source of energy results from fatty acid β-oxidation (~80%) (Lopaschuk and Jaswal, 2010).

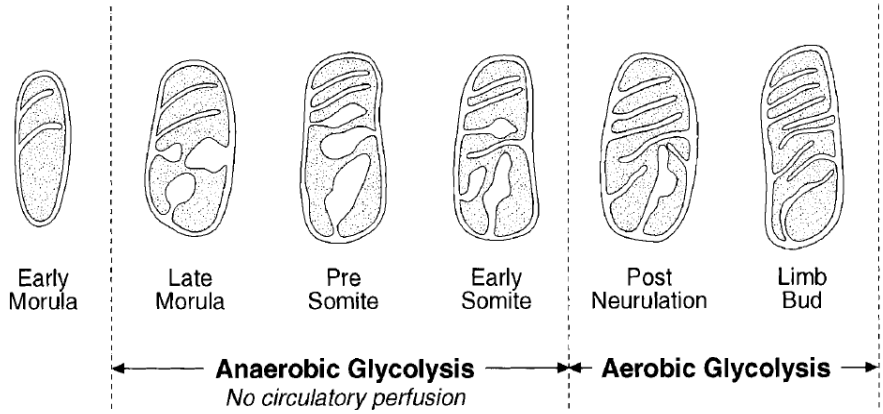

Figure 16 - Illustration displaying the proposed formation of mitochondrial cristae from blebbing of inner mitochondrial membrane during heart development. With maturation, the blebs collapse to form lamellated mature cristae. Adapted from Shepard, 1998.

1.5.4 - Ion channels and calcium handling properties

The electrochemical activity of CMs changes during cardiac development as a result of shifts in the expression of distinct ion channels. In general, early developmental stages exhibit lower expression levels of ion channels, as compared to more mature stages. To exemplify, in freshly isolated cells, transient outward current (I_{to}) density has been shown to double at day 15 as compared with day 5 rat neonatal CMs (Guo et al., 1996). In canines, the only K^+ channel expressed in young ventricles is I_{Kr}, whereas both I_{Kr} and I_{Ks} are present in adult canine myocardium (Obreztchikova et al., 2003). Also in immature CMs, the lower levels of sodium channel Nav1.5, results in slower upstroke velocities, while the reduced expression of LTCCs leads to a shorter or completely absent plateau phase (Sartiani et al., 2007). The low expression of ion channels, such as the I_{K1} channel, has been also suggested to interfere with the resting membrane potential. Lastly, the higher resting potentials detected in immature CMs (~-50 mV) contrast with their mature counterparts (~-90 mV) (Hansen et al., 2010, Nunes et al., 2013).

Calcium handling has a central role in CM contractility. It has been demonstrated that immature cells, such as hPSC-CMs, express critical Ca^{2+} handling proteins and exhibit Ca^{2+} transients. Nevertheless, it is not clear the extent of this expression and the exact mechanisms of functioning (Yang et al., 2014b). Studies have shown that PSC-CMs are relatively insensitive to drugs that interfere with SR Ca^{2+} release or reuptake (Dolnikov et al., 2006). In addition, key SR regulatory proteins such as calsequestrin or phospholambam have not been detected (Liu et al., 2002). Therefore,

the increase of Ca^{2+} transients in hPSC-CMs results from trans-cytoplasmatic entry via calcium channels and not from internal Ca^{2+} stores. Additionally, rodent models also showed underdeveloped SR Ca^{2+} stores at the same developmental stages (Liu et al., 2002, Escobar et al., 2004). Contrasting with these observations, other reports characterizing hPSC-CMs demonstrated that these possessed functional SR Ca^{2+} stores (Satin et al., 2008, Itzhaki et al., 2011), thus supporting the hypothesis that SR-dependent Ca^{2+} handling is an early event in the maturation process. These diverging conclusions concerning Ca^{2+} handling properties may result from CMs at different stages of maturation, obtained by different differentiation protocols.

1.5.5 - Pharmacological response

Cellular response to pharmacological agents is one of the most complete assessments that can be performed to an engineered tissue. This cellular response translates the degree of functionality of the pharmacological target. As an example, it has been demonstrated that the β-adrenergic agonist, isoproterenol, induces a dose-dependent increase of the frequency of spontaneous beating hESC-CMs (Pillekamp et al., 2012). Nevertheless, this increase in frequency was not accompanied by a significant change in the contraction force. Similarly, electrical stimulation at a constant rate (0.3–1.9 Hz) also did not reveal changes in actuation forces. Despite a clear chronotropic response after β-adrenergic stimulation, the lack of an inotropic response likely indicates immaturity of the sarcoplasmic reticulum. However, some studies have reported positive inotropic effects of epinephrine on hiPSC- and hESC-CMs (Yokoo et al., 2009, Liu et al., 2012a).

1.6 - Strategies for enhancing cardiac tissue function *in vitro*

To enhance CM activity and/or maturation several platforms have been suggested including: i) increasing culture time (Shinozawa et al., 2012, Kamakura et al., 2013, Lundy et al., 2013), ii) specific culture media composition (Tchao et al., 2014, Chattergoon et al., 2012), iii) optimizing oxygen and nutrient supply (Tandon et al., 2009), and iv) the use of particular scaffolds designs. This section will summarize the most important advances related to the use of scaffolds to enhance CM activity and/or maturation.

1.6.1 - Topography

Cells sense physical cues and adhere to the extracellular environment through processes mainly mediated by integrins. Cell phenotype and orientation can be modulated by the pattern and availability of integrin binding domains, and reorganization of the cytoskeleton tensional forces (Kim et al., 2013, Iskratsch et al., 2014, Stoppel et al., 2015b). Therefore, cells are extremely sensitive to topographical cues towards which they respond by changing their cytoskeleton, morphology, and ultimately their behaviour. The use of patterned substrates to align cells is a useful tool for *in vitro* engineering of cardiac tissues, since specific spatial orientation of cells has been shown to translate directly to improved functional properties. Alignment of cardiac cells not only affects electrical properties, including action potential duration and transient calcium direction (Bursac et al., 2002, Chung et al., 2007), but also impacts cell body morphology and nuclear elongation (Aubin et al., 2010, Kai et al., 2011). These parameters are known to associate with increased cellular differentiation and maturation.

CMs showed improved alignment and activity in micropatterned substrates (width between 5 and 80 μm). hESC-derived CMs seeded in Matrigel® and fibronectin coated glass slides with groove widths between 30 μm and 80 μm showed an increase in sarcomere alignment relative to the long axis of the pattern (Salick et al., 2014). In another report, stem cell-derived CMs cultured for two weeks on fibronectin-coated PDMS microgrooved substrates (10 μm apart, 10 μm wide, 4 μm deep), demonstrated improved cellular alignment and organized sarcomeres, with a decrease in the time to peak amplitude of their calcium transients (Rao et al., 2013). Moreover, CMs seeded in substrates with narrow grooves (up to 65 μm in width) showed higher CM elongation and faster propagation of action potential than control cells cultured on flat PS surfaces (Thomas et al., 2000). In a separate study, laminin lines varying from 5 to 50 μm in width, created by microcontact printing on non-adhesive polystyrene surfaces (McDevitt et al., 2003) showed elongated myocyte

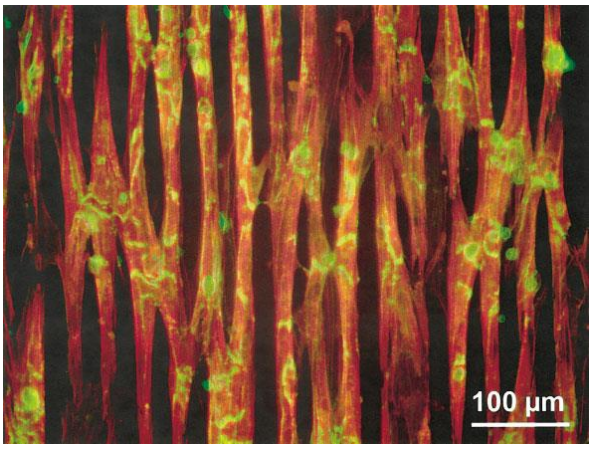

Figure 17 – **Immunostaining of patterned CMs seeded on spin-cast poly(urethane) films**. CM patterns (15x20 μm lanes) fixed at 4 days in culture, stained with an antibody to N-cadherin (green), and counterstained with phalloidin (actin filaments, red). Adapted from (McDevitt et al., 2003).

morphology, synchronous contraction and upregulation of Cx43 at cell–cell borders and intercalated disks (Figure 17). Similarly, CMs cultured in microabraded polyvinyl chloride cover slips with microgrooves ranging from 0.5 to 5 μm-wide and 0.2 to 2 μm-deep, and in micro-contacted printed lanes of fibronectin with 12 or 25 μm (Bursac et al., 2002) showed alignment of a rat cardiac cell layer, as well as increased longitudinal to transverse conduction velocity ratio, a measure of the anisotropy of the action potential.

CMs also showed improved alignment and activity in nanopatterned substrates (width between 150 and 800 nm). Rat CMs seeded on nanogrooved poly(ethylene glycol) substrates (substrates with width 150-800 nm, spacing of 50-800 nm, height of 200-500 nm) showed improved elongation and alignment, anisotropic contractions and action potential generation and Cx43 upregulation (Kim et al., 2010). Importantly, CMs demonstrated different sensitivities to the nanogroove dimensions: cells cultured on 800 nm-wide and 800 nm-spaced scaffolds showed larger size, highest Cx43 expression upregulation and the fastest longitudinal conduction velocity than other nanopatterned and flat PEG scaffolds.

Cardiac tissue constructs generated with electrospun PCL fibres, with diameters ranging from 100 nm to 5 μm, demonstrated excellent cell attachment and synchronized contractions (Shin et al., 2004). Due to the porosity of the scaffolds, these cardiac monolayers could be stacked up to 5 layers without core ischemia (Ishii et al., 2005). The lack of an anisotropic organization seen in these reports was later addressed by using post-processing of uniaxial stretch and rotary jet spinning. Neonatal cardiac rat cells cultured on aligned fibre scaffolds with an average diameter of 1 μm, demonstrated elongation and alignment along the orientation of the fibres (Zong et al., 2005, Orlova et al., 2011). Another report compared aligned and random electrospun poly(urethane) scaffolds with an average fibre diameter of 2.0 μm. Here, a more mature CM phenotype was seen on aligned electrospun scaffolds, while comparing to random electrospun scaffolds and tissue culture PS (Rockwood et al., 2008). Besides the organizational features, an additional advantage of aligned fibre scaffolds lays in their ability to mimic cardiac muscle differential stiffness. This results from the particular radial and circumferential directions present in fibre-based scaffolds (Courtney et al., 2006, Ott et al., 2008).

1.6.2 - Stiffness

Rigidity or stiffness is another property of the ECM that modulates mechanosensing. The degree of stiffness of a substrate has an impact in the establishment of focal adhesion points by the cell, therefore affecting cell cytoskeleton and cell spreading (Figure 18). This interaction between the cytoskeleton and integrins modulated by substrate rigidity has been shown to influence many cell phenotypes including morphology, polarity, migration, differentiation, and maturation (Engler et al., 2006, Murphy et al., 2012). Typically, CMs have been cultured in PS culture dishes that have a rigidity near 1 GPa, a much higher value when compared to the muscle tissue stiffness (Freedman et al., 2015). Hence, cell culture on conventional PS dishes is not the best platform to preserve/enhance CM activity.

Figure 18 – Comparative testing of cell response on substrates with different stiffness properties. Adapted from (Stoppel et al., 2015b).

Mechanical analysis of excised cardiac tissue demonstrates that tissue stiffness changes throughout the course of development (Jacot et al., 2010) and it has a strong impact in the development of contraction force (Berk et al., 2007, Freedman et al., 2015). Atomic force microscopy measurements of developing murine heart tissue showed that the tissue stiffens drastically after birth (embryonic ~12 kPa, neonatal ~32 kPa) (Jacot et al., 2010), which is in agreement with uniaxial tension measurements (embryonic ~10 kPa, neonatal/adult ~20 kPa) (Gershlak et al., 2013). Similarly, through micropipette aspiration method, the elastic modulus of healthy neonatal rat heart tissue was determined to be ~7 kPa and the healthy adult rat heart tissue to be ~30 kPa (Figure 19) (Bhana et al., 2010).

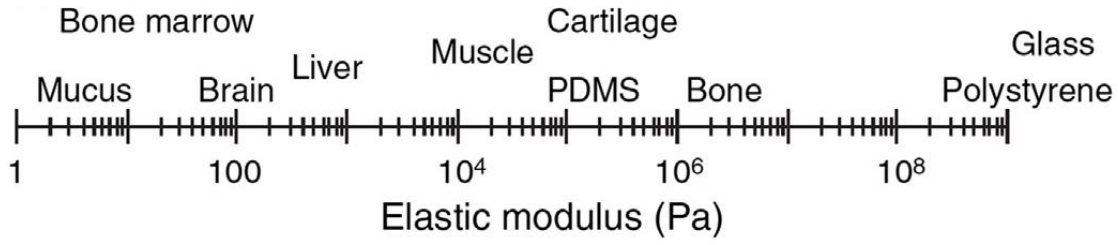

Figure 19 – Comparison of the stiffness on different tissues and materials, as measured by the elastic modulus. Adapted from Freedman et al, 2015.

To evaluate the role of substrate stiffness in CM phenotype, neonatal cardiac cells have been plated in poly(acrylamide) gels with different elastic modulus (1-144 kPa) and a collagen I coating (Jacot et al., 2010, Bhana et al., 2010). In gels with low elastic modulus, cells had reduced cell density, excitation threshold, force of contraction, and CM elongation, but increased cTnI staining. In gels with high elastic moduli, CMs exhibited unaligned striations with long, large stress fibres, combined with reduced cTnI staining, increased CF density, and poor electrical excitability. Gels with an elastic modulus similar to embryonic tissue displayed defined and aligned striations and the greatest action potential. Overall, these results confirm that collagen-coated substrates that are stiffer than healthy cardiac tissue (~50 kPa) prevents the physiological maturation of isolated CMs *in vitro*. Conversely, softer substrates that mimic the mechanical environment of heart tissue at earlier stages in development can enhance some aspects of CM maturation.

Another study as reported the culture of chick embryonic heart cells on substrates with an elastic modulus that increased slowly over time, thus mimicking the stiffening of heart tissue during development (Young and Engler, 2011). The substrates were composed of HA hydrogels crosslinked with PEG diacrylate, being the stiffness controlled by changing the crosslinker's molecular weight. CMs plated on the hydrogels coated with collagen I showed increased maturation as measured by a greater sarcomere length and increased expression of cTnT, as compared to cells cultured on a static substrate modulus. This report demonstrated that time and duration of the mechanical stimulation have impact on CTC function, a direct correlation to the native tissue, since time dependent physical changes are observed during development (Ivashchenko et al., 2013, Veerman et al., 2015).

1.6.3 - Mechanical stimulation

External forces, such as cyclic tension/stretch and contraction/compression forces, constantly modulate the activity of cardiac cells. These forces result from the particular rhythmic contraction and the pressure associated with the filling of the heat. In the last years, mechanical stimulation has been investigated to enhance CM activity and maturation. Strategies for mechanically altering cells include i) passive material stiffness (Figure 18), ii) step-wise stretching (Figure 20A), and iii) dynamic stretching (Figure 20B). Step-wise or static stretch is characterized by either an increase in the percentage of stretch over time or an initial stretch after plating that is maintained over

the time of culture. On the other hand, dynamic stretch aims to mimic the cyclic filling of the ventricles with blood during diastole.

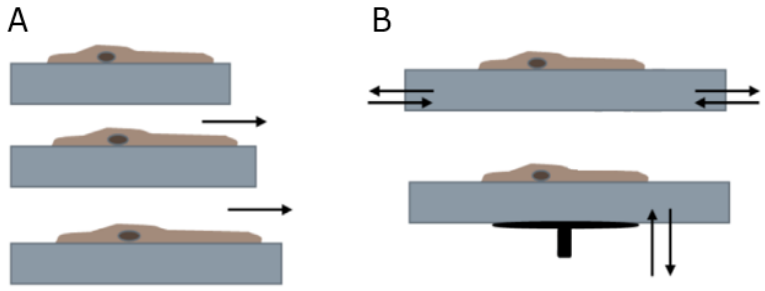

Figure 20 – **Strategies of mechanical actuation over cultured cells. A)** Sequentional analysis on incremental strech displacements; **B)** Aplication of cyclic mechanical stimuli with or without diferential directions of actuation. Adapted from (Stoppel et al., 2015b).

To determine the role of stretch and integrin binding in CM maturation, isolated neonatal CMs were cultured on collagen and laminin coated elastic wells and subjected to a step-wise increase in strain (25%) over four days (Vandenburgh et al., 1996). With stretch, CMs demonstrated improved alignment, higher total MHC content, an increase in the number of binucleated CMs, and greater cell area, when compared to the non-stretched controls. The increase in binucleation and longitudinal area is indicative of physiological hypertrophic growth, while the increase in alignment and both α- and β-MHC isoform content suggests improved maturation. Though, it is known that CMs elongate and MHC isoform expression shifts during development and maturation (Nadal-Ginard and Mahdavi, 1989, Boheler et al., 1991), the definition of mature CM requires the presence of additional markers. Further studies have shown that mechanical stretch is a key component for maintaining proper excitation-contraction coupling *in vitro*. CMs cultured with step-wise stretch displayed differences in microfibrillar architecture and turnover (Simpson et al., 1996), the activity of stretch activated ion channels (Sigurdson et al., 1992), the organization of focal adhesions (Sharp et al., 1997), and overall gene expression (van Wamel et al., 2000).

Compared to stepwise stretch, dynamic stretch offers a closer reproduction of the natural mechanical forces occurring in the heart. Several reports have shown that dynamic stretch affects intracellular organization, intra- and extracellular tension, focal adhesion formation, gene and protein expression (Komuro et al., 1996, Fink et al., 2000, Malhotra et al., 2010, Dhein et al., 2014). Commercially available systems allow mechanical stimulation of cells plated on top of elastic substrates. The Flexcell systems (Flexcell International, Inc.) have been used in several cardiac tissue related studies, especially those that evaluate the combined role of stretch and small molecules or growth factors delivery on CM phenotype (Salameh et al., 2010a, Leychenko et al.,

2011). Mechanical stimulation has also been performed in cells encapsulated in 3D scaffolds. Neonatal rat CMs encapsulated in a Matrigel matrix, forming a tubular engineered tissue constructs or ring-shaped constructs were mechanically stimulated resulting in improved contraction force and well-organized sarcomeres (Zimmermann et al., 2000, Zimmermann et al., 2002).

1.6.4 - Electric stimulation and conductivity

Several studies have reported positive functional and phenotypic changes induced by external electrical stimulation of CMs. Intracellular changes include: i) shifts in gene expression profile (McDonough and Glembotski, 1992, Xia et al., 1998, Passier et al., 2000, Chan et al., 2013), ii) formation of extensive and organized myofibrils (McDonough and Glembotski, 1992), iii) increased levels of structural proteins, such as MHC, MLC, Cx43, and cTnI (Radisic et al., 2004a, Chan et al., 2013, Baumgartner et al., 2015), and iv) contributions to cell mitochondria proliferation (Xia et al., 1998). At the morphological level it has been reported enlargement of CM cell body (McDonough and Glembotski, 1992), enhanced intercellular coupling, better ultrastructural organization and alignment (Radisic et al., 2004a, Tandon et al., 2009). In terms of cellular function, studies show stable synchronous contractions alongside with greater contraction forces, increases in the maximum pacing frequency and appropriate physiological response to drugs (Berger et al., 1994, Radisic et al., 2004a). In overall, these results provide evidence that electrical cues have a significant role in cell phenotype modulation *in vitro*, particularly in hypertrophy related mechanisms (Xia et al., 2000, Passier et al., 2000).

The electrical functions of the muscle tissues are subjected to the physical cues present in them, in fact, these well-organized cues favour the effective conduction of the electrochemical signal that causes the unidirectional contraction of cardiac muscle. To study the combinatorial effect of topographic cues and electrical stimulation, microgrooved surfaces were simultaneously used with electrical field stimulation, in parallel and perpendicular to the groove directions (Au et al., 2007). After seven days of culture and stimulation, neonatal CMs showed contraction, alignment along the microgrooves and Cx43 localization near cell-cell junctions, as opposed to the punctate expression in unstimulated neonatal CMs. Additionally, when the orientation of the microtopography was perpendicular to the electric field, neonatal rat CMs aligned accordingly to the topographical cues rather than the electrical field direction.

Conversely, in the condition where electrical stimulation was parallel to the microgrooves, cells showed increased elongation, alignment, and increased electrical functionality.

The electrical stimulation of CMs has been also tested in 3D environments. hESC- and hiPSC-derived CMs encapsulated in a collagen gel have been electrically stimulated by a wire in the middle of the matrix (Nunes et al., 2013). In the electrically stimulated conditions, cells displayed better ultrastructural organization, denoted by higher myofibril organization, shown by α-actinin and cTnT staining and imaging of intercellular junctional complexes. Action potential related processes were also characterized demonstrating increased conduction velocity and maximum capture rate, decreased excitation threshold, and improved Ca^{2+} handling properties (as shown by response to the chronotropic agent epinephrine). Taken together, these observations suggest that engineering strategies that combine multiple aspects of the cardiac microenvironment lead to better CM function.

Several conductive polymers have also been explored in cardiac tissue engineering. Poly(aniline), a conductive polymer, has been blended with other polymers, such as PCL (Jun et al., 2009) and gelatin (Li et al., 2005), to form a mesh of nanofibers (60 to 800 nm of diameter). Gelatin/poly(aniline) blends supported attachment, migration, and proliferation of H9C2 rat cardiac myoblasts. Gold nanowires/nanoparticles have been also used in scaffolds to make them electrically conductive. Gold nanoparticles were embedded in an elastic blend of hydroxyethyl methacrylate (HEMA) and thiol-HEMA (You et al., 2011), while gold nanowires have been dispersed in alginate scaffolds (Dvir et al., 2011). In both studies the composite scaffolds maintained the neonatal rat CM population for 8 days. These cells showed upregulation of Cx43 in the absence of exogenous electrical stimulation. Additionally, higher amounts of Cx43 and α-sarcomeric actinin were also detected, alongside scaffold wide calcium transients that were not detected in the absence of the nanowires.

Carbon nanotubes is another class of materials tested to enhance electrical conductivity in scaffolds. Carbon nanotubes have been included in methacrylated gelatin hydrogels (CNT-GeIMA) (Shin et al., 2013) and chitosan scaffolds (CNT-chitosan) (Martins et al., 2014). On CNT-GeIMA hydrogels, CNTs provided electric conductivity to collagen nanofibres resulting in increased cell adhesion and maturation, demonstrated by the higher levels of α-actinin and cTnI. Though the increase in Cx43 expression was

moderate, cross-striation of α-actin and partial cell alignment denoted stimulation of cell-cell electrical coupling. Additionally, when exposed to an inhibitor of cell-cell coupling (heptanol) and a cardiotoxic drug (doxorubicin), the CNT-GeIMA hydrogels showed to have a protective effect. CNT-chitosan scaffolds supported cardiac cells for 14 days and enhanced some cardiogenic parameters without external electrical stimulation, e.g. higher metabolic activity, and upregulation of Troponin C Type 1 and Cx43.

1.6.5 - Combinatorial strategies

1.6.5.1 - Mechanical-based systems

Studies have demonstrated that 3D constructs promote alignment of plated cells, improves CM gene and protein expression, as well as tissue function (Black et al., 2009, Stoppel et al., 2015a). These results were further improved with the addition of more features such as mechanical stimulation. In fact, several designs of bioreactor systems allow to cyclically stretch 3D engineered cardiac tissues (Birla et al., 2007, Kluge et al., 2011). One of the first bioreactor designs to show functional improvement of cardiac tissues used freshly isolated neonatal rat and chick cells encapsulated within Matrigel® supplemented collagen I gels (Fink et al., 2000). CTCs formed from either neonatal rat or chick CMs were uniaxial stretched in collagen gels and after 4 days they exhibited improved CM organization, denoted by the increased cell size and myofilament length (40% increase in sarcomeric α-actin). Also, improved mitochondrial density was followed by an upregulated metabolic activity.

In another study, neonatal rat CMs were included in a similar matrix forming tubular engineered tissue constructs (Zimmermann et al., 2000). Results showed a positive correlation of Matrigel® concentration and CTC function, suggesting that complex 3D matrix impacts CM maturation. In addition to demonstrating an increase in contraction force overtime, these neonatal rat CTCs exhibited a positive force-length and negative force-frequency relationship. Subsequent improvements to this design came in the form of ring-shaped constructs. The resulting constructs displayed highly organized sarcomeres, as well as increased adherence and gap junctions, after 7 days of culture with continuous mechanical stimulation (10% strain, 2 Hz) (Zimmermann et al., 2002).

Passive tension was tested in the gels suspended between two parallel PDMS posts (Legant et al., 2009, Galie et al., 2015). The deflection of the posts allowed for the determination of force exerted by the cells in the hydrogels as the system contracted and the collagen gel compacted. Later, stiffness modulation was added to the system by replacing the soft PDMS pillars with stiffer rods, thus recreating *in vitro* the pathological increase of cardiac afterload (Hirt et al., 2012).

1.6.5.2 - Perfusion-based biorectors

Bioreactors have been designed to provide both media perfusion, to improve nutrient and small molecule delivery, and electrical stimulation. A first example includes an aligned scaffold system of poly(glycerol sebacate) coated with laminin used for plating neonatal rat CMs. The resulting CTC showed increased contraction amplitudes and cTnT expression when cultured with both perfusion and electrical stimulation (3 V/cm, 3 Hz), when compared to either parameters alone or in static culture (Maidhof et al., 2012). These results suggest that the improvements seen were not just due to the addition of improved oxygen and nutrient supply afforded by perfusion of the construct.

An improvement to the previous design included electrical stimulation and perfusion of wire-based constructs that mimic the cardiac bundle found in native tissue (Nunes et al., 2013, Xiao et al., 2014). The perfusion system allowed for the delivery of different small molecules and relative automatization of the system demonstrated its applicability as a drug-testing platform. Electrical stimulation (1 ms duration, 1.2 Hz, 3.5-4 V/cm) increased the Cx43 positive area over cTnT positive area in images taken after 4 days of stimulated culture compared to non-stimulated controls. Furthermore, results demonstrate that the orientation of CM alignment and the direction of electrical field stimulation affects functional outputs such as excitation threshold (Xiao et al., 2014).

1.6.5.3 - Electro-mechanical platforms

Innovative designs have been developed for bioreactor systems that combine electrical stimulation and mechanical stretch with 3D scaffolds (Wang et al., 2013, Lu et al., 2013, Morgan and Black, 2014, Miklas et al., 2014). The main goal is to appropriately time tissue contraction with mechanical stimulation thus mimicking ventricular filling. In all reported designs, electrical stimulation is applied through field

stimulation of the entire construct and mechanical stimulation is controlled by physically stretching the construct.

One reported design includes individual bioreactor units (Morgan and Black, 2014) where electrical stimulation was applied by two carbon rods added to the media surrounding the construct. The underlying principle was to provide physiologically relevant timing of combined electrical and mechanical stimulation. Neonatal CMs cultured in fibrin hydrogels were electrically stimulated 0.49s after the start of the mechanical stimulation, thus mimicking the timing of isovolumetric contractions. Results showed superior SERCA2a and Akt1 expression when compared to static culture and the individual application of each stimuli. The fine control over the coordination of signals in the milieu offers the possibility of applying electrical and mechanical stimulation in non-physiological regimes, thus allowing the modelling of pathological contexts.

A larger scale bioarector design has also been proposed. This system contains eight microtissues and two stimulating electrodes, so that each electrode pair stimulates four constructs at one time, providing greater high-throughput compared to previous designs (Miklas et al., 2014). Static stress is applied to the CTCs by using a pneumatically driven stretch device. A pair of PDMS posts inside each microwell chamber allows for the calculation and verification of the stretch applied to each tissue. The CMs cultured under a static 5% strain and an electrical stimulation of 3–4 V/cm with a frequency 1.1 Hz electrical demonstrated enhanced sarcomere alignment (cTnT) and expression of gap junction proteins (Cx43) after 3 days compared to either mechanical or electrical stimulation alone.

1.7 - *In vitro* cardiac tissue modelling

1.7.1 - The importance of cardiotoxicity testing

Nearly 40% of new drug candidates that are able to reach the last phases of clinical trials fail to enter the market due to ineffectiveness and/or unforeseen toxicities (Kola and Landis, 2004). The total investment to bring a drug from pre-clinical trials to the market costs around €1.5 thousand million, a process that can take 10 to 15 years.

Additionally, many drugs are later withdrawn from the market due to side effects and toxicity. As an example, from 2000 to 2007 several drugs, including cisapride, rofecoxib and tegaserod, were all withdrawn from the United States market following unforeseen clinical cardiotoxic and/or arrhythmogenic toxicities (Mordwinkin et al., 2013).

Cardiotoxicity is the leading cause of regulatory delay in approval and market withdrawal of newly developed drugs (Kola and Landis, 2004, Kannankeril and Roden, 2007). Members of several non-cardiovascular drug classes, including the anthracyclines, non-steroid anti-inflammatory drugs, and certain antipsychotics, have been labelled with cardiovascular-related black-box warnings (Mordwinkin et al., 2013) (Table 3). This has led the regulatory authorities to extend requirements on cardiotoxicity testing, thus making nonclinical cardiotoxicity assessment during pre-clinical studies an important part of the regulatory procedure. Currently, specific guidelines set by the International Conference on Harmonization of Technical Requirements for Registration of Pharmaceuticals for Human Use (ICH) and the European Medicines Agency describe the requirements for electrophysiology testing *in vitro* and *in vivo*. In particular, these tests should contribute to revealing disrupted organ functions, which are not readily detected by standard toxicological testing.

Trade name (generic name)	Indication(s)	Black box warning and associated cardiotoxicity
Anthracyclines including Adriamycin (doxorubicin), Cerubidine (daunorubicin), and Ellence (epirubicin)	Anticancer	Black box warning (cardiotoxicity)
Avandia (rosiglitazone)	Type 2 diabetes	Black box warning (congestive heart failure and myocardial infarction)
Betapace (sotalol)	Antiarrhythmic	Black box warning (proarrhythmic effects)
Clozaril (clozapine)	Antipsychotic	Black box warning (myocarditis)
Cordarone, Pacerone (amiodarone)	Antiarrhythmic	Black box warning (proarrhythmic effects)
Herceptin (trastuzumab)	Breast cancer	Black box warning (cardiomyopathy)
Inapsine (droperidol)	Antiemetic and antipsychotic	Black box warning (QT prolongation and TdP)
Mellaril (thioridazine)	Antipsychotic	Black box warning (QT prolongation and TdP)
Novantrone (mitoxantrone)	Anticancer and multiple sclerosis	Black box warning (cardiotoxicity)
NSAIDs including Anaprox (naproxen), Cataflam (diclofenac), Celebrex (celecoxib), Orudis (ketoprofen), and Motrin (ibuprofen)	Pain and inflammation	Black box warnings (increased cardiovascular risk)
Sporanox (itraconazole)	Antifungal	Black box warning (congestive heart failure)
Tambocor (flecainide)	Antiarrhythmic	Black box warning (ventricular arrhythmias)
Tasigna (nilotinib)	Leukemia	Black box warning (QT prolongation and TdP)
Tikosyn (dofetilide)	Antiarrhythmic	Black box warning (proarrhythmic effects)
Tyrosine kinase inhibitors including Gleevec (imatinib) and Sprycel (dasatinib)	Anticancer	No black box warnings (reports of cardiotoxicity)

Table 3 – Aproved drugs with cardiovascular-related black box warnings. Adapted from Mordwinkin et al 2013.

The interference of drugs in ventricular repolarization has been a topic of increasing interest by regulation agencies and research groups. The concerted activity of several cardiac ion channels is important in ventricular repolarization and alterations may increase the risk of ventricular tachycardia arrhythmia. Essentially, the main mechanism to be evaluated is the compound's capability to inhibit the cardiac human Ether-à-go-go channel (hERG) channel, which consequently results in the prolongation of the QT interval in repolarization events on CMs.

1.7.2 - Engineered cardiac tissue models versus cell models

Cardiotoxicity assays have been performed typically in rodent-based cell models, cultured in 2D substrates. These tissue monolayers have provided a relatively simple tool for drug screening and toxicology assessment, however, they are limited in CM maturation and functionality (Liau et al., 2012, Radisic and Christman, 2013, Hirt et al., 2014b). Nowadays, more advanced strategies are being explored based in engineered cardiac tissues. These CTCs aim to reproduce with more accuracy the *in vivo* heart tissue and thus the biological information obtained in drug screenings will be more reliable.

Rat and human CTCs have been used to assess the cardiotoxicity of pro-arrhythmic drugs (Hansen et al., 2010, Schaaf et al., 2011). Rat CTCs were insensitive to specific blockers of rapid delayed rectifier potassium current, a gene related to the hERG channel. In contrast, human CTCs were highly sensitive to hERG blockers (Hirt et al., 2014b). These results demonstrate that rat cell-based models are not suitable for detecting hERG-dependent proarrhythmic effects, nevertheless, they are a good test system to detect hERG-independent effects, which seem to be more prevalent.

Human iPSC-derived CMs have provided several relevant advantages over animal models for cardiotoxicity, nevertheless, they still exhibit limitations. Firstly, using flat culture systems may not reflect the human disease phenotype, as they lack relevant epigenetic and environmental factors that influence cellular function. Secondly, disease models using solely pure populations of CMs cannot exhibit disease phenotypes at the tissue level, such as decreased conduction velocity, fibrosis, myocyte disarray, and tissue-level electromechanical coupling. Lastly, several reports confirm that pluripotent stem cell-derived CMs are at an embryonic/fetal developmental stage, evident by their distinct gene expression profiles, when comparing with adult cells (Burridge et al., 2012).

1.7.3 - Functional read-outs

The use of engineered cardiac tissues for drug screening and toxicology assessment should be compatible with automatization and miniaturization in order to allow high content readouts. An assay for evaluating CM function should include bioanalytical sensors which are compatible with the target cells. Considering that adequate cell material is available, these sensor devices should be merged and configured with electrical, optical or other analytical transducers for sufficiently accurate recording of key physiological or biochemical alterations occurring in the cells.

Micro- electrode arrays (MEA) have been used successfully for high-throughput drug screening analyses. These arrays include metal electrodes integrated in cell culture plates that can register the electrical field potentials of spontaneously beating or electrically stimulated clusters of CM layers plated directly on the plate dishes (Caspi et al., 2009, Braam et al., 2010). hESC-CM have been cultured up to 2 weeks on MEA dishes, meanwhile allowing on-line monitoring of some electrophysiological processes. When a desirable phenotype is reached, cumulative dose–response experiment with increasing concentrations of a pharmacologically relevant drug can be performed. Increase of the throughput capacity can be achieved by transferring the assay from multi-electrode single-well approach into a multi-well layout with a limited number of electrodes per well. Automation can be increased by using a compatible liquid handling robot. In addition, the integration of a data acquisition and analysis software may assist the user to obtain report sheets with dose–response curves and analysis of the pro-arrhythmic potential of the target drug.

Several compounds, including lidocain, quinidine, amiloride and nifedipine, have been tested using MEA (Mandenius et al., 2011). hESC-CM have been plated on MEAs and the effect of the compounds evaluated in terms of cardiac field potential, beating frequency and amplitude of depolarization. Some results were not clear and the data obtained could not be correlated with results from studies with primary CMs and clinical data. This was likely due to the heterogeneity of CM phenotype or to technical issues such as limited drug diffusion into the cell layers which may compromise the interpretation of the results. For this reason, several other criteria other than the ones referred should be assessed to properly validate the inclusion of the hESC- CM in a screening system.

Cellular respiration rate is an indicator of cellular metabolic activity and may be used as a simple readout for the effect of drugs on cardiac cells. The use of cost-effective techniques that allow detection of molecular oxygen by luminescence has provided opportunities for a wide range of applications in biological, biomedical, pharmaceutical and biotechnological fields (Papkovsky, 2004, Papkovsky et al., 2006). Commercially available platforms such as Oxoplates® (96- well) and OxoDishes® (24 well), are based in luminescence measurements and offer rapid screening of oxygen uptake rates (Deshpande et al., 2004, Beckers et al., 2010). While using a reading system that can be placed in an ordinary cell culture incubator, cellular respiration of hESC- CM clusters can be measured. Incubation with the drugs doxorubicin and quinidine allowed the calculation of representative EC50 values in real-time (Mandenius et al., 2011). Additionally, since this method is non-invasive, the supernatants and cells can be further used/processed with other methods.

Metabolic rates are affected by intracellular processes and modulated by environmental factors and toxic effects. Metabolome analysis can involve extracellular and/or intracellular metabolite and the most frequent methods of analysis includes nuclear magnetic resonance (NMR) and chromatographic techniques combined with mass spectrometry. Metabolome analysis together with metabolic network models also provide the basis for intracellular and exchange cellular fluxes (Niklas et al., 2010). Extracellular analysis can be applied for cells as well as for isolated whole organs (Vo and Palsson, 2006). Detailed analysis of metabolic fluxes is possible using ^{13}C labelled substrates, e.g. glucose or amino acids (Wittmann and Heinzle, 1999, Wiechert and de Graaf, 1997). For example, cells from a mouse CM cell line, HL-1, were exposed to subtoxic doses of verapamil and flux analysis revealed a drastic reduction in glycolysis but insignificant changes in other metabolic activities. These techniques can also be applied at smaller scales and for high- throughput analysis, as has been shown, for example, with yeast (Velagapudi et al., 2007).

Quantification of CM secretion factors has also been used for high-throughput drug screening analyses. hESC-CMs exposed to a cardiotoxic insult released detectable levels of two clinically relevant cardiac biomarkers, cTnT and fatty acid binding protein 3 (Andersson et al., 2010). These proteins have been monitored by surface plasmon resonance in a high-throughput approach. Quantification of cardiac cell number by fluorescence methods can also be used for high-throughput screening. Real-time

measurements and high- throughput screening can be easily done through automated fluorescence readers while using standard cultivation microplates. As an example, HL-1 cells have been used in a multiwell microplate (Fritzsche et al., 2009). The autofluorescence signal of these cells presumably correlates to the protein content, which in the present of toxic substances decreases due to inhibition of cell growth or cell death.

Chapter 2

Materials and Methods

2.1 - Preparation of MNF and MNF+PIEZO scaffolds

MNFs were prepared by the combined use of a sacrificial layer and spin coating (Ricotti et al., 2010, Taccola et al., 2011). Initially, a solution of PVA (1% w/v, in water; 1 ml; Mw = 25.000, 88% hydrolysed; Polysciences, Inc) was added to the surface of a silicon wafer (400 μm thick, 2 × 2.5 cm; Primewafers) and spin-coated (Spincoat G3P-8, Pi-Kem) at 4000 rpm for 20 s. Then a suspension of superparamagnetic magnetite/maghemite nanoparticles (10 mg/mL; EMG1300; diameter of 10 nm; FerroTec Co., USA) suspended in a PCL solution (20 mg/mL in chloroform; Mw=80000, Aldrich) was added to the wafer and spin-coated according to the previous spinning parameters. For MNF experimental group, the polymer-coated wafer was immersed in water, the PVA sacrificial layer was dissolved, releasing a freely suspended insoluble nanofilm. For MNF+PIEZO experimental group, the polymer-coated silicon wafers were fixed to a home-made rotating collector for the deposition of aligned fibres (rotator motor: Heidolph RZR2020; rotative collector was made as an aluminium circular frame with the following measurements: 100 mm of diameter, 18 mm of thickness). The fibres were generated from a solution of poly(vinylidene fluoride–trifluoroethylene) (70:30 w; Solvay) dissolved in methylethylketone (Labor Spirit) acording to a methodology described elsewhere (Weber et al., 2010b). The parameters used were: voltage (10-12 kV), polymer solution concentration (20%) (w/v), tip to collector distance 12 cm, injection rate 2 mL/h, relative humidity 40-50% at room temperature and collector's rotation speed 2000 rpm. The selected collection time was 4 minutes.

2.2 - Scaffold characterization

2.2.1 - AFM analyses

Imaging was performed with a Veeco Innova Scanning Probe Microscope (Veeco Instruments Inc., Santa Barbara, CA) in dry state, operating in tapping mode, with oxide-sharpened silicon probes (RTESPA-CP, Veeco Instruments Inc.) at a resonant frequency of ~300 kHz. The sample was scanned across the edge of the scratch over a 50 μm × 50 μm area, recording 128 × 128 samples. The resulting scan data were elaborated using the Gwyddion SPM analysis tool (http://gwyddion.net). Scan data were leveled with the facet level tool to remove sample tilt, and then the film thickness was evaluated as the difference between the average heights of a region of interest (ROI) selected on the nanofilm surface and the average height of the ROI on the silicon wafer.

2.2.2 - Mechanical tests

Mechanical properties were evaluated by measuring their strain in response to an applied unidirectional stress. An INSTRON 4464 Mechanical Testing System was used, equipped with a ±10 N load cell. Traction tests were performed on ten samples for each sample typology. The nanofilms were detached from the substrate, by immersing them in water, then gently fished up and allocated between two aluminium clamps. All specimens were pulled at a constant speed of 5mm/min, until reaching sample failure. Data were recorded at a frequency of 100 Hz. The stress was calculated as the ratio between the load and the cross-section area of a tensile specimen, while the strain was calculated as the ratio between its extension and its initial length. The Young's modulus for each tested sample was extracted from its stress/strain curve, according to a standard procedure (Callister, 2003).

2.2.3 - SEM analysis

A Phenom Pro tabletop SEM was used for analyses. At least 3 image sets were taken per each sample. Fibre diameter was determined by using ImageJ's measuring tool set on SEM images of the tested conditions. Regarding the evaluation of fibre anisotropy, each picture taken to the tested conditions were processed by following the analysis protocol described by Boudaoud, A. *et al* (Boudaoud et al., 2014b). Briefly, quantification of the orientation and anisotropy of fibrillar structures in raw images is done using the image analysis software ImageJ, where computation on the basis of the gradient of pixel intensity level is performed over a region of interest in the image.

2.2.4 - Impedance measurements and scaffold deformation

Scaffold impedance spectra were analysed by using an impedentiometer (Agilent) in the 40 Hz – 20 kHz frequency range. Charge generation capacity of the piezoelectric fibres was determined by using custom designed flexible gold electrodes coupled to a mix signal oscilloscope (InfiiVision, Agilent Technologies). Deformation of the PIEZO fibre layers was achieved by using two Delrin cylinders featured by two different diameters, thus obtaining two pre-defined deformation curvatures for the tested substrate (curvature I – 84 mm cylinder diameter, curvature II – 105 mm cylinder diameter). A flexible polyethylene thin-film was used as non-piezoelectric control condition.

2.2.5 - Piezoresponse force microscopy (PFM) measurements

PFM measurements were performed using a Ntegra Prima scanning probe microscope (NT-MDT, Russia). All measurements were done using conductive TiN coated cantilevers NT-MDT FMG01/TiN (resonance frequency of the used cantilevers was 70 - 75 kHz). Topography mapping was done in a tapping mode. PFM was performed in the contact mode by placing a tip at a certain points without scanning. Driving AC voltage with 150 kHz frequency and in the range 1÷10 V (amplitude) was applied to the tip under ambient conditions. Pt coated Si was inserted between the film and the substrate and served as a grounded bottom electrode

2.3 - Coating of the scaffolds for cell culture

The scaffolds were coated with poly(dopamine) and then with a gelatin solution (1%, w/v). The poly(dopamine) coatings were prepared as described by Haeshin Lee *et al* (Lee et al., 2009). Briefly, scaffolds were immersed in a dopamine solution (2 mg of dopamine/HCl per mL of 10 mM Tris buffer pH 8.5) typically overnight and rinsed with water for further use. The scaffolds were afterwards mounted in a Cellcrown (Scaffdex Oy, Finland) before cell seeding. Next, the structures were sterilized while immersed in a disinfection solution of 1000U/ml Penicillin-Streptomycin (Life Technologies) and 10 µg/ml amphotericin B (Fluka) for 24 hours. Afterwards, the nanofilms mounted in Cell Crowns were exposed to UV light for 30 minutes and stored at 4°C. Prior to cell culture, the antibiotics/amphotericin solution was removed and the supports were coated with a 1% gelatin in solution for 12 hours.

2.4 - Isolation and culture of rat fetal CMs

Fetal CMs were obtained from Wistar rat fetus (17-18 days of gestation) sacrificed according to European Union directives. After sacrifice the hearts were removed, the atria were excised and the ventricles were placed in Hank's Balanced Salt Solution (HBSS, pH 7.4, Ca^{2+} and Mg^{2+} free, Sigma). Next the ventricles were placed in a new Petri dish (30-40 per plate) containing a trypsin-EDTA solution (0.1%, w/v, Gibco) and maintained at 4ºC overnight for digestion. After 18 h, the partially digested tissues were brought to 30-37ºC and type II Collagenase (75 U/mL, Worthington Biochemical Corporation, USA) was added for 30-45 minutes. The digested tissue was mechanically dissociated and filtered through a cell strainer (40 µm, nylon; Falcon), the cell suspension was then purified by plating the cells in a 1% (w/v) gelatin-coated plate for

3 hours. The non-adherent cells were then counted and platted at a density of 450000 cells per scaffold (effective area of the scaffold is 0.8 cm^2) in Dulbecco's modified Eagle's medium (DMEM) supplemented with 10% (v/v) fetal bovine serum (FBS), 100 IU mL^{-1} penicillin and 100 µg mL^{-1} streptomycin. The average cell yield was of 130×10^4 per heart.

2.5 - Cardiac beating analysis

Videos of the samples were recorded (Camstudio) using a light microscope at a magnification of 20×. The videos had an average of 300×300 pixels of area. One recording was performed per replicate for each experiment. These recording focused on a hot spot, i.e., an area where synchronous beating was clearly visible. The number of beatings was obtained by manually counting each beat during the time span of the videos. It is important to note that since the resolution of the recorded videos was low it was not possible to use automatic imaging processing methods.

2.6 - Finite element model simulations of the contracting scaffold

FEM simulations were carried out by using the Matlab®R2013a (MathWorks) and Abaqus 6.13 (Dassault Sys-temes) software environments. Matlab was used to design the system in a parametric way and to manage data, while Abaqus was used to perform FEM simulations.

Simulation conditions for the layer used in the model were retrieved from experimental data of MNF+PIEZO scaffolds, i.e. thickness of 4.5µm and an elastic modulus of 5 MPa. Cell related conditions contained experimental data extracted from fluorescence image analysis, which provided the total value of 306 cells per area of layer, and defined the cell dimensions and distribution configurations. After creating the substrate in the Abaqus environment (1.4 x 1.4 x 0.0045 mm^3), by using the Python language, experimental data (stress-strain curves) of the MNF+PIEZO scaffold were imported by exploiting the Hyperplastic module supported by the program. In the Abaqus Step module, an explicit dynamic behaviour was defined. Appropriate fixed constraints were applied to the four membrane edges, thus resembling the real situation (Chapter 3, Fig. 1A). A quad element-based mesh was implemented with 10 µm as characteristic dimension. Cells were modelled with 40 x 40 μm^2 squares, spaced of 40 µm each other and anisotropically oriented along one preferential direction (data

extracted from fluorescence images). Cell contraction force and orientation angle were extracted from literature data, which indicate a stress of 4 mN/mm^2 for primary cardiomyocytes and an angle of ~ 20° between focal adhesion average axis and the substrate plane. Von Mises stresses and overall displacement values were recorded for each simulation.

2.7 - Immunocytochemistry analysis

At specific time points, cells were fixed in 4% (v/v) paraformaldehyde for 10 min and permeabialized with 0.1% (v/v) Triton or with methanol for 10 min when it was recommend by the antibody supplier. Following the blocking step with 1% (w/v) BSA for 30 min the cells were incubated with the primary antibody for 1 h at room temperature. The primary antibodies used were: anti-vimentin (rabbit, Abcam), anti-α-actinin (mouse, Sigma), anti-connexin 43 (rabbit, Sigma), anti-Troponin I (goat, Santa Cruz) anti-calsequestrin 2 (goat, Santa Cruz), anti-dihydropyridine receptor alpha-1 (mouse, Thermo Scientific), hERG (rabbit, Santa Cruz). After extensive washes with PBS cells were incubated with the secondary antibody for 30 min at room temperature and counterstained with DAPI.

Cellular alignment was quantified on confocal microscopy images taken on samples (63x) labelled for alpha-actinin (mouse, Sigma; CM population), vimentin (rabbit, Abcam; CF population) and DAPI (cell nucleus). Each image was processed by following the analysis protocol described by Boudaoud, A. *et al* (Boudaoud et al., 2014b). Briefly, quantification of the orientation and anisotropy of fibrillar structures in raw images was done using the image analysis software ImageJ, where computation on the basis of the gradient of pixel intensity level is performed over a region of interest in the image.

Cellular morphology of cells cultured in MNF+PIEZO was performed after the harvest of the cells using a type II collagenase and trypsin-EDTA solution for at 5 to 7 minutes. Cells were then plated at low density (~50.000 cells) in cover glasses coated with gelatin for 6 hours and next fixed as described previously.

Fluorescence intensity analysis was performed while using ImageJ image analysis tool set. Briefly, a region of interest (ROI) was selected by using a drawing/selection tool. Next, measuring settings “Area”, “Integrated density” and “Mean grey value” were selected at the “Analyse - Set measurements" menu. Measurements were done for the

ROI and for the respective background levels (3 measurements per image). Afterwards, the measured values were used to calculate the corrected total cell fluorescence (CTCF) as follows:

$$CTCF = Integrated\ Density - (Area\ of\ ROI\ X\ Mean\ Fluorescence\ of\ background)$$

2.8 - Western blot analysis

Cell protein extracts were diluted in SDS sample buffer (2.5% SDS, 0.0625 M Tris-HCl, 10% glycerol, 5% 2-mercaptoethanol, 0.05% bromophenol blue, pH 6.8) and boiled for 5 min at 95ºC. Proteins (30 µg) were separated by SDS/PAGE [10% (v/v)] and transferred onto PVDF membranes by electroblotting. The membranes were blocked with 5% skim milk in Tris-buffered Saline-Tween (TBS-T, 20 mM Tris-HCl, 150 mM NaCl, 0.1% Tween 20) and then probed with an antibody for connexin 43 (produced in rabbit, Sigma), for troponin I (produced in goat, Santa Cruz) or for alpha actinin (produced in mouse, Sigma). After extensive washings with TBS-T, the blots were incubated with an alkaline phosphatase-conjugated secondary antibody (GE Healthcare, Buckinghamshire, UK). Immunoreactive complexes were detected by chemifluorescence using the ECF reagent (GE Healthcare). Fluorescence was detected with a Molecular Imager FX scanner (Biorad). To ensure an equal protein loading, antibody for CsQ2 (Santa Cruz) was used as internal control. The intensity of the bands was analysed using the TotalLab TL120 software (Nonlinear Dynamics).

2.9 - Viability tests

For the assessment of cellular growth and viability two different methods were performed: MTT assay (thiazolyl blue tetrazolium bromide, Sigma) and PrestoBlue (Invitrogen). Briefly, for the MTT assay the cells were incubated with medium (DMEM, Biochrom) supplemented with MTT (5mg/ml) for 1 h. Then, cells were washed with PBS and DMSO was added for 20 min so that the MTT salts could be solubilized. After a centrifugation step the absorbance of the supernatant was read at 540 nm and 620 nm. For the PrestoBlue, cells were incubated for 2h.30m with a 10% solution of the reagent and medium. The resulting supernatant was diluted (1:1) with medium and fluorescence readings were made at excitation 535 nm and emission 615 nm.

2.10 - FACS analysis

Cardiac cells after isolation (see protocol above; 1.25-2.5 × 10^5 cells per condition) were fixed in 4% (v/v) paraformaldehyde (Electron Microscopy Sciences) solution for 15 min and then washed two times with PBS. Cells were then permeabilized with saponin (0.5%, Sigma) and labelled with antibodies against cardiac fibroblasts (anti-vimentin, rabbit, Abcam), CMs (anti-α-actinin, mouse, Sigma) or endothelial cells (anti-CD31, mouse, ThermoFisher Scientific). After a washing step, cells were characterized by a FACS Calibur (BD) and the data analyzed by Cell Quest software. Twenty thousand events were collected in each run.

2.11 - In vivo testing

The acute animal model was performed in Wistar rats (16 weeks) assigned to 2 groups: DOXO and Vehicle. One group received a single dose of DOXO, 20 mg/kg by intraperitoneal injection, while the other group received the equivalent volume of the vehicle solution (in this case 0.9% NaCl) by intraperitoneal injection. Both treatments were carried out for 24 h before sacrifice. The sub-chronic animal model was performed also in Wistar rats (8 weeks old) assigned to 2 groups: DOXO and Vehicle. In this case, animals were injected subcutaneously weekly in the scruff or flank with 2 mg/Kg DOXO or with equivalent volume of vehicle solution (0.9% NaCl), during 7 weeks. At the end, animals were allowed to rest for 2 weeks before being sacrificed. Animals were euthanized by cervical dislocation followed by decapitation, confirming death of the animal. Extraction of the heart with the aortic stump from the thorax was quickly performed, and heart was washed in a cold (4ºC) Tyrode´s buffer in order to temporarily stop its beating and preserve it from ischemic injury prior to perfusion.

2.12 - NMR spectra acquisition/analysis

Cells were cultured in Dulbecco's Modified Eagle's Medium (D5030, Sigma) supplemented with 1.0 g/L [1,6-^{13}C2]glucose (Cambridge isotopes), 0.584 g/L L-glutamine (Life Technologies), 3.7 g/L sodium bicarbonate (Sigma) and 10% FBS (Alfagene). ^{1}H-NMR spectra were acquired in a 600 MHz Varian VNMRX spectrometer using a 3 mm broadband NMR probe. Each NMR spectrum consisted of 32k points covering a sweep width of 7.2 kHz. An interpulse delay of 10 s and a 45° radiofrequency reading pulse were used to ensure full relaxation of all nuclei in the sample. A total of 16 scans were averaged to ensure adequate signal to noise for quantitative purposes.

Before Fourier transformation each free induction decay (FID) was multiplied by a 0.2 Hz Lorentzian apodization function. NMR spectra deconvolution was achieved by NUTSproTM NMR software using the line-fitting subroutine which allows deconvolution of individual lines. Each NMR sample consisted of 20 μL culture media plus 200 μL of a 2.5 mM sodium fumarate (internal standard) phosphate buffered D2O (99.9%) solution.

2.13 - Live cell Ca^{2+} analysis

For the assessment of intracellular Ca^{2+} transients Rhod-3 Calcium Imaging Kit (Life Technologies) was used in cells at 6 days of culture on the tested conditions. First, the assessment media was removed from the cells and these were washed twice in HBSS. Then, cells were incubated in the dark at room temperature for 30–60 minutes with the loading buffer. Afterwards, the cells were washed and DMEM media without phenol red (Thermo Scientific HyClone) supplemented with 10% FBS, was used for the live recording. Analysis of the fluorescence intensity was performed for each frame of the resulting live recording. Fluorescence intensity analysis was performed with the ImageJ image analysis tool described previously (see Immunocytochemistry analysis). Results are shown by fluorescence intensity as a function of time. The raw data was normalized towards the background signal and adjusted by using the "Fluorescence Recovery After Photobleaching" ImageJ's plugin. Briefly, the FRAP profiler plugin analyses the intensity of a bleached ROI over time and normalize it against the intensity of the whole cell. After that it will find the minimum intensity in the bleached ROI and fit the recovery with this point in mind.

2.14 - Total RNA extraction and quantitative real-time RT-PCR (qRT-PCR)

For the *in vitro* conditions, total RNA was extracted with TRIzol Reagent (Invitrogen) and immediately stored at -80ºC. In the case of the *in vivo* rat samples extraction of the RNA samples from the collected heart tissue was performed with an RNA extraction kit (Qiagen). RNA was quantified in a NanoDrop ND-1000 Spectrophotometer (NanoDrop Technologies, Inc., USA) by spectrophotometry at 260 nm. The cDNA was reverse transcribed from 1 μg of total RNA, using TaqMan Reverse Transcription Reagents kit (Invitrogen) according to the manufacturer's instructions. The cDNA obtained was stored at -20ºC until further analysis by real time PCR using the fluorescent dye SYBR Green and the 7500 Fast Real Time PCR System (Applied Byosystems). Specific sets of primers were designed by SIGMA (see table below).

Quantification of target genes was performed relative to the reference CsQ2 or TBP (TATA box binding protein). Genes relative expression= $2^{[-(Ct_{sample}-Ct_{reference})]}$. The mean minimal cycle threshold values (Ct) were calculated from quadruplicate reactions.

Gene	Sequence
Myl7_Rat_S	GGCAACATCGACTACAAG
Myl7_AS	ACAGAGTTTATTGAGGTGAC
Myh7_S	GCAGAAAGAGATTATCACATTT
Myh7_AS	GAACGCATAATCGTAGGG
Acta1_S	CAAGCGAGGTATCCTGAC
Acta1_AS	ATCTTCTCCATGTCGTCC
Myl2_S	CCAGATCCAGGAGTTCAA
Myl2_AS	CCTTAGGTCATTCTTGTCAAT
Myh6_S	CTACCAGATCCTGTCCAA
Myh6_Rat_AS	TGAGAGACGAAGGCATAG
Actc1_S	AGCCCTCTTTCATTGGTA
Actc1_AS	TACAGGTCTTTGCGGATA
Cacna1s_S	AAAAAGACCCTTATTGCTTCC
Cacna1s_AS	TTTCTGACTTTTGGTCATGG
Cacna1c_S	TTAAAAGTGATTGCCTACGG
Cacna1c_AS	CACTAAAAAGCCCTACAACC
Cacna1d_S	CTCAGATATAGTAGCTGAAGAGG
Cacna1d_AS	GTCAAAATTAGTGATGCCTCC
Cacna1f_S	CTCTACCCAAGTTAAGAGAAAC
Cacna1f_AS	TGAGTACTTCCTTCTTCTGG
Scn1a_S	TCTTTACCAACTGACATTGC
Scn1a_AS	TTTATCAGGTAGAATGAGCCC
Scn3a_S	ATTTTAACTCCGCTAAACCC
Scn3a_AS	CTACATTCTTTGTCCAGTCG
Scn5a_S	ATCTACACCTTTGAGTCTCTG
Scn5a_AS	TGACCGATATAGTTTTCAGGG
Scn7a_S	CCCAAGAAGATGGAAATGATG
Scn7a_AS	TATAACCTTCTGGACACAGG
Kcnq1_S	CATCAGCTATCAGGGGTATC
Kcnq1_AS	AAAGTAGGAGGAGAAGATGAG
Kcnh2_S	CATAGCACCCAAGATAAAAGAG
Kcnh2_AS	GCAGCTTATATTCAGGAAGC

S – Sense a.k.a. Forward; AS - Anti-sense a.k.a Reverse

2.15 - Statistical analysis

An unpaired *t* test or one-way ANOVA analysis of variance with Bonferroni post test was performed for statistical tests using GraphPad Prism. Results were considered significant when $P < 0.05$.

Chapter 3

Results

3.1 - Flexible nanofilms coated with aligned piezoelectric microfibres preserve the long-term contractility of cardiomyocytes

3.1.1 - Introduction

Several scaffolds that mimic the architecture and biophysics of the myocardial extracellular matrix (ECM) have been proposed for the generation of engineered cardiac tissue (Eschenhagen and Zimmermann, 2005, Hirt et al., 2014b, Vunjak-Novakovic et al., 2010). Most of the cardiac tissue engineering approaches have used preformed scaffolds such as the one based on poly(glycerol sebacate) (Engelmayr et al., 2008) and hydrogels such as alginate (Nunes et al., 2013), fibrin (Radisic and Christman, 2013), fibronectin (Gerecht-Nir et al., 2006), tropoelastin (Annabi et al., 2013) and collagen (Naito et al., 2006). Carbon nanotubes (Shin et al., 2013) and gold nanowires (Dvir et al., 2011) have been embedded in scaffolds to improve electrical signal propagation between cells and thus enhancing cellular excitability and proper cellular organization. On the other hand, approaches that shape the surface of the scaffolds to replicate the aligned organization of the heart have been proved useful in improving cell-cell interaction and tissue cohesion (Motlagh et al., 2003, Shah et al., 2010, Shin et al., 2004).

Cardiotoxicity assessment is of paramount importance in the development of new drugs. Cardiac toxicity has been implicated in nearly 28% of drug withdrawals over the last 30 years (Gwathmey et al., 2009). Although the use of cardiomyocytes (CMs) in a culture dish or microfluidic systems (Mathur et al., 2015) have been reported, the use of engineered cardiac tissue for high-throughput drug screening/toxicology assessment remains largely unexplored. A miniaturized and automated method based on engineered heart tissue has already been reported (Hansen et al., 2010). Unfortunately, more than 20% of the cardiac cells died over a period of 3 days and the variability in the force and frequency between cardiac constructs was relatively high. The development of tissue engineered cardiac tissue for drug screening requires the development of scaffolds that can be easily produced and miniaturized, flexible, and preserve the long-term contractility of CMs, ideally in the absence of electrical stimulation.

Here we propose a scaffold that reproduces aspects of cardiac ECM that preserves the contractility of rat fetal CMs for at least 12 days. The scaffold is formed by a nanofilm composed of poly(caprolactone) (named MNF from now on) and piezoelectric microfibres (PIEZO) composed of poly(vinylidene fluoride–trifluoroethylene) (PVDF-TrFE) that have been deposited on top of the nanofilm (MNF+PIEZO). When a mechanical force is applied to a piezoelectric material, a change in the polarization density occurs due to the shifting or rotation of the constitutive dipole crystals, resulting in the generation of a transient electric charge. Therefore, PIEZO fibres may act as Purkinje cells, which in the native tissue are responsible for initiating and synchronizing cardiac beatings (Baruscotti et al., 2010). We hypothesized that i) a MNF will create a flexible support for cell contraction and ii) the aligned PIEZO fibres deposited on top of the MNF will create conditions for cell alignment and electrical stimulation of the seeded cells.

3.1.2 - Preparation and characterization of MNF+PIEZO scaffolds

To prepare the MNFs, poly(caprolactone) (PCL) dissolved in chloroform was deposited on silicon wafers coated with a sacrificial layer of poly(vinyl alcohol) (PVA) and finally spin-coated (Figure 1A). Superparamagnetic nanoparticles (SPIONs) were added to the PCL solution before the spin coating, to facilitate MNF manipulation by an external magnet. We employed PCL to generate the nanofilms due to its elasticity as well as its long history in biomedical applications.

For the preparation of nanofilms we have screened concentrations of PCL to yield a stable ultrathin polymeric film with low elastic modulus (Figure 2). After this screening process, we prepared a nanofilm with 2 $\times$ 2.5 cm, a thickness of 400 nm as measured by scanning electron microscopy (SEM), an average surface roughness (Ra) of 0.09 ± 0.03 μm as measured by atomic force microscopy (AFM) and an elastic modulus of 0.06 $\pm$ 0.04 MPa as evaluated by traction test (Figure 1D.1).

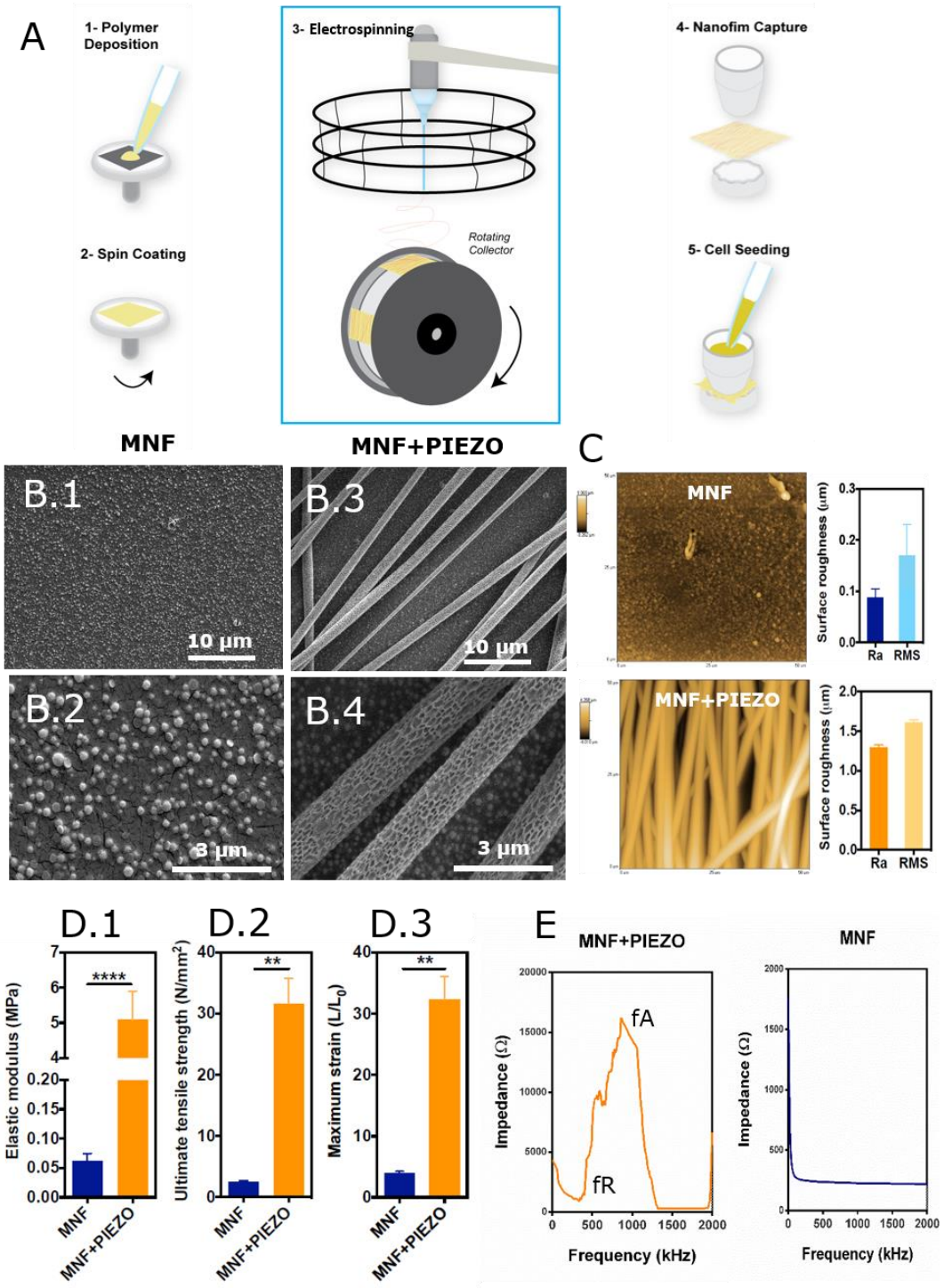

Figure 1 - **Preparation and characterization of MNF and MNF+PIEZO scaffolds**. **A)** Scheme showing the methodology used for the preparation of MNF and MNF+PIEZO. Initially, a sacrificial layer of PVA was deposited in a silicon wafer and spin-coated. This was followed by the spin-coating of a solution of PCL, deposition of PIEZO fibres by electrospinning, mounting the scaffold in a cell crown system and culture the cells on top of it. **B)** SEM images of the surface of MNF (B.1 and B.2) and MNF+PIEZO (B.3 and B.4). **C)** AFM images of MNF and MNF+PIEZO (tapping mode; height imaging). Scan areas of 50×50 μm^2 were used. **D)** Mechanical properties of MNF and MNF+PIEZO scaffolds obtained by stress-strain measurements, including elastic modulus (D.1), maximum strain (D.2) and ultimate tensile strength (D.3). The nanofilms were immersed in water to remove them from the silicon substrate and allow their fixation into the mechanical testing system. Results are Mean±SEM, n=10. **E)** Impedance spectra of MNF and MNF+PIEZO scaffolds. The MNF+PIEZO spectrum has two characteristic frequencies (resonance frequency, fR and anti-resonance frequency, fA), typical of piezoelectric materials. The MNF spectrum has no measurable impedance signal in the frequencies tested.

The resulting free-standing nanofilm is brownish (due to the presence of SPIONs), very flexible and can be manipulated with tweezers or a magnet (Figure 2A).

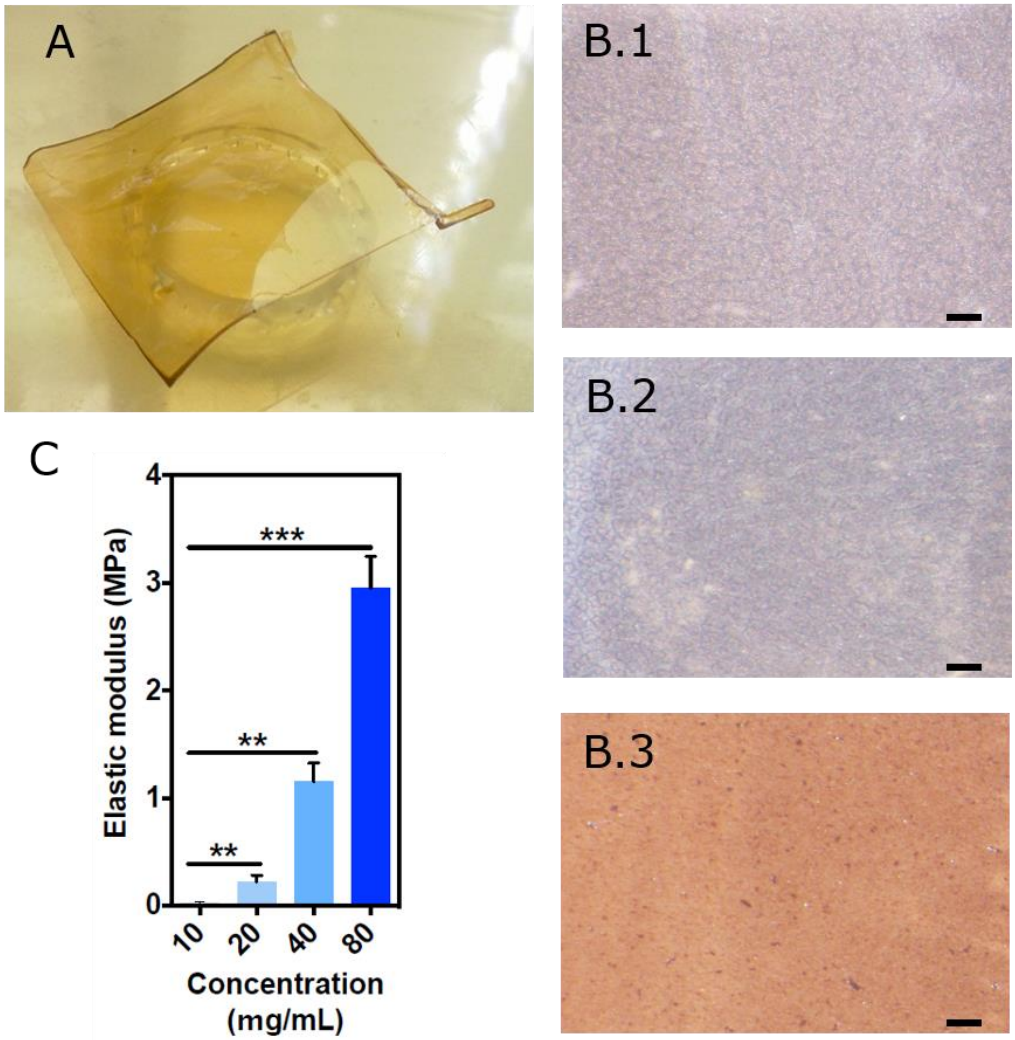

Figure 2 - **Morphology and mechanical properties of the nanofilms. A)** Nanofilm removed from the silicon wafer and immersed in water. **B)** Morphology of the nanofilms prepared with different concentrations of PCL (B.1: 20 mg/mL; B.2: 40 mg/mL; B.3: 80 mg/mL) as evaluated by light microscopy. Bar corresponds to 500 µm. **C)** Mechanical properties of nanofilms prepared with different concentrations of PCL. Results are Average ± SEM, n=3-5. * Denotes statistical significance: *P<0.05, **P<0.01, ***P<0.001, ****P<0.0001.

To prepare PIEZO fibres, a solution of PVDF-TrFE (20%, w/v) was electrospun. This copolymer was chosen because it has spontaneous dipolar orientation after a electrospinning step (Mandal et al., 2011a) and good biocompatibility properties (Fine et al., 1991, Weber et al., 2010a). The electrospinning production conditions were optimized to generate fibres with relative low diameter and high anisotropy after deposition in a PCL nanofilm substrate (Figure 3).

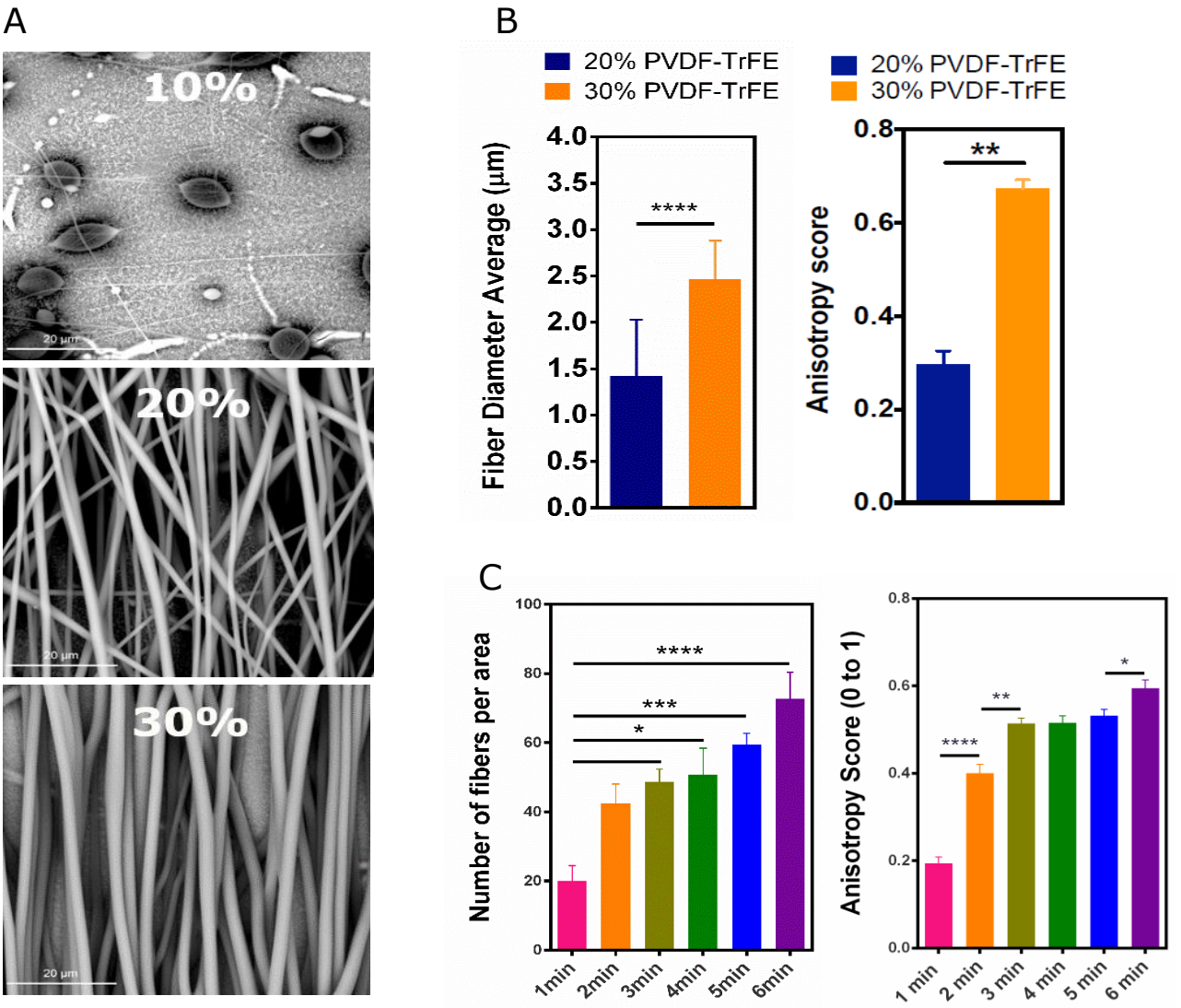

Figure 3 – **Morphology, diameter and anisotropy of the PIEZO fibres. A)** SEM images of the PIEZO fibres deposited on top of the PCL nanofilm. Concentrations of P(VDF-TrFE) (%, w/v) are indicated on top of the images. Bar corresponds to 20 µm. **B)** Diameter (n>950 fibres) and anisotropy (n=4) of fibres prepared from a solution of 20 and 30 % (w/v) of PVDF-TrFE. Results are Average ± SEM. Anisotropy of 1 indicates perfectly ordered arrays. **C)** Number of fibres per area and anisotropy score of the fibres as a function of deposition time on top of the nanofilm. Results are Average ± SEM, n=4. In B and C, * denotes statistical significance: *P<0,05, **P<0,01, ***P<0,001, ****P<0,0001.

In the tested conditions (Figure 1B, 1C and Figure 3), porous fibres with an average diameter of 1.24 ± 0.13 µm (average ± SEM, n=3) were obtained. These fibres have piezoelectric properties as determined by piezoresponse force microscopy (PFM), a local probe-based technique for non-destructive high-resolution piezoelectric domain imaging and manipulation (Kholkin et al., 2010). Following the topography acquisition in tapping mode, the AFM was switched to the PFM in which the conducting tip was scanned in contact mode while an *ac* voltage (V_{ac}) is applied between the tip and Au electrode (Figures 4A.1 and 4A.2). Over different points of the fibres, the surface

amplitude of the piezoresponse varied between 3.5 ($d_{33(min)}$) and 11.1 pm/V ($d_{33(max)}$) (Figure 4A.3).

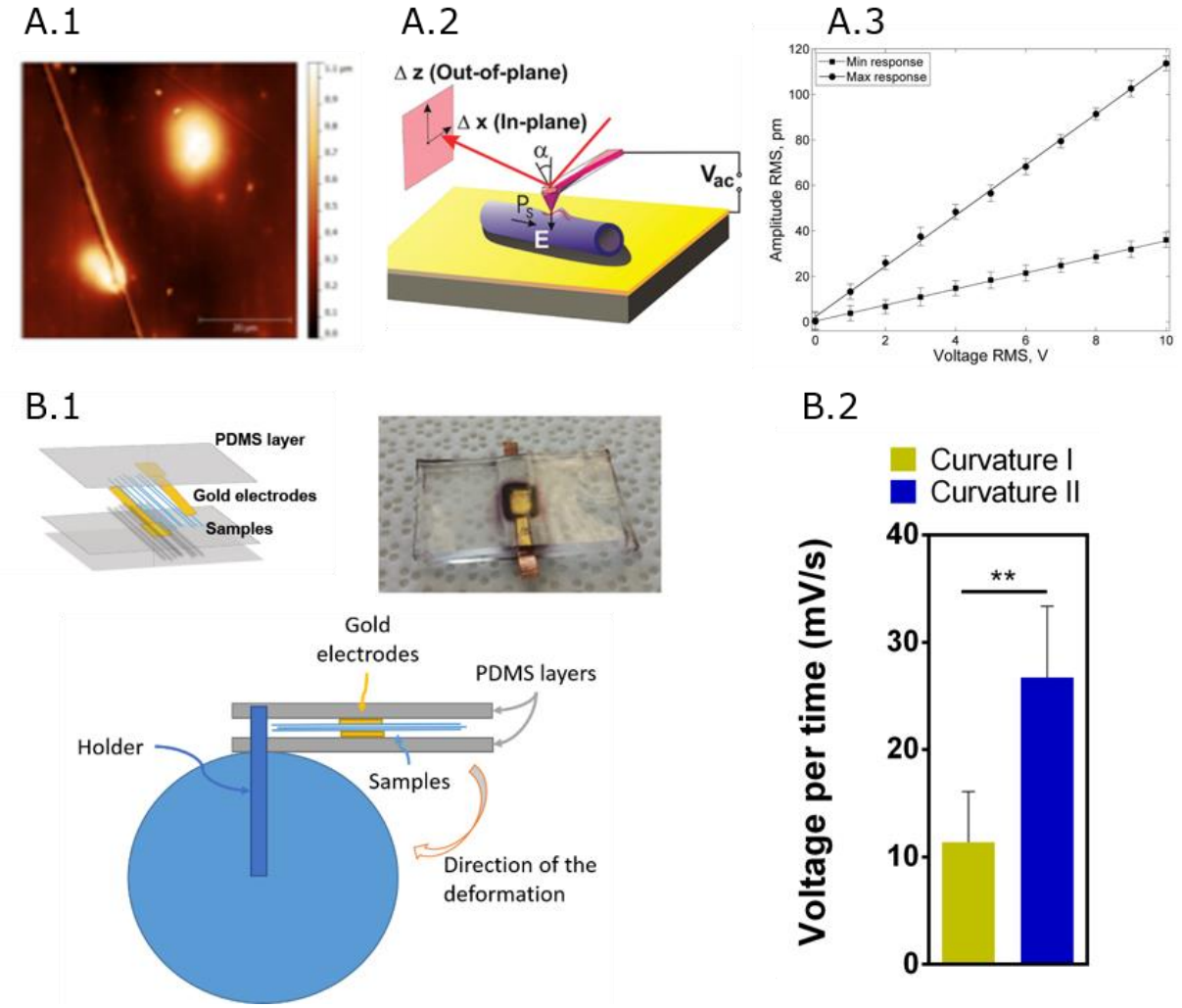

Figure 4 - Piezoelectric properties of PIEZO fibres and MNF + PIEZO scaffolds. A) Assessment of piezoelectric properties of PIEZO fibres by PMF. **A.1)** AFM images of the PIEZO fibre. **A.2)** Procedure for the determination of piezoelectric properties. **A.3)** Amplitude of displacement as a function of *ac* voltage applied to the samples. The determined piezoelectric charge constant, d, refers to the induced strain in direction 3 per unit electric field applied in direction 3 (d_{33}). Results are Average ± SEM, n=5. **B.1)** Methodology for the assessment of the piezoelectric properties in the MNF + PIEZO scaffolds. **B.2)** Assessment of the direct piezoelectric effect by subjecting samples of the PVDF-TrFE fibre mesh to mechanical deformation in two different curvature values (curvature I refers to the substrate deformed over the external surface of a Delrin cylinder showing a diameter of 84 mm; curvature II refers to the substrate deformed over the external surface of a Delrin cylinder showing a diameter of 105 mm), while registering the amount of voltage generated over time (values normalized towards control; Mean= 0,00263 mV/s). Results are Average ± SEM, n=10. * denotes statistical significance: **P<0.01.

MNF + PIEZO scaffold showed an average surface roughness (Ra) of 1.30 ± 0.06 µm, as measured by AFM (Figure 1C), and an elastic modulus of 5.08 ± 0.82 MPa (average ± SEM, n=3), as measured by indentation analyses (Figure 1D.1), showing that the presence of the PIEZO fibres led to mechanically stronger constructs than MNF

alone. Impedance measurements were also performed to evaluate both the piezoelectric and conductive properties of the constructs. The results demonstrate that the MNF scaffold has stable impedance values for all frequencies, while MNF+PIEZO scaffold shows a spectrum with two peaks, a resonance (f_R) and an anti-resonance frequency (f_A) (Figure 1E), typical of piezoelectric materials (Yasuda et al., 2006, Shin et al., 2013). To further evaluate the capacity of charge generation by the piezoelectric fibres, mechanical deformation tests were performed (Figure 4B). Readings were accomplished by using a custom designed flexible gold electrode coupled to a mix signal oscilloscope. Deformation of the PIEZO fibre layers was done with two different pre-defined deformation curvatures (curvature I – 84 mm, curvature II – 105 mm) and a flexible polyethylene thin-film was used in the non-piezoelectric control condition (Figure 4B.2). We registered a nearly 2-fold increase (from 11.4 mV/s to 26.7 mV/s) of the charge generated with the increase of the deformation curvature.

3.1.3 - MNF+PIEZO scaffolds enhance cellular stratification and cell alignment

To evaluate the *in vitro* biocompatibility of the scaffold, primary prenatal rat heart cells (59.5 ± 2.9 %, CM; 32.1 ± 2.4 % cardiac fibroblasts (CF) and 5.1 ± 4.7 % endothelial cells; Figure 5) were seeded on top of the scaffolds and cultured for 12 days. We selected 12 days for our analyses to allow the organization of the cells in the constructs while being primed by the ECM for a maturation process. The time is also a good compromise to allow the use of the engineered cardiac tissue for drug screening by the pharmaceutical industry. Cell viability and proliferation was assessed at day 1 after seeding (T1) and at day 12 (T12) by a MTT viability assay (Figure 6A). Cells cultured on polystyrene (PS) and cells cultured on MNF without PIEZO fibres were used as controls. Results at T1 show that the scaffolds (MNF and MNF+PIEZO) are cell adhesive and allow cell population growth and proliferation from day 1 (T1) to 12 (T12).

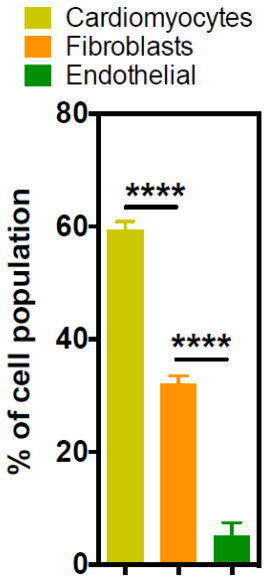

Figure 5 - Characterization of cardiac cell population. Rat fetal cardiac cells after isolation were characterised by Fluorescence-activated cell sorting (FACS). Cells were fixed with a 4% paraformaldehyde solution and then permeabialized with saponin. Afterwards each population was marked with different fluorescence marker targeting a specific subpopulation of the cardiac tissue: anti-vimentin for CF, anti-α-actinin for CM and anti-CD31 for endothelial cells. Results are Average ± SEM, n=4. * Denotes statistical significance: ****P<0.0001.

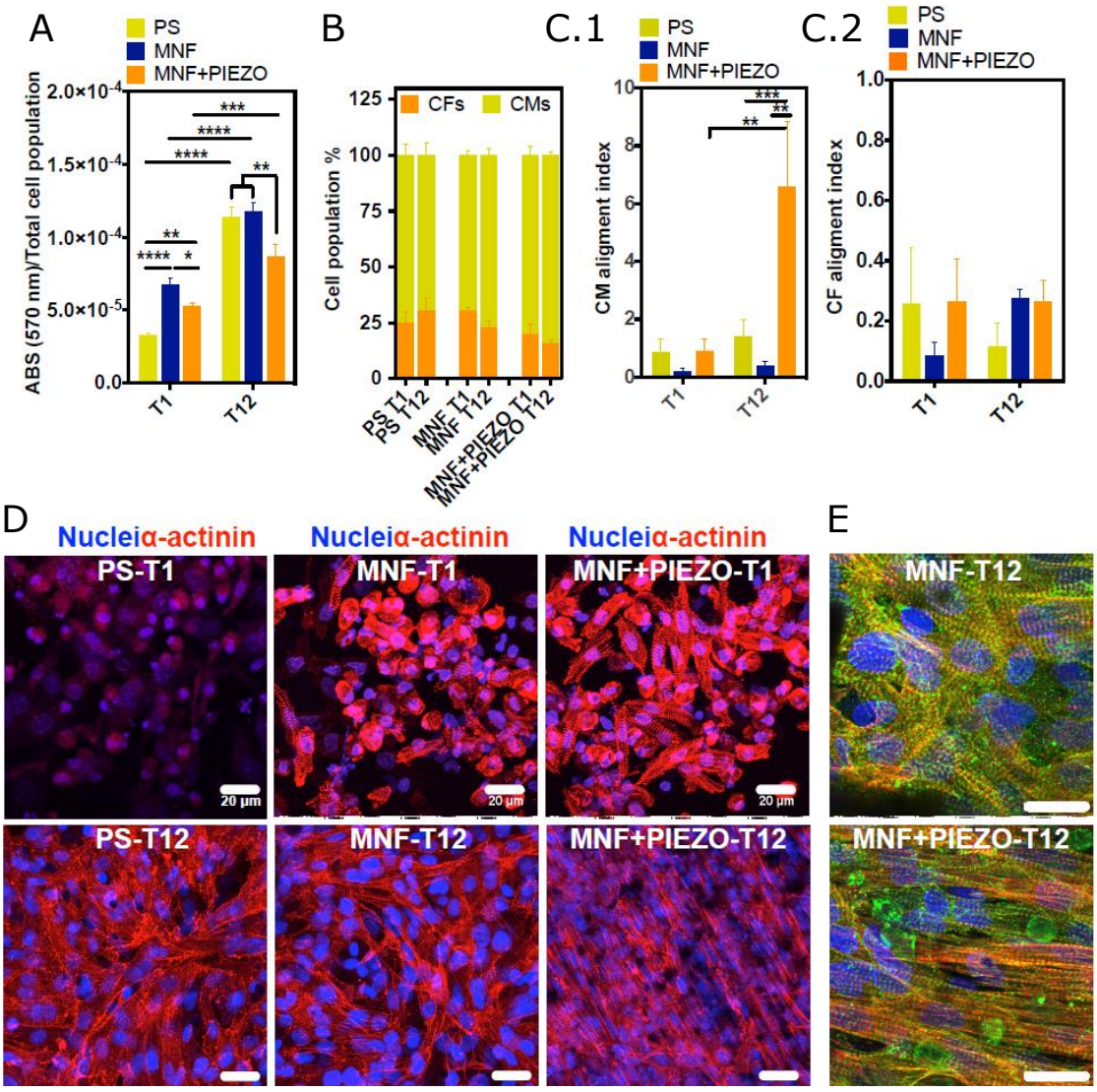

Figure 6 - Viability, composition and alignment of cardiac cells cultured in different scaffolds. A) Cell viability/proliferation as assessed by a MTT assay. Results are Mean ± SEM, n=6. **B)** Quantification of CM and CF total population per culture area (0.8 cm^2) by confocal microscopy (the quantifications were performed in immune-stained samples (63×). The quantifications were performed in substrates collected from three independent experiments, having each experiment three technical replicas. Results are Mean ± SEM, n=3. **C)** CM and CF sub-population alignment index in different substrates. The alignment was calculated in confocal microscopy images (63×) of immuno-stained samples. Cellular alignment was quantified by taking account the deviation (20º degrees) towards a common reference line. CM population was identified as positive for α-actinin staining, while CF population was identified as positive for vimentin. Results are Mean ± SEM, n=3 (three independent experiments; each experiment having 3 technical replicates). **D)** Representative confocal microscopy images of cardiac cells cultured in the different substrates tested for 1 day (T1) and 12 days (T12) after seeding. Cells were stained for α-actinin. Scale bar represents 20 µm. (E) Representative confocal images of positive α-actinin and troponin I CMs cultured under different substrates at T1 and T12. In A and C.1, * denotes statistical significance: *P<0.05, **P<0.01, ***P<0.001, ****P<0.0001.

We then asked whether the cell population in the scaffold was altered during time. CM and CF were identified by the expression of α-actinin and vimentin, respectively (Figure 6B, 6D and 6E). At day 1, approximately 75% of the cells were CM

and only 25% were CF (slight variations in this ratio are observed between conditions). This cell ratio was not statistically different at day 12 (Figure 6B). Altogether, our results show that MNF+PIEZO scaffolds support cell adhesion and proliferation and maintain CM:CF ratio from day 1 to day 12. Previous studies using other scaffolds have shown a marked decrease in CM population overtime (Tiburcy et al., 2011, Radisic et al., 2008). The maintenance of CM:CF ratio is important because CFs produce ECM that increases tissue's resistance to mechanical tension (Banerjee et al., 2007) and they establish important intercellular contacts with CMs (Porter and Turner, 2009).

MNF+PIEZO scaffolds, but not MNF or tissue culture poly(styrene), enhanced cellular stratification. At T12, CMs were located in the proximity of the fibres of the MNF+PIEZO scaffold, while CFs were located on top of CMs and therefore distant from the PIEZO fibres (Figure 7). The reason for such stratification is not clear. It has been shown that cells respond differently to the microtopography (Biela et al., 2009) and stiffness (Discher et al., 2005) of the substrates. An attractive possibility is that this stratification is linked to the piezoelectric properties of the fibres and their capacity to generate electrical charge, which may constitute a source of tropism for CMs.

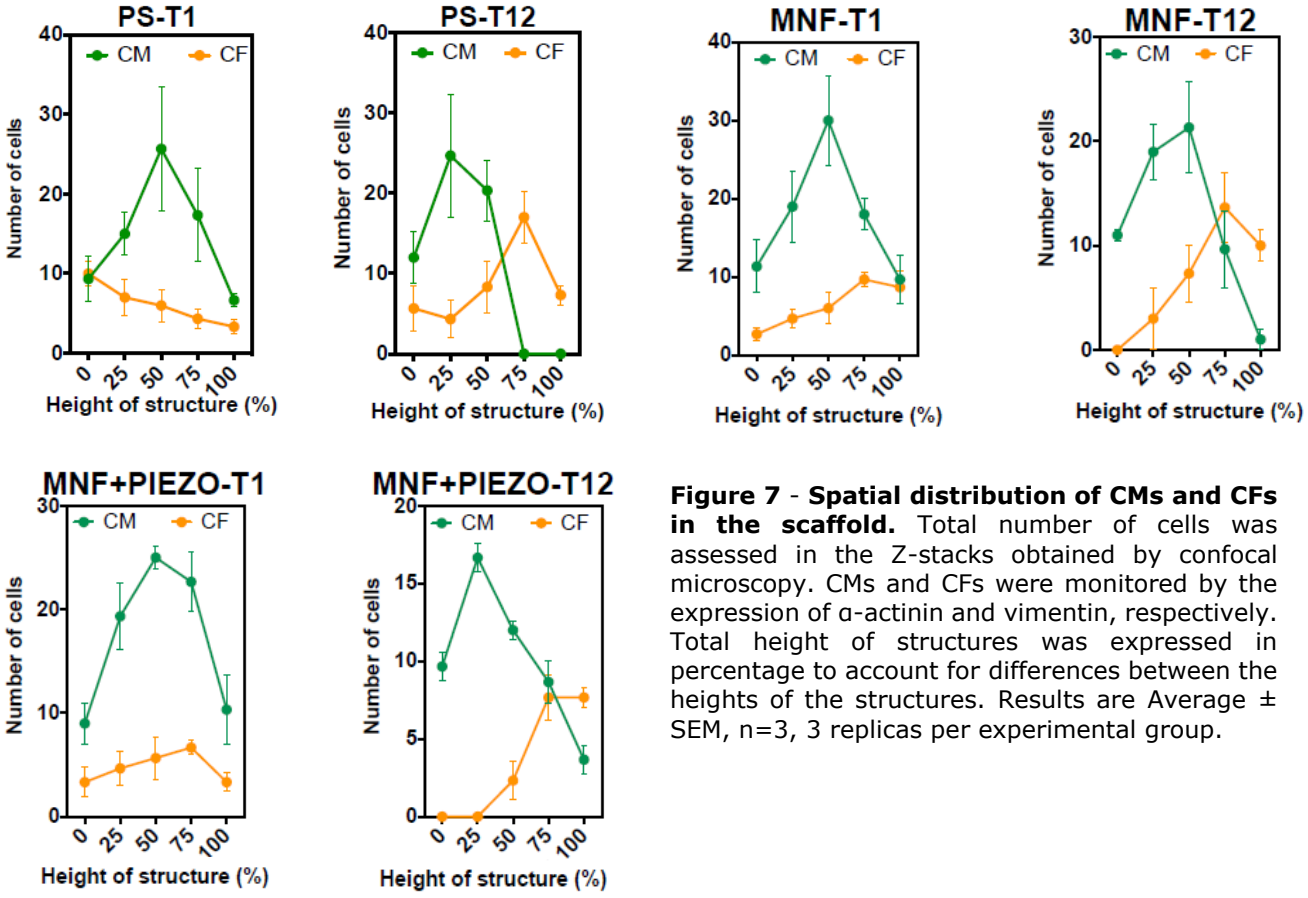

Figure 7 - **Spatial distribution of CMs and CFs in the scaffold.** Total number of cells was assessed in the Z-stacks obtained by confocal microscopy. CMs and CFs were monitored by the expression of α-actinin and vimentin, respectively. Total height of structures was expressed in percentage to account for differences between the heights of the structures. Results are Average ± SEM, n=3, 3 replicas per experimental group.

Previous studies have shown that cell alignment is of utmost importance to generate contractile cardiac-like tissue. For example, CM aligned by the use of micro- and nanopatterned biomaterials have high action potential conduction velocity and express high levels of cell-cell coupling proteins such as Cx43 (Kim et al., 2010, Annabi et al., 2013). To evaluate whether MNF+PIEZO scaffolds enhanced cell alignment, local cell alignment index was quantified by image processing (Boudaoud et al., 2014a). For this purpose α-actinin and vimentin filament orientation was identified for analysis of CM and CF population, respectively (Figures 6C.1 and 6C.2). Cells seeded on MNF+PIEZO scaffolds show a nearly 3-fold increase alignment at day 12 as compared to day 1, while no significant alignment is observed for the other conditions (PS and MNF scaffolds) in the same time scale. Cells cultured on top of MNF+PIEZO scaffolds align with respect to the fibres, showing a clear orientation of the sarcomeric α-actinin fibres relative to the PIEZO fibres, indicating a clear positive impact of topography over cellular organization (Figures 6C.1 and 6E). Regarding the CF population, cell alignment was absent or poor in all conditions (Figures 6C.2). Overall, MNF+PIEZO scaffolds enhanced CM but not CF alignment. Selective CM alignment might be ascribed to the stratification effect described above, i.e., to the proximity of CMs to the piezoelectric fibres. Although cell alignment on ultrathin polymeric films has been reported recently on poly(styrene) (Fujie et al., 2013) and poly(lactic-*co*-glycolic acid) (Shi et al., 2014) nanofilms, this was achieved by the use of a poly(dimethylsiloxane) mould with microgrooved motifs. Our study is the first to report the use of electrospun microfibres on top of nanofilms to control cell alignment.

3.1.4 - MNF+PIEZO scaffolds increase CM area and sarcomere organization and enhance cell-cell communication

MNF+PIEZO scaffolds enhanced sarcomere alignment and increased cell surface area in CMs. To further elucidate the impact of the architecture and biophysics of our scaffolds in CMs, we analysed the overall cellular morphology and intracellular organization of sarcomeres at a single cell level (Figure 8). Our results show that CMs cultured in MNF+PIEZO scaffolds for 12 days have approximately 2-fold higher cell surface area as compared to the other experimental groups (MNF and PS), and 3-fold higher sarcomeric alignment than cells cultured in PS. The increase in the area of CMs is a sign of CM maturation. In postnatal rodent CMs, the increase of CM size can be up

Chapter 4

Discussion

The impact of MNF+PIEZO scaffolds in cardiac cell physiology was initially evaluated at gene level by quantitative real-time polymerase chain reaction (qRT-PCR). In rodents, CM maturation encompasses an increase in cardiac α-actin (α-cd) and a decrease in skeletal α-actin (α-sk) transcripts, as well as a shift from β-(fetal/slow)-myosin heavy chain (β-MHC) to α-(adult/fast)-MHC (α-MHC) (Radisic et al., 2004a, Tiburcy et al., 2011, Tandon et al., 2009). Analysis of α-MHC and β-MHC expression shows that cells cultured in MNF+PIEZO scaffolds have a significant decrease in α-MHC expression but a significant increase in β-MHC expression from T1 to T12 (Figure 9). However, the ratio of α-MHC/β-MHC decreased from T1 to T12, contrarily to the profile observed in the maturation of CMs in rodents (see fetal and adult CM expression). The analyses of α-cd and α-sk transcripts by qRT-PCR shows that cells cultured in MNF+PIEZO scaffolds have increased levels of both α-cd and α-sk, although not statistical significant ($P>0.05$) (Figure 9). The remaining conditions showed either maintenance (PS) or decrease (MNF) in the expression of α-cd and α-sk.

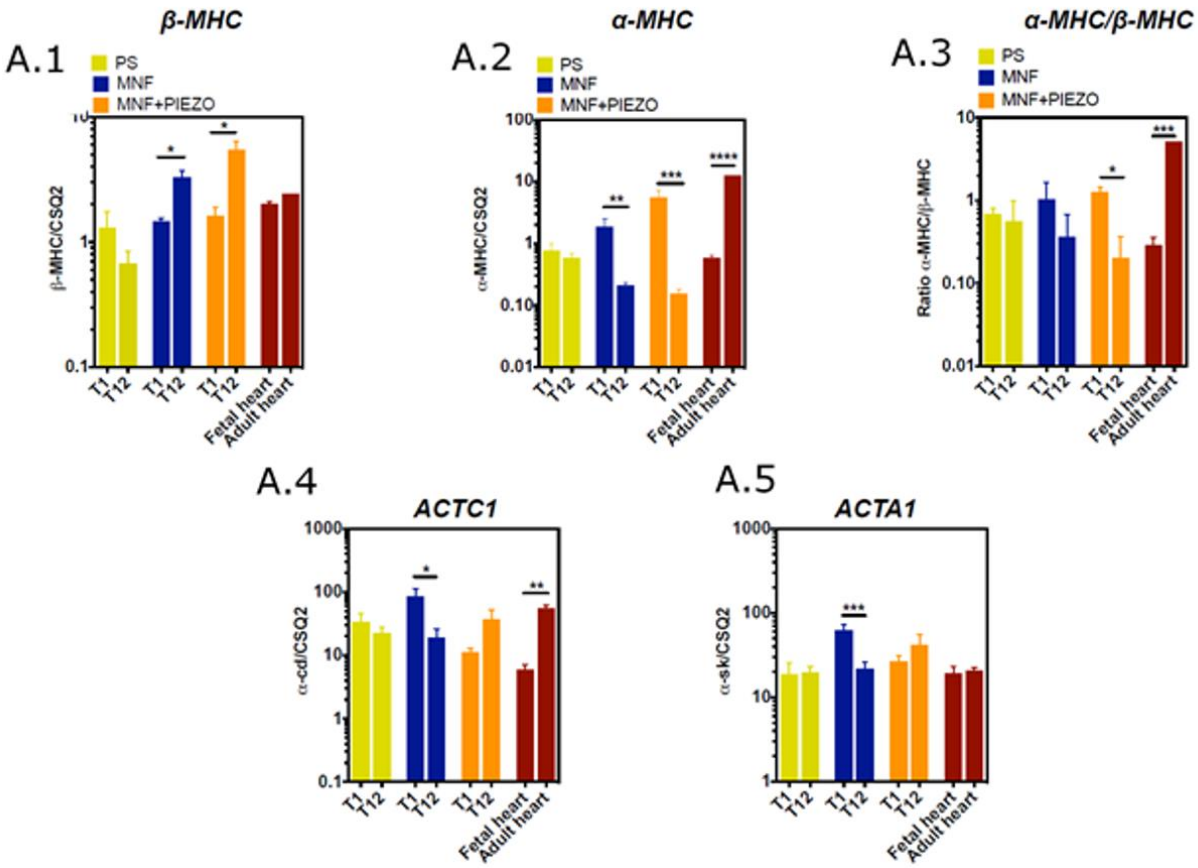

Figure 9 - **Maturation of CMs as evaluated by qRT-PCR analysis.** Cells were cultured on PS, MNF or MNF+PIEZO scaffolds for T1 or T12. Fetal or adult rat heart cells were used as controls. Expression of *β-MHC* (A. 1), *α-MHC* (A.2), ratio *α-MHC/β-MHC* (A.3), α-cd (*ACTC1*; A.4) and α-sk (*ACTA1*; A.5). The expression of genes was normalised by the expression of *CSQ2* gene. Results are Average ± SEM (n=3, 3 replicates at minimum). *Denotes statistical significance: *P<0.05, **P<0.01, ***P<0.001, ****P<0.0001.

To complement the gene expression studies, the phenotype of the cells cultured in MNF+PIEZO for 12 days were evaluated by western blot analysis for α-actinin, troponin I and connexin 43 (Cx43) (Radisic et al., 2004a, You et al., 2011, Tiburcy et al., 2011). The band corresponding to the phosphorylated Cx43 (pCx43), and thus active form of the protein (Mordwinkin et al., 2013, Zimmermann et al., 2006a, Marquez-Rosado et al., 2012, Zhang et al., 2013), was quantified and normalized by total Cx43 levels (phosphorylated plus non-phosphorylated Cx43). Our results show that the ratio pCx43/totalCx43 was statistically higher ($P<0.05$) on CMs cultured on MNF or MNF+PIEZO scaffolds than on PS at T12 (Figure 10A). Cx43 has been shown to regulate cell-cell communication and to promote a contractile phenotype in CM (Ando et al., 2005). The enhanced expression of the active form of Cx43 (pCx43) in CMs seeded on both MNF and MNF+PIEZO scaffolds indicates that both scaffolds promote cell-cell interaction.

To further characterize the phenotype of CMs, the expression of both α-actinin and troponin I was also assessed by western blot and normalized by the expression of calsequestrin 2 (CSQ2), a CM specific protein (Tiburcy et al., 2011). No changes in the expression of α-actinin were observed for all the experimental conditions tested (Figure 10B). An increase in the expression of troponin I was observed for cells cultured in MNF+PIEZO, although no statistical significant difference ($P>0.05$) was observed between the conditions tested (Figure 10C). It is possible that in both cases (α-actinin and troponin I) the variation occurs in the phosphorylated forms of the proteins but not in the total levels of the proteins. For example, it is known that the phosphorylation levels of troponin I regulates its activity (Radisic and Christman, 2013). Moreover, previous studies have shown that contractile CMs cultured in 3D scaffolds for 12 days have similar levels of α-actinin expression to day zero (Hansen et al., 2010). Altogether, the higher levels of Cx43 phosphorylation suggest that the MNF+PIEZO scaffolds promote the establishment of cell-cell communications, likely influencing electrical coupling and promoting contractile behaviour, as compared to CMs cultured in PS. Similar results have been previously reported for cardiac tissues cultured under electrical stimulation or conductive scaffolds (You et al., 2011, Radisic et al., 2004a, Dvir et al., 2011). Our results further show a discrete increase in the expression of markers related to contractile cellular apparatus such as troponin I (protein level) and cardiac α-actin (gene level). The profile obtained is somehow less clear than the one obtained in previous studies showing cardiac maturation in scaffolds (Hansen et al.,

2010). However, discrepancy in the expression of maturation markers was also observed, such as: i) an increase in α-cd but a decrease in the α-MHC/β-MHC ratio (Hansen et al., 2010); ii) the down-regulation of gene fetal markers such as atrial natriuretic peptide, brain natriuretic peptide, α-myosin heavy chain (MYH6) but not at protein level (Nunes et al., 2013); and iii) no significant down-regulation of atrial natriuretic factor during cardiac tissue maturation (Thavandiran et al., 2013).

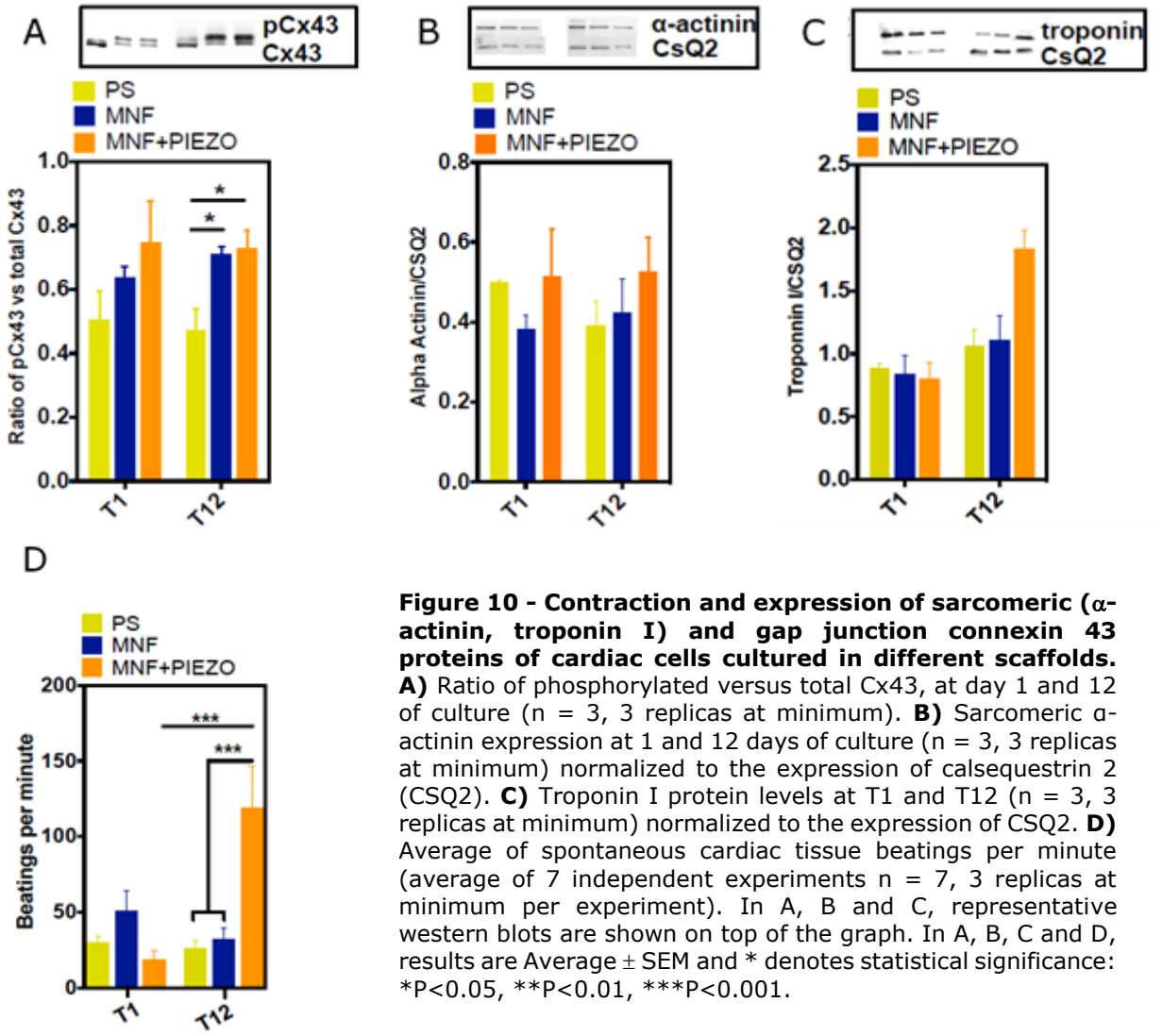

Figure 10 - Contraction and expression of sarcomeric (α-actinin, troponin I) and gap junction connexin 43 proteins of cardiac cells cultured in different scaffolds. A) Ratio of phosphorylated versus total Cx43, at day 1 and 12 of culture (n = 3, 3 replicas at minimum). **B)** Sarcomeric α-actinin expression at 1 and 12 days of culture (n = 3, 3 replicas at minimum) normalized to the expression of calsequestrin 2 (CSQ2). **C)** Troponin I protein levels at T1 and T12 (n = 3, 3 replicas at minimum) normalized to the expression of CSQ2. **D)** Average of spontaneous cardiac tissue beatings per minute (average of 7 independent experiments n = 7, 3 replicas at minimum per experiment). In A, B and C, representative western blots are shown on top of the graph. In A, B, C and D, results are Average ± SEM and * denotes statistical significance: *P<0.05, **P<0.01, ***P<0.001.

3.1.5 - MNF+PIEZO scaffolds preserve CM contractility and Ca^{2+} handling properties

The frequency of heartbeats in rats is around 360 beats per min (6 Hz) (Loe and Edwards, 2004). To evaluate whether MNF+PIEZO scaffolds preserve CM contractility, the number of spontaneous synchronous beating per minute was monitored at day 1 and 12 cell post-seeding (Figure 10D). While the average rate of beats on cells cultured

in PS and MNF scaffolds were similar at day 1 and day 12, a significant increase in beats/minute of the cells cultured in MNF+PIEZO scaffolds (from 18 to 106 beats/min) was observed. This indicates that MNF+PIEZO scaffold provided a better environment to preserve the spontaneous contractility of CMs than the other experimental groups. Therefore, for subsequent experiments we focused in the MNF+PIEZO scaffolds. To understand whether the preservation was due to the piezoelectric properties of the fibres, we have prepared another MNF scaffold having on top aligned PCL fibres, as substitutes of the PIEZO ones (Figure 11).

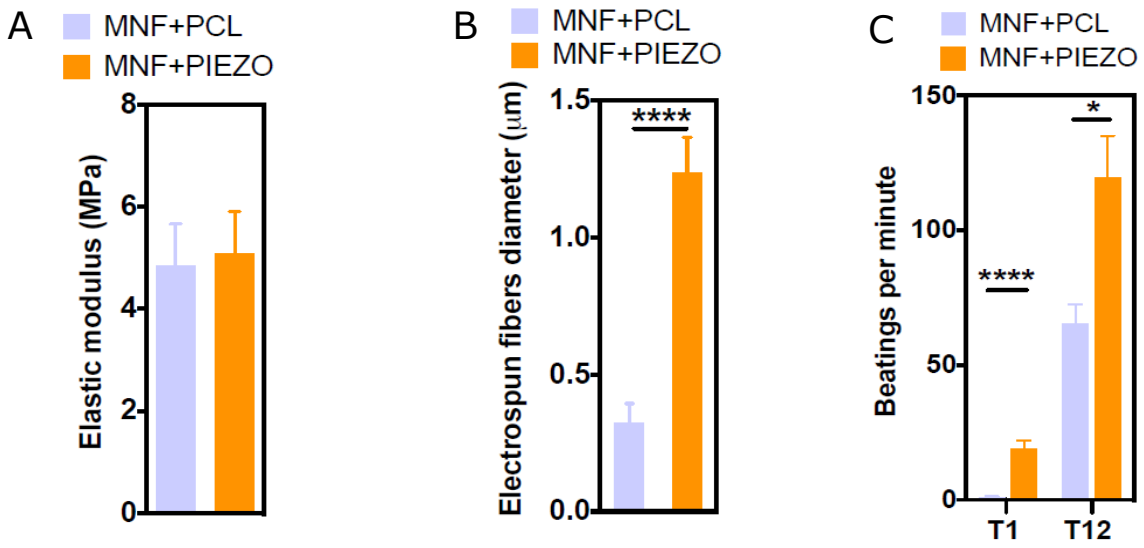

Figure 11 - **Properties of MNF+PCL fibre scaffolds. A)** Elastic modulus. **B)** Diameter of electrospun fibres. **C)** Beatings per minute of scaffolds seeded with CMs at days 1 and 12. In A-C, results are Average ± SEM, n=4. * Denotes statistical significance: *P<0.05, **P<0.01, ***P<0.001, ****P<0.0001.

The PCL-based scaffold ability to maintain CM contractility was significantly lower than that of the scaffold based on PIEZO fibres. The high beating rates observed in cells cultured in MNF+PIEZO scaffolds are likely due to the positive effect of the electric charge generated by the PIEZO fibres after being deformed/bent. Therefore, to confirm this hypothesis, finite element model (FEM) simulations were performed to show that the MNF+PIEZO scaffold undergoes a significant deformation during CMs beating. Local stresses up to ~0.5 MPa (Figure 12B.1) and displacement values up to ~0.2 mm (Figure 12B.2) have been registered.

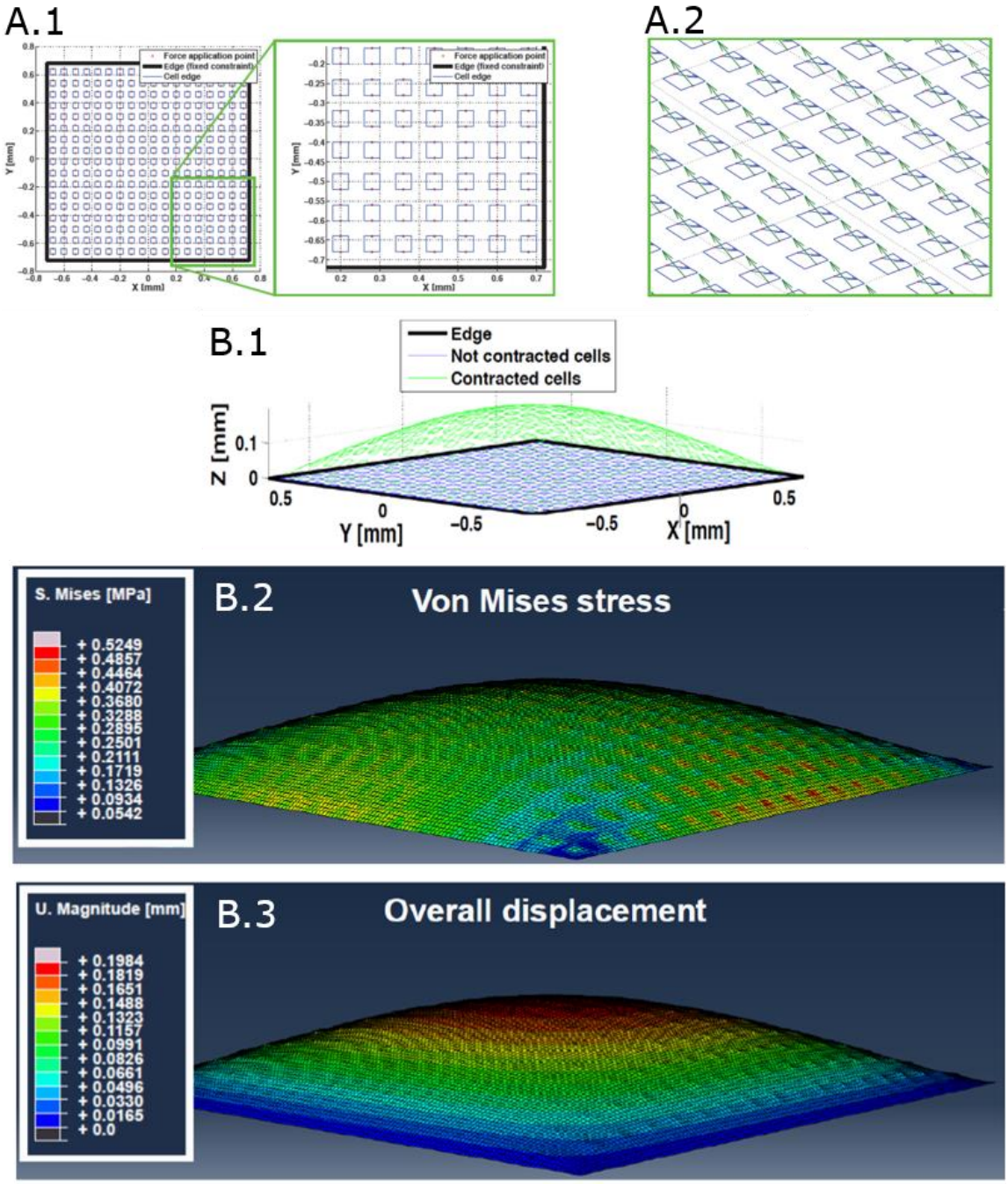

Figure 12 - FEM simulations of scaffold deformation under CM contraction. A) Substrate model, a 1.4x1.4 mm^2 membrane, parametrically designed in the Matlab environment and implemented in the Abaqus simulation environment. Simulation conditions included values for thickness and elastic modulus of the membrane imported from MNF+PIEZO experimental data. Cell dimensions and distribution (A.1) were extracted from fluorescence image analysis, while the imposed cell contraction force and the angle between the contraction force vectors and the substrate surface (A.2) derived from literature data (Feinberg et al., 2007, Carisey et al., 2013). **B)** 3D representations of simulated deformation under the influence of beating cells. Deformation displacement in the absence and presence of CM contraction (B.1); von Mises stress (MPa) distribution over the surface of the simulated layer while under CM beating denotes a generally elastic deformation occurs during this process (B.2); Scalar representation of surface point displacement (in mm) demonstrates higher shifts in the central region of the surface during CM induced deformation (B.3).

The contraction frequency observed in CMs seeded on MNF+PIEZO is higher than the one observed for other constructs such as scaffolds formed by elastin (ca. 40

beats/min, day 12) (Annabi et al., 2013), methacrylated gelatin (ca. 20 beats/min, day 12) (Annabi et al., 2013), methacrylated gelatin containing carbon nanotubes (ca. 45 beats/min, day 9) (Shin et al., 2013) and Matrigel with fibrin (ca. 70 beats/min, day 15; average of 6 series) (Hansen et al., 2010). Furthermore, neonatal rat CMs cultured in MNF+PIEZO exhibit an increase in the contraction frequency overtime while cells cultured in hyaluronic acid patterned glass surfaces or Matrigel® exhibit a decrease in their contraction frequency within 7 days of culture (Khademhosseini et al., 2007, Radisic et al., 2004b).

To further evaluate CMs physiology cultured in MNF+PIEZO scaffolds we monitored the intracellular Ca^{2+} levels by a fluorescent probe (Rhod-3), in the presence or absence of norepinephrine (Sigma). Norepinephrine activates β adrenergic receptors, which induces the permeability of Ca^{2+} channels at the cell membrane and sarcoplasmic reticulum, which in turn leads to an increase of intracellular Ca^{2+} concentration. In the absence of norepinephrine, cells cultured in PS showed fluorescence signal in small foci with low intensity, while cells cultured in MNF+PIEZO showed intense and well distributed fluorescence signal in the cytoplasm (Figure 13A-B). In addition, cells cultured in PS showed almost no variation in the intracellular calcium levels overtime, while cells cultured in MNF+PIEZO showed cyclic variations in the intracellular levels of calcium corresponding to cycles of cell contraction (Figure 13C). In the presence of norepinephrine (1 μg/ml), cells cultured in MNF+PIEZO showed ca. 3-fold higher total intracellular Ca^{2+} fluorescence as compared to the ones cultured in PS (Figures 13A-B). Moreover, cells cultured in MNF+PIEZO pulsed with norepinephrine showed higher number of fluctuations of Ca^{2+} than cells not exposed to norepinephrine (Figure 13C). Overall, our results show that cardiac cells cultured in MNF+PIEZO, but not in PS, have spontaneous fluctuations of intracellular calcium due to significant cell contraction. In presence of norepinephrine, cells cultured in PS responded with low number and amplitude of Ca^{2+} transients, while cells cultured in MNF+PIEZO responded with high number and amplitude of Ca^{2+} transients. Although the pharmacological stimulation of cardiac tissue has been described for short periods of time (up to 7 days) in previous studies (Nunes et al., 2013), it is unclear the outcome for longer periods of time, making difficult any comparison between our results and previous ones.

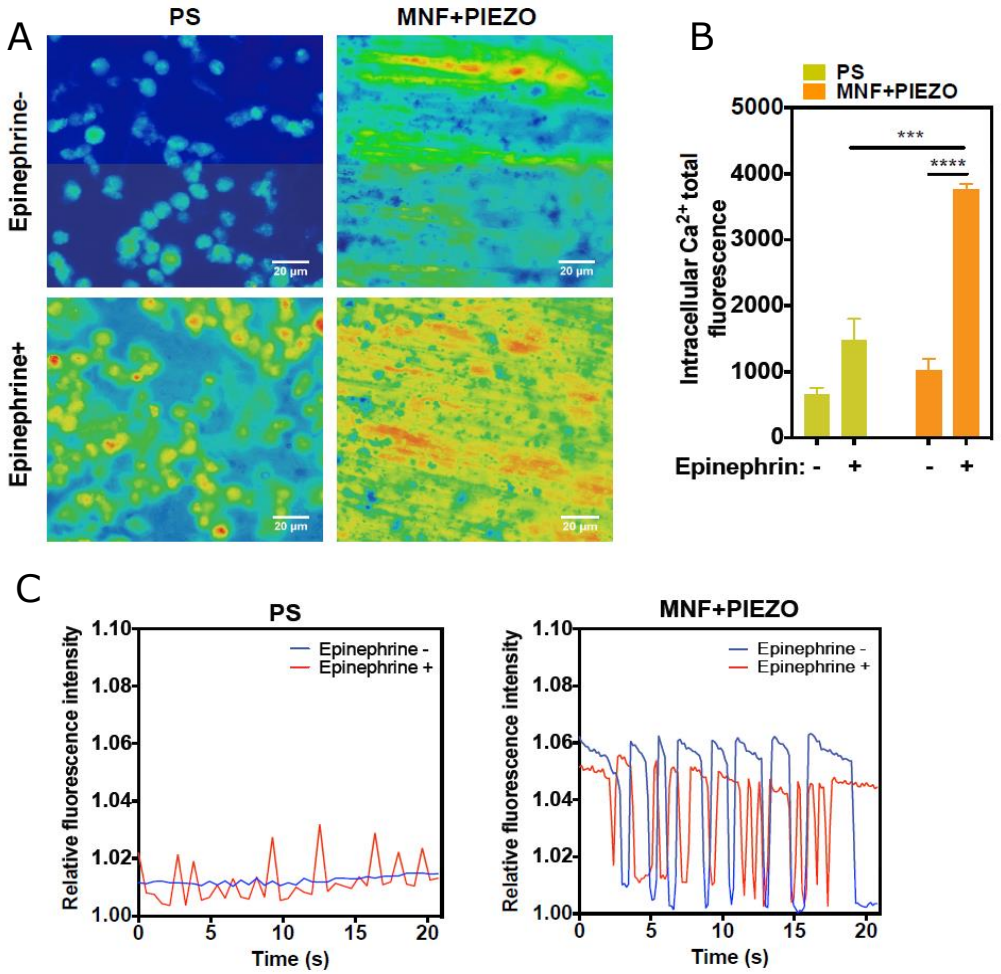

Figure 13 - **Live cell imaging of intracellular Ca^{2+}.** Cardiac cells were cultured in MNF+PIEZO or PS for 6 days before analyses. **A)** Intracellular calcium levels as monitored by a Rhod-3 probe in cardiac cells cultured in PS and MNF+PIEZO, in the absence and presence of norepinephrine. Bar indicates 20 µm. Images were taken by a confocal microscope. **B)** Normalized fluorescence signal in cardiac cells cultured in PS and MNF+PIEZO, in the absence and presence of norepinephrine. Fluorescence intensity values in each experiment were normalized by the minimum background intensity registered during that recording. **C)** Profile of the fluorescence intensity versus time (s) in the absence and presence of norepinephrine. *Denotes statistical significance: *P<0.05, **P<0.01, ***P<0.001.

To complement the previous functional studies related to CM response to pharmacological agonists, we evaluated by qRT-PCR the expression of 8 ion channels subunits important in mammalian CM electrophysiology (Zhang et al., 2013) (Figure 14). With the exception of *CACNA 1S*, there was a statistical significant increase in mRNA levels for all ion channel subunits (*CACNA1C*, *CACNC1D*, *SCN1A*, *SCN5A*, *SCN7A*, *KCNQ1*, *KCNH2*) from T1 to T12 in cells cultured on MNF+PIEZO scaffolds. Furthermore, cells cultured on MNF+PIEZO showed higher expression of 5 ion channels subunits (*CACNA1C*, *CACNA1D*, *SCN5A*, *KCNQ1*, *KCNH2*) than cells cultured on PS. *CACNA1C* and *CACNA1D* transcripts codify, respectively, alpha 1C and 1D subunits of L-type Ca^{2+} channels; *SCN5A* encodes an alpha subunit of voltage-gated Na^{+} channel; and *KCNQ1* and *KCNH2* transcripts encode a voltage-gated potassium channel and a voltage-activated potassium channel (hERG), respectively.

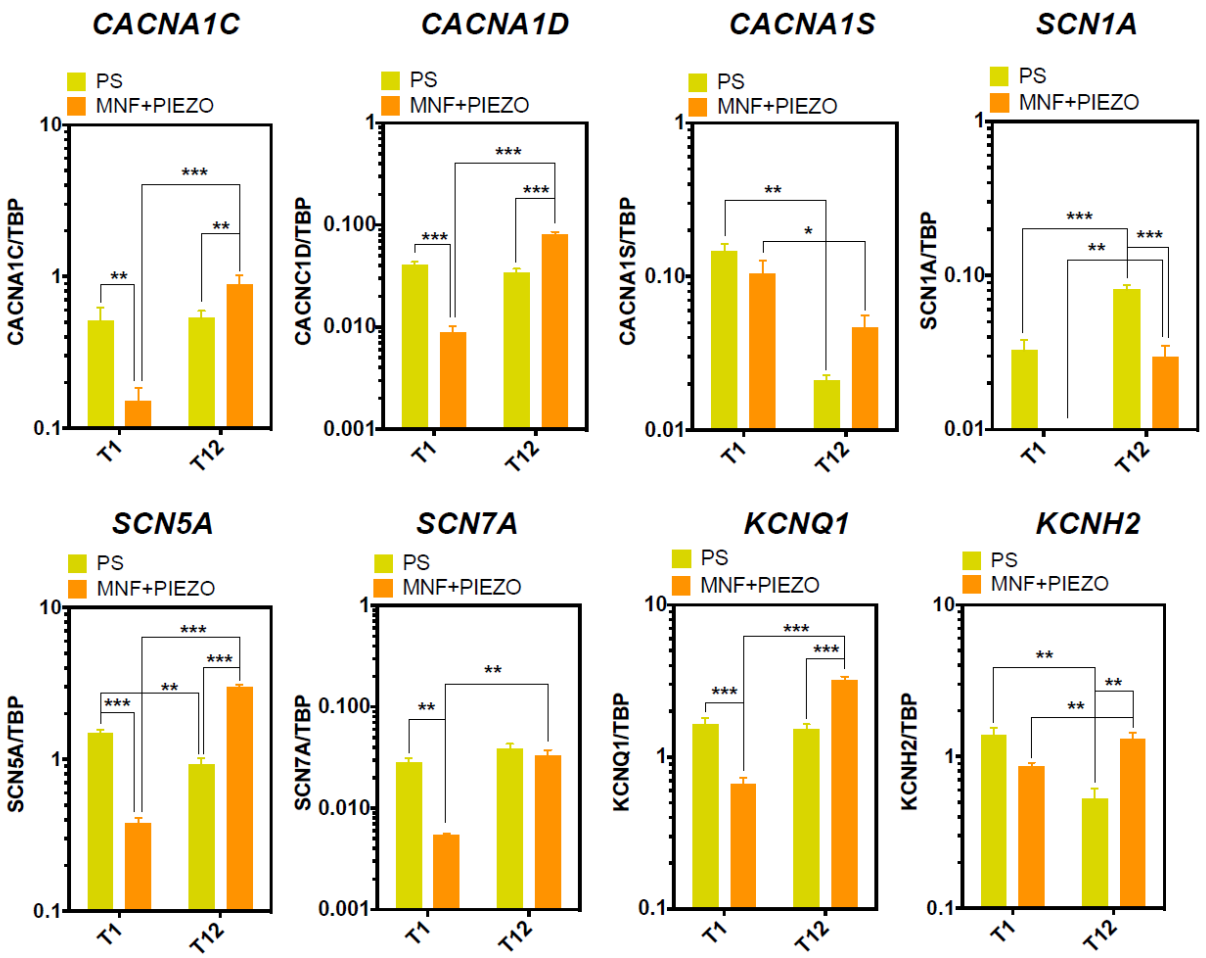

Figure 14 - **Cellular expression of ion channels as evaluated by qRTPCR.** Cells cultured on PS or MNF+PIEZO at day 1 and day 12 were used for these analyses. Target genes include: voltage gated Ca^{2+} channel subunits Cav1.1 (CACNA1S), Cav1.2 (CACNA1C), Cav1.3 (CACNA1D), voltage gated Na^{+} channel subunits Nav1.1 (SCN1A), Nav1.5 (SCN5A), Nax (SCN7A), voltage gated K^{+} channel subunits Kv7.1 (KCNQ1), Kv11.1 (KCNH2). Target genes were normalized against TBP gene expression. Results are Average ± SEM, n=4. *Denotes statistical significance: *P<0.05, **P<0.01, ***P<0.001.

We complemented gene analysis by assessing the expression of hERG and L-type Ca^{2+} channels (Su et al., 2011) (Figure 15). No significant statistical difference was observed in the expression of hERG in cells cultured in both PS and MNF+PIEZO. However, our results show significant differences in cellular distribution and expression of the L-type Ca^{2+} channel, with an approximately 15% increase in the corrected total cell fluorescence (CTCF) levels from PS to the MNF+PIEZO condition. During cardiac development, expression of distinct channel types occurs with time. It is known that L-type channels are more expressed in adult than immature CMs (Yang et al., 2014b). Therefore, our immunofluorescence results indicate signs a promotion in Ca^{2+} homeostasis in CMs cultured in MNF+PIEZO scaffolds.

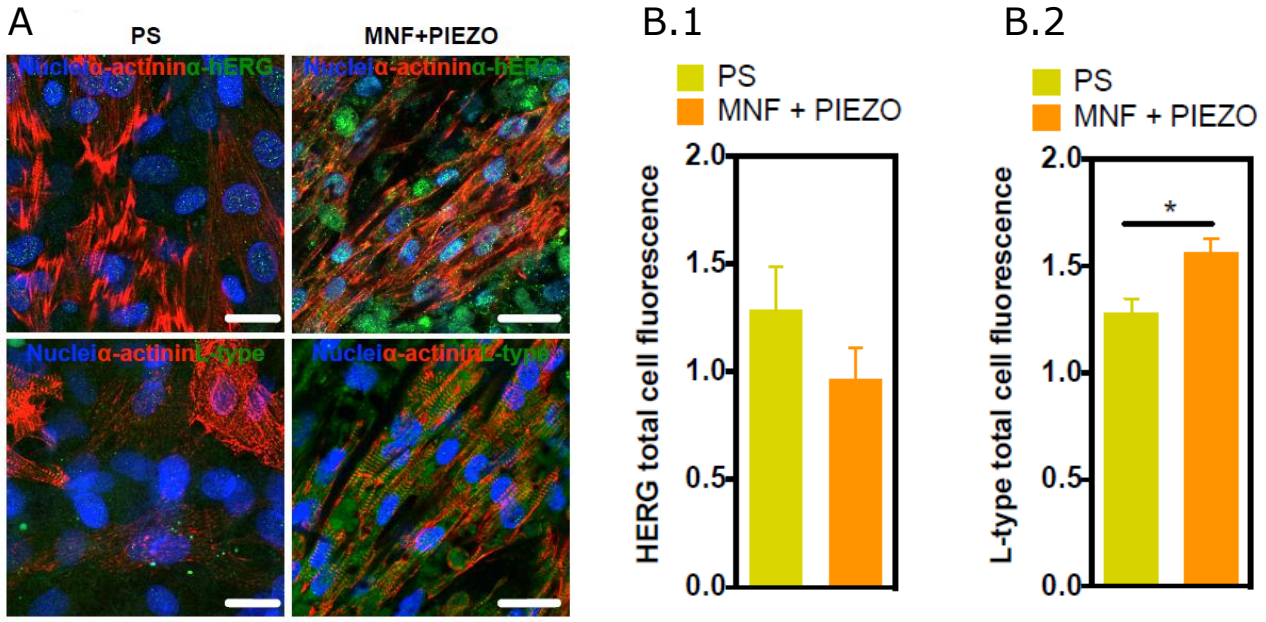

Figure 15 - **Expression of voltage-activated potassium channels (hERG;KCNH2) and L-type calcium channels (anti-dihydropyridine receptor alpha-1 channels) in cardiac cells at day 12. A)** Confocal microscope images of cardiac cells cultured in PS, MNF or MNF+PIEZO for 12 days. Images show the localisation and expression of hERG and L-type calcium channels. Scale bar represents 20 μm. **B)** Quantification of hERG and L-type calcium channels from confocal microscope images. Results are Average ± SEM, n=4. *Denotes statistical significance: *P<0.05, **P<0.01, ***P<0.001.

3.1.6 - Engineered cardiac tissue in MNF+PIEZO scaffolds responds to cardiotoxic compounds.

During early cardiac development, glycolysis is a major source (80%) of energy however, as CMs matures, mitochondrial oxidative capacity increases and fatty acid β-oxidation (80%) becomes the major source of energy (Lopaschuk and Jaswal, 2010). To complement the previous functional and physiological studies, we evaluated the metabolic profile of cells cultured in MNF+PIEZO scaffolds by nuclear magnetic resonance (NMR). Cardiac cells in MNF+PIEZO or PS were cultured for 24 h in media containing [1,6-$^{13}C_2$]-glucose and their metabolic profiles followed by [1,6-$^{13}C_2$]-glucose consumption and [3-^{13}C]-lactate production (Figure 16A). An expanded region of ^{1}H NMR spectra of culture media removed at 2, 4 and 24 h (Figure 16B) shows a doublet at ~1.44 ppm, that is one half of the resonance due to [3-^{13}C]-lactate. Over time, the levels of [3-^{13}C]-lactate increased considerably in the media, denoting an active glycolysis and lactic fermentation in both preparations. Rates of lactate production are however considerably higher in cells cultured in PS, denoting a less oxidative metabolic phenotype of CMs. Altogether, the metabolic profile observed for cardiac cells cultured in MNF+PIEZO scaffolds (i.e. less glycolytic) indicates a metabolic maturation process. Previous studies with engineered cardiac tissues have shown an increase in the number

of mitochondria in more mature CMs (Nunes et al., 2013). However, as far as we know, metabolic studies in engineered cardiac tissues were not reported.

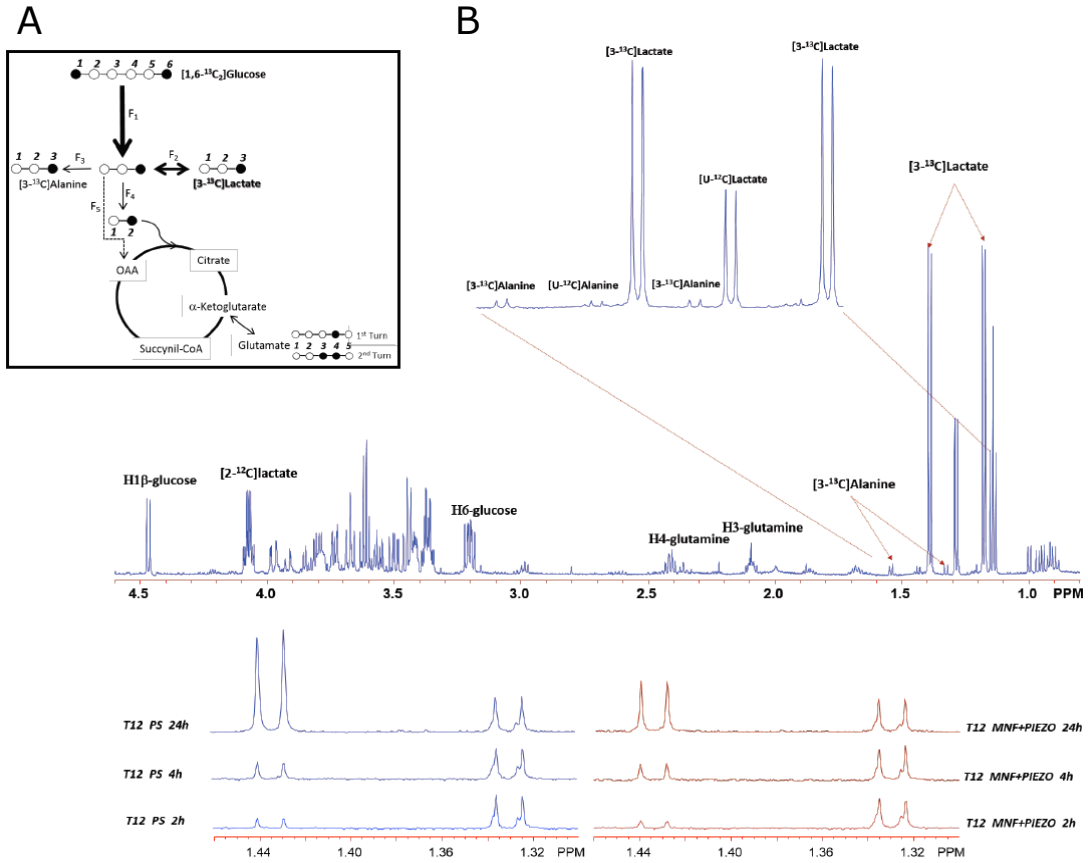

Figure 16 - **Cellular metabolic evaluation using the carbon tracer [1,6-^{13}C2]-glucose and proton nuclear magnetic resonance spectroscopy (1H-NMR)**. **A)** Schematic representation of the metabolic fluxes: F1-glucose consumption; F2-lactic acid fermentation; F3-pyruvate transamination; F4-pyruvate oxidation; F5-pyruvate carboxylation. Through glycolysis, [1,6-^{13}C2]-glucose gets converted into two molecules of [3-^{13}C]-pyruvate, that can follow any of the previously mentioned pathways/fates. **B)** 600 MHz 1H-NMR spectrum of culture medium. The expansion shows the spectral region due to the methyl resonances of lactate and alananine. [3-^{13}C]-lactate is easily distinguished form unenriched lactate due to heteronuclear (JHC) scalar coupling. The two satellites for both lactate and alanine refer to the [3-^{13}C]-isotopes for each metabolite and allow the evaluation of the fluxes F2 and F3. The temporal evolution (2, 4 and 24 h incubation) of the lactate resonances allow an indirect evaluation of the glycolytic flux by determining the rates of lactate accumulation in cell culture medium. By determining the rates of [1,6-^{13}C2]-glucose consumption and [3-^{13}C]-lactate production, the oxidative character of the cardiomyocytes can be effectively evaluated. Resonances for abundant metabolites in culture medium, glucose and glutamine, are also identified in the 1H-NMR spectrum.

Next, we assessed the potential of the engineered cardiac tissue in MNF+PIEZO scaffolds to respond to cardiotoxic compounds. The drug model used was doxorubicin (DOXO), often used in the clinic to treat patients with leukaemia and solid tumours, whose cardiotoxic effect has been widely reported being the primarily target the mitochondria (Octavia et al., 2012) (Ichikawa et al., 2014). Cells cultured in MNF+PIEZO and PS for 12 days were pulsed with 500 nM of DOXO for 24 h. This concentration of DOXO is in the range of concentrations typically used in the clinic (Frost et al., 2002). Cells were then characterized for viability and qRT-PCR for gene

expression related to cell damage (*p53*, *BAX*, *GADD45*) (Vikhanskaya et al., 1995, Zhang et al., 2009b) (Figure 17A). Our results show that cells cultured in MNF+PIEZO scaffolds for 12 days are more sensitive to the effect of DOXO than cells cultured in PS for the same time, since 40% *versus* 20% of the cells died after 24 h of exposure to DOXO, respectively. At gene level, no significant differences were observed for the expression of *BAX* and *GADD45* in cells cultured in MNF+PIEZO or PS. As expected for a cell damage process, both cardiac cells showed an up-regulation in the expression of both genes after exposure to DOXO. Interestingly, cells cultured in MNF+PIEZO scaffolds were more sensitive to p53 than the ones cultured in PS. Our gene expression results were then compared with the gene expression profile of hearts in animals exposed to acute or sub-chronic exposure to DOXO (Figure 17C-D). In this case, animals received a single (acute) or multiple (sub-chronic) doses of DOXO for a certain period of time. Animals exposed to multiple doses of DOXO (sub-chronic animal model) showed an up-regulation of BAX and GADD45, but not p53 in the heart cells, while animals exposed to a single dose of DOXO (acute animal model) showed only an up-regulation of BAX in heart cells. Therefore, our *in vitro* results correlate better with the results obtained in the sub-chronic animal model.

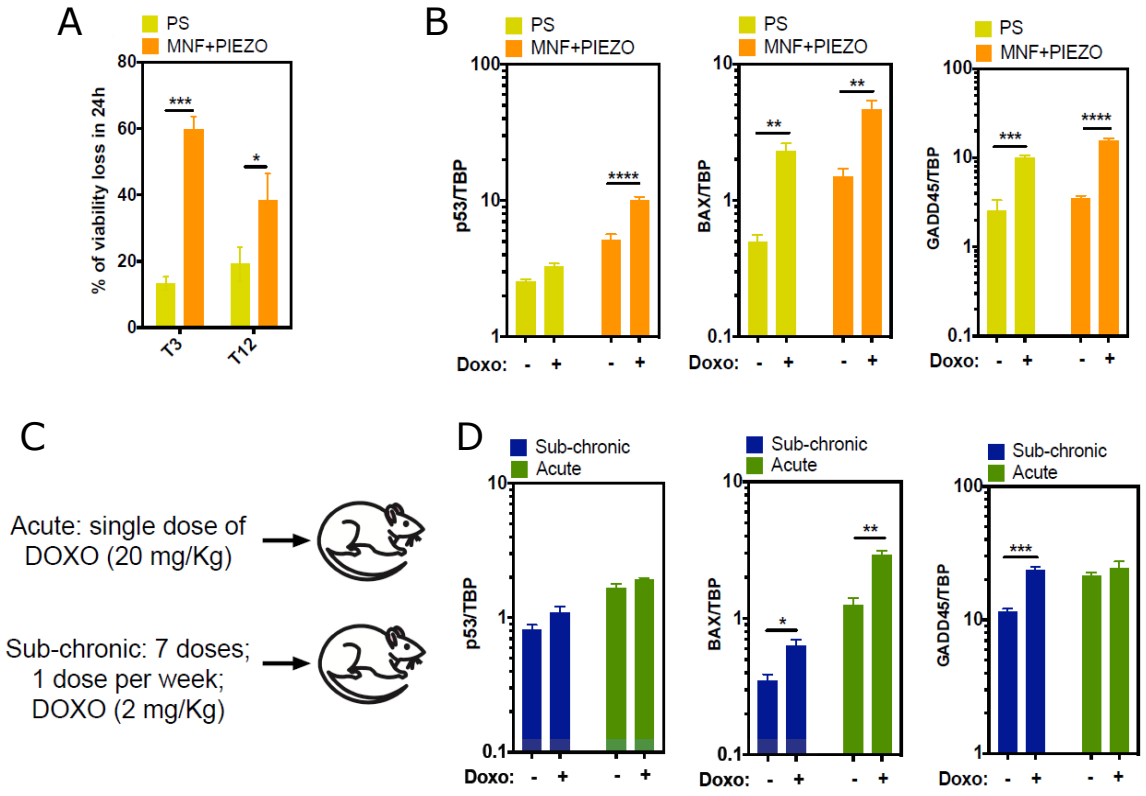

Figure 17 - **Response of cardiac cells cultured in MNF+PIEZO or PS to a cardiotoxic drug (doxorubicin).** (A-B) Cells were exposed to 500 nM of doxorubicin (DOXO) for 24 h and then cellular viability or gene expression evaluated. **A)** Cellular viability, as quantified by a PrestoBlue assay, at day 3 (T3) and day 12 (T12). Results are Average ± SEM (n = 3, 3 technical replicates per each independent experiment). **B)** qRT-PCR analysis of transcripts for 3 genes related to cellular stress response at day 12

of culture. Expression results were normalized to the expression of TBP. Results are Mean ± SEM (n = 3, 3 technical replicates per each independent experiment). **C)** Scheme showing the experimental set-up used to evaluate the acute and sub-chronic effect of DOXO in Wistar rats. To evaluate the acute response to DOXO, animals received a single dose of the drug (20 mg/Kg; DOXO dissolved in NaCl 0.9% solution) by intraperitoneal (IP) injection while the other animals received an equivalent volume of the vehicle solution (NaCl 0.9%). To evaluate the sub-chronic response to DOXO, part of the animals received weekly injections of Doxo (2 mg/Kg; DOXO dissolved in NaCl 0.9% solution) for 7 weeks by subcutaneous injection, while the remaining animals received weekly injections of the carrier (0.9% NaCl). **D)** qRT-PCR analysis of transcripts for 3 genes related to cellular stress response in the heart of the animals. Expression results were normalized to the expression of TBP. Results are Mean ± SEM (n=4). In A-D, * denotes statistical significance: *P<0.05, **P<0.01, ***P<0.001, ****P<0.0001.

To extend the previous viability and gene expression studies, we performed metabolic profiling in cells cultured in MNF+PIEZO by NMR. As in the previous studies, cells cultured in MNF+PIEZO or PS for 12 days were pulsed with DOXO (500 nM) for 24h. Our results showed that cells cultured in MNF+PIEZO became more glycolytic after exposure to DOXO while cells cultured in PS had similar levels of glycolysis before or after exposure to DOXO (Figure 18). The increase of glycolysis on cells cultured in MNF+PIEZO is consistent with the impact that DOXO has on mitochondria. Exposure to DOXO leads to an inhibition of mitochondrial oxidative metabolism that needs to be compensated by glycolysis (Figure 18).

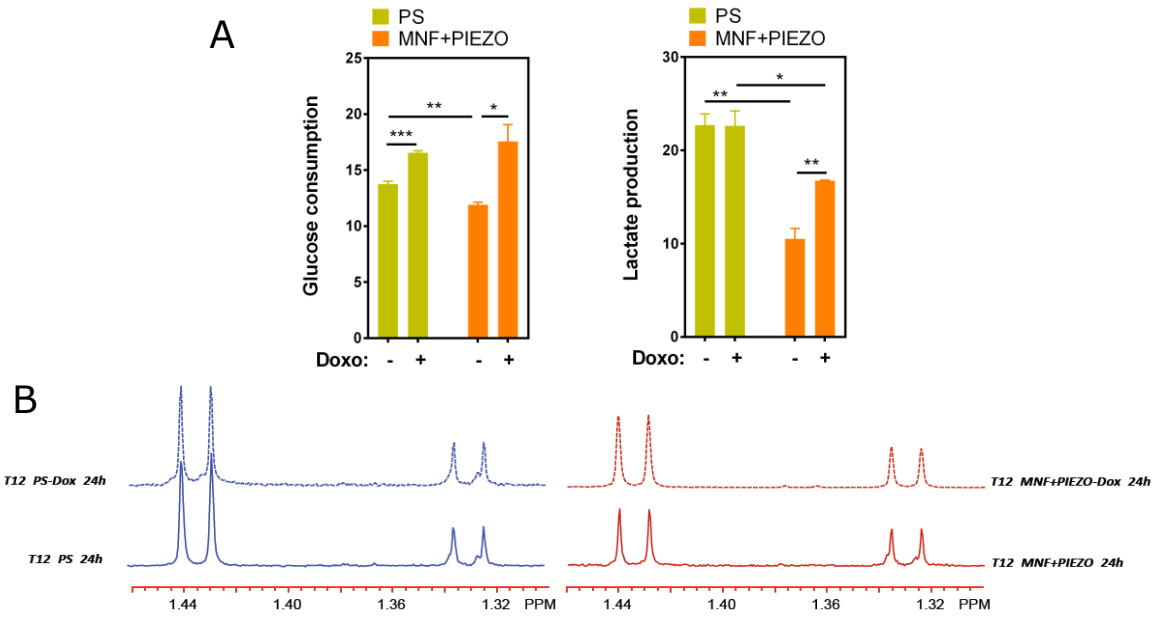

Figure 18 - **Effect of DOXO in cellular metabolism. A)** Rates of glucose consumption and lactate production in the presence (+) and absence (-) of DOXO. Results are Average ± SEM, n=3. *Denotes statistical significance: *P<0.05, **P<0.01. DOXO treatment causes significant increase in glucose consumption, in both PS and MNF+PIEZO groups. This fact results from an increased dependency in the less efficient glycolic pathway to meet cell's energetic demands. Consequently, an increase in lactate production can be observed, particularly in the MNF+PIEZO group. These observations suggest that CMs in the PS group are more glycolytic than in the MNF+PIEZO. **B)** Representative expanded regions of the 1H-NMR spectrum of culture medium showing the lactate methyl resonances due to [U^{12}C]-lactate (1.33 ppm) and [3-^{13}C]-lactate (one of the satellites; 1.44 ppm).

Overall, our viability, gene expression and metabolic profiling results indicate that engineered cardiac tissues in MNF+PIEZO scaffolds respond to cardiotoxic compounds to a level that is not possible to achieve using cells cultured in regular conditions (in this case cultured in PS). The higher sensitivity of our engineered cardiac tissue is likely due to a high mitochondrial function and metabolic maturation. Although a previous study has demonstrated the utility of engineered cardiac tissues to screen cardiotoxic compounds the readout was based in the contraction of the cell construct, which might not be so sensitive as metabolism selected in this work (Hansen et al., 2010).

3.1.7 - Conclusions

In summary, we have engineered a scaffold that combines several features to preserve CM contraction overtime and to promote cardiac maturation. Overall, our results indicate that MNF+PIEZO scaffold promotes cardiac cell attachment and alignment, maintains the ratio of cell populations (CMs:CFs) overtime, promotes cell-cell communication, and preserves CM contractility for at least 12 days. In addition, we have indications that MNF+PIEZO scaffold promotes CM maturation as shown by the increase of CM area, high sarcomeric alignment, up-regulation of α-cd gene, Ca^{2+} handling properties, expression of ion channels, metabolic profile, and response to cardiotoxic compounds that target mitochondria. Although other scaffolds have been used to engineer cardiac tissues, such as collagen gels (Nunes et al., 2013, Thavandiran et al., 2013), methacrylated tropoelastin gels (Annabi et al., 2013), macroporous nanowire electronic scaffolds (Tian et al., 2012), carbon-nanotube embedded methacrylated gelatin gels (Shin et al., 2013), our scaffold is unique in the sense that integrates piezoelectric fibres that align cells and convert mechanical stress in electrical current. Furthermore, the nanofilm is flexible to allow cell contraction, and the system can be easily adapted for high-throughput screenings using cell metabolism as readout (nowadays easily to monitor by commercially equipment and not necessarily by NMR).

Chapter 4

Discussion

4.1 - Significance of the study

A cardiac tissue construct (CTC) suitable for high-throughput screening was developed in this thesis. The CTC had the ability to reproduce aspects of cardiac physiology because it showed a i) high organized cardiomyocyte (CM) ultra-structure, ii) a regular action potential profile comparable to the native tissue, iii) an adequate response to known pharmacological and toxicological agents, and iv) an aerobic-based metabolic activity (Hirt et al., 2014b, Yang et al., 2014b, Keung et al., 2014). The work presented here also shows that the combination of different elements in the scaffold (topography, stiffness and electrical properties) which play an important role to preserving cardiac function. It further highlights the use of metabolism as a final readout for high-throughput drug screening studies.

4.2 - Scaffold design

The scaffold developed in this thesis was able to promote cardiac cell survival for at least 12 days. The scaffold comprised a poly(caprolactone) (PCL) nanofilm onto which a piezoelectric fibre mesh was deposited. The scaffold offered a stable matrix for cardiac cell attachment and proliferation. Our results contrast with previous results on CTCs reporting decreasing numbers of cardiac cells over time of culture (Radisic et al., 2008, Hansen et al., 2010, Tiburcy et al., 2011). The enhanced cell viability observed in our study is likely ascribed to the low thickness of our CTC (few micrometers versus millimetres in other studies) and the substrate conditions to keep cell functionality.

The scaffold developed here was able to preserve the contractile properties of CMs for longer time than previous studies. Contracting CMs by deforming the piezoelectric fibres of P(VDF–TrFE) leads to a local generation of electric charge. This charge subsequently can stimulate further the contraction of CMs by changing cell membrane surface potential. Therefore, the piezo fibres can act as substitutes of pacemaker cells. The stimulation strategy adopted in the present work is more suitable for high-throughput screening than the one based in electrode-activation of cardiac cells. Indeed, most electrical stimulation set-ups described in the literature use two electrodes to provide electrical impulses to cardiac cells (Tandon et al., 2009, Chan et al., 2013). The scaffold shown here provides electrical stimuli to cells at the micro-level without the need of complex external apparatus such as electrode-based systems. Consequently, piezoelectric scaffolds offer greater flexibility for scale-up and integration in high-throughput systems. Moreover, by using anisotropic piezoelectric fibres the

scaffold provides stable cues for cardiac cell alignment, which has been shown to be a strong determinant of CM function (Au et al., 2007) (Table 1). This is in clear contrast with previous reports that tested electrical stimulation without adequate mechanical support and lacked the appropriate aligned topographical cues (Dvir et al., 2011, Nunes et al., 2013, Xiao et al., 2014) (Table 1).

Material	Elastic moduli (kPa)	Type of electrical stimuli	Conductive material	Anisotropy	Reference
Collagen I	61	N	N	N	(Wang, Li et al. 2005)
Hyaluronan benzyl ester	18-60	N	N	N	(Boublik, Park et al. 2005)
Fibrin	1200	External field	N	Y	(Black, Meyers et al. 2009)
Poly(aniline) + Gelatin	600-1400 x 10^3	N	Y	N	(Li, Guo et al. 2006)
Carbon nanotubes + Gelatin-methacrylate	10-32	External field	Y	N	(Shin, Jung et al. 2013)
Alginate + Nanowires	3,5	External field	Y	N	(Dvir, Timko et al. 2011)
Melanin + PCL + Gelatin	7,1-39,2 x 10^3	External field	Y	Y	(Kai, Prabhakaran et al. 2013)
Poly(vinyl carbonate)	N/A	External field	N	Y	(Au, Cheng et al. 2007)
Poly(methyl-glutarimide)	N/A	External field	N	Y	(Orlova, Magome et al. 2011)
MNF+PIEZO scaffold	5,08 x 10^3	*In situ* electric charge generation	Y	Y	-

Table 1 – Comparison of studies exploring the impact of electrical stimuli, stiffnes, and/or topography.

P(VDF–TrFE) was chosen in this PhD work to produce microfibers with piezoelectric properties. The polymer PVDF crystallizes into a non-piezoelectric phase (α and/or γ phases) and has to be mechanically stretched and poled to form a piezoelectric crystal phase (β phase). In contrast, the presence of TrFE in the copolymer causes steric hindrance forcing PVDF into an all-trans configuration, similar to the β phase, thus eliminating the need for mechanical stretching and poling (Eberle et al., 1996). In addition, P(VDF–TrFE) was also chosen for displaying a higher piezoelectric coefficient, meaning that higher polarizations are achieved upon application of a stress than in other polymers of the same class (Ribeiro et al., 2015).

P(VDF–TrFE) microfibers were obtained by electrospinning after selection of the best parameters to have aligned small-diameter fibres. Different concentrations were

selected for testing (10-30%, w/v), however stable fibres were only obtained at concentrations equal or higher than 20%. Increased polymer concentrations resulted in fibres with large diameter (ranging from 1.4 μm at 20% to 2.4 μm at 30%). This is in line with previous studies reporting a similar dependency between polymer concentration and fibre diameter (Pham et al., 2006). Regarding fibre alignment, it was observed an anisotropy score of 0.29 for 20% and 0.67 for 30% (where 1 represents 100% fibre alignment). A previous study has reported P(VDF-TrFE) fibre alignment of approximately 0.9 with concentrations of 15% and 25% (w/v), however it was not clear which fabrication conditions were used other than polymer concentration and type of collection plate (Lee et al., 2011).

The fabricated P(VDF-TrFE) fibres showed piezoelectric properties that were confirmed through piezoelectric force microscopy analysis and direct voltage measurements after mechanical deformation. In this last case, manual deformations were applied to the fibre meshes during a time frame while using two distinct curvatures. These deformations induced voltages between 11.4 mV/s and 26.7 mV/s. Other studies with the same polymer have reported higher voltage peaks between ~400 mV (Beringer et al., 2014) and ~800 mV (Mandal et al., 2011b). It is important to note that these values were detected in anisotropic P(VDF-TrFE) fibres produced with lower concentrations (12-15%, w/w), through near-field electrospinning (Beringer et al., 2014) and a distinct set-up for dynamic fibre collection (Mandal et al., 2011b). On the other hand, strategies using direct electrical stimulation on CMs, used monophasic impulses between 3 and 6 V/cm (Nunes et al., 2013, Chan et al., 2013) and biphasic impulses from -2 to +2 V/cm (Hirt et al., 2014a, Pietronave et al., 2014). During CM contraction the action potential signal varies approximately 100 mV (VanPutte et al., 2015). Therefore, the range of electrical stimulation offered by the piezo fibres described here is much closer to what is observed in the native tissue. This is in contrast to what cells are subjected in artificial electric stimulation set-ups that need supra physiological stimuli to induce a response.

Although it was not possible to measure the voltage generated during cell culture, simulations done with a finite element model (FEM) suggest that CMs can deform the scaffold. Therefore, it is likely that electrical charge is generated in the process of CM contraction. Other studies report electric charge generation driven by CM contraction (Xia et al., 2014, Ishisaka et al., 2006) however, the cells were not in direct contact with the piezoelectric fibrous component. Consequently, the direct impact of the

piezoelectric effect onto cardiac cells was not assessed. Studies that indeed report testing CM seeding directly on a piezo material (Alford et al., 2010, Liu et al., 2014) did not explored in detail the impact of the material and the effects of direct piezoelectric properties on the cells. In contrast, the work presented here attempts to described for the first time the impact of a P(VDF-TrFE) fibre-based scaffold on CM function and maturation.

The scaffold developed in this thesis offers advantages to other reported scaffolds combining electrical stimulation and topography. Firstly, being a free-floating scaffold it can provide the necessary mechanical compliance to allow the free contraction of CMs, as simulated by FEM. This feature has been rarely reported in the literature (McDevitt et al., 2003) and the majority of the 3D matrixes used in the past did not allow free compliance to contraction (Aubin et al., 2010, Bouten et al., 2011). Secondly, by modifying bulk properties, such as film thickness, the degree of mechanical resistance offered to CM contraction can be tuned. This allows for a closer replication of physiological and pathological workloads. Similar rationale can be found in previous studies reporting the use of hydrogels anchored between flexible micro-posts (Legant et al., 2009, Galie et al., 2015). However, such design depends on expensive fabrication processes and in complex set-ups.

The fibres fabricated for the MNF-PIEZO substrate have relatively higher fibre diameter (1.4 μm) compared with the nanosized cues reported for native collagen ECM fibres (~100 nm) (Perumal et al., 2008, Kim et al., 2010). Nevertheless, this is still within the range that has been reported to show superior tissue fidelity in 2D fabricated scaffolds (0.8 to 5 μm) (Bursac et al., 2002, Kim et al., 2010). Furthermore, AFM data shows that the MNF+PIEZO scaffolds are porous (Ra=1,30 ± 0,06 μm), a parameter that can be further controlled by the time of deposition of the fibres. One must also consider that the resulting anisotropic mesh is in fact a sequential deposition of fibres. The density of the mesh and the size of the fibres creates a complex microenvironment with much more contact area for cell adhesion than any 2D substrate can offer. Another factor to take into account, is that a reduction of fibre size (i.e. fibre mass) would imply a reduction in the piezoelectric coefficients obtained (Lian and Sottos, 2000, Park et al., 2006, Lusiola et al., 2015). Consequently, this would lower the efficacy of generating electrical charges through deformation of the piezo material. Overall, the current fibre size is a compromise between effective micro-scale topographical cues and significant piezoelectric properties.

Although piezoelectricity has been reported in biological tissues before (Shamos and Lavine, 1967), few studies have reported the impact of P(VDF-TrFE) electrospun fibres in cells (Ribeiro et al., 2015). P(VDF-TrFE) fibres have only been used in cultures of human skin fibroblasts (Weber et al., 2010b), neurons (Lee and Livingston Arinzeh, 2011), and an immortalized cell line (Beringer et al., 2014). It is important to point out that these studies were performed in static conditions therefore the impact of the piezoelectric effect was not proven. In addition, all the tested cell types were unable to dynamically actuate over the material in order to induce the piezoelectric effect. This is in contrast with the work shown in this PhD thesis because the pre-natal rat CMs have a rhythmic contractile function. Overall, this is the first study to assess the effect of P(VDF-TrFE) fibres in direct contact with contractile cells.

4.3 - Structure of the engineered cardiac tissue

CMs cultured in MNF+PIEZO scaffold had higher alignment (approx. 3-fold) as compared to CMs cultured in control conditions (MNF and PS). This has been also observed in previous studies that explored the independent or combined use of electrical stimulation and topographical cues (Radisic et al., 2004a, Kim et al., 2010, Nunes et al., 2013). Topography was found to be the major cue responsible for CM alignment (Au et al., 2007). Moreover, as the electrical charge of the piezoelectric fibres does not have any directional field, the topography provided by the anisotropic fibres should be the main mediator of CM alignment in our system.

CMs cultured in MNF+PIEZO scaffolds had increased size. This observation correlates with what occurs *in vivo*, where an increased cell area is associated with the maturation of CMs (Lundy et al., 2013). In addition, higher cell surface area correlates with better action potential propagation and greater contractile force (Spach et al., 2004b). This contrasts with results reported in other culture systems, where elongation of the cell body occurs at the expense of a reduction in cell width (Tiburcy et al., 2011). Aside from morphology and cellular alignment, ultrastructure analysis provides useful insights on the degree of maturation of CMs (Robertson et al., 2013, Yang et al., 2014b). In our system, the analysis of ultrastructural markers (α-actinin, troponin I) in the MNF+PIEZO condition showed highly organized sarcomeric structures, denoted by alignment of components such as Z-disks. Protein analysis showed an increase of both proteins from day 1 to day 12, although not statistically different. Additional characterization would be needed to have further insight about the activity of these

proteins, including the analysis of other isoforms and post-translational modifications (Radisic and Christman, 2013).

4.4 - *Functionality of the engineered cardiac tissue: inter-cellular communication and ion dynamics*

CMs cultured in MNF+PIEZO scaffolds showed enhanced intercellular communication, as confirmed by increasing levels of functional connexin 43. In addition, CM contraction was also uniform across the construct and beating rates reached maximum values above of what has been reported by other groups (Hansen et al., 2010, Annabi et al., 2013, Shin et al., 2013). Nonetheless, the beating profile observed in CMs cultured in MNF+PIEZO scaffolds was not as high as in the native rat tissue. This is likely due to the fact that CMs cultured in MNF+PIEZO express slow fetal isoform of myosin heavy chain, β-MHC. These results indicate that action potential signalling was indeed stimulated in the MNF+PIEZO scaffolds however, the contractile machinery was not fully mature.

CMs cultured in MNF+PIEZO scaffolds showed higher Ca^{2+} transients. Cardiac cells cultured in MNF+PIEZO showed higher and well-distributed fluorescence signal across the cytoplasm than the ones cultured in polystyrene. In addition, cyclic variations of fluorescence were detected, suggesting improved Ca^{2+} handling properties. Moreover, only on the MNF+PIEZO condition it was possible to detect waveform signals spreading across the preparation, which indicates an adequate cell-cell communication. To further evaluate the degree of maturation of intracellular Ca^{2+} handling mechanisms, the cardiac tissue constructs were incubated with the chronotropic agent, norepinephrine. In the presence of norepinephrine, Ca^{2+} fluorescence signal increased in both the control and MNF+PIEZO condition, however the increase was superior (3 fold) in CMs cultured in MNF+PIEZO scaffolds. Our results are in line with the ones expected after activation of β1-adrenergic receptors (Tank and Wong, 2011, Nunes et al., 2013).

CMs cultured in MNF+PIEZO scaffolds showed higher transcript levels of ion channels (5 in 8 ion channels analysed) than CMs cultured in polystyrene. In addition, immunofluorescence analyses showed that L-type Ca^{2+} channel expression was higher in CMs cultured in MNF+PIEZO than in the control conditions, while hERG potassium channel expression was similar in both conditions. These results indicate that the MNF+PIEZO scaffold favours transmembrane transients of Ca^{2+}. However, it is not

possible to determine if the observed enhancement in intracellular Ca^{2+} results solely from increased transmembrane mobilization or from more developed intracellular Ca^{2+} storages. Elucidation of this matter is relevant since developed intracellular Ca^{2+} storages are a known marker of CM maturation (Satin et al., 2008, Robertson et al., 2013).

4.5 - *Functionality of the engineered cardiac tissue: cell metabolism and toxicity response*

The heart has high metabolic demands and the analysis of how this organ uses carbon to fuel energy production can give important insights about the state of development and in the distinction between health and disease (Rana et al., 2012). In the context of CTCs, electrophysiology has been the most common tool used for accessing functional maturation. Though it can provide detailed information regarding action potential generation and signal propagation, little to no information can be obtained regarding metabolic development. On the other hand, the development of a set-up for electrophysiology measurements in cells growing in the nanofilm would be a difficult task. Therefore, we used cardiac cell metabolism to assess cell maturation and cardiotoxicity. Cellular metabolism was evaluated by nuclear magnetic resonance (NMR). Our results show that cardiac cells plated on MNF+PIEZO were more dependent on the oxidative phosphorylation to meet their energetic needs than cardiac cells cultured in polystyrene. The transition from a glycolytic (anaerobic) to an oxidative (aerobic) metabolism coincides with the morphologic development of the heart and myocyte differentiation (Porter et al., 2011, Folmes et al., 2012). As an organism continues to mature, the development of mitochondrial respiration capacity is crucial to meet the energetic demands resulting from the increasing workload placed upon the heart muscle (Porter et al., 2011, Vega et al., 2015). Therefore, the result obtained on our experiment shows that MNF+PIEZO scaffolds increased the metabolic maturation of CMs.

The cardiotoxic response of our engineered cardiac tissue was evaluated against doxorubicin (DOXO). The toxic effect of DOXO in CMs is mainly mediated by i) an induction of superoxide generation through eNOS reductase and NADPH oxidase activation and ii) interference with iron sequestration resulting in the increase of free radical generation. The mitochondria is a direct target of DOXO. It is known that DOXO may be retained in the mitochondrial inner membrane and form a nearly-irreversible

complex with cardiolipin (Goormaghtigh et al., 1980). This phospholipid plays an important role in the electron transport chain reaction and by disrupting its function, DOXO causes the production of more superoxide (Schlame et al., 2000). In addition, DOXO can interfere with proteins responsible for the transfer of carnitine, an important mediator in mitochondrial beta-oxidation of long-chain fatty acids (Kashfi et al., 1990). A direct result from cardiolipin and carnitine impairment is the reduction of long-chain-fatty acid oxidation, accompanied by an increase in glucose metabolism (Carvalho et al., 2010). Therefore, the DOXO causes a clear shift from aerobic to anaerobic metabolism in cardiac cells. Mitochondrial aerobic function accounts for the production of around 90% of the ATP utilized by CMs (Ventura-Clapier et al., 2004). Consequently, the damage caused to mitochondria by DOXO leads to a reduction in ATP production, which culminates in the disruption of ATP mediated processes (Gabrielson et al., 2007). Such shift was clearly seen in cardiac cells cultured in the MNF+PIEZO scaffold when subjected to DOXO. At the same time, higher cell death was detected, when comparing with the control condition. Interestingly, these observations contrast with what has been observed in another report, where carbon nanotubes imbedded in a hydrogel protected the CMs from DOXO induced damage (Shin et al., 2013).

Cardiac cell metabolism is an excellent biomarker of cardiotoxicity. Cardiotoxic drugs can induce cardiac cell damage much ahead of any visible change in cardiac function (Gianni et al., 2008) and thus, common read-outs such as beating rates and electrophysiological analyses, might not detect early on cell damage. This is particularly relevant when the drug targets mitochondrial function, such in the cases of imatinib and sunitinib (Adao et al., 2013).

Chapter 5

Future studies

5.1 - Future studies

Future studies should further analyse the degree of maturation of CMs cultured in MNF+PIEZO scaffolds. For example, it will be important to quantify in CMs cultured in MNF+PIEZO scaffolds the presence of atrial natriuretic factor and brain natriuretic factor, both associated with fetal stages of development (McDonough and Glembotski, 1992, Miklas et al., 2014),. In addition, it will be important to characterize the transmission of action potential in cardiac cells by electrophysiology analysis.

Future studies should evaluate the performance of the engineered cardiac tissue against cardiotoxic drugs that modify ion channel function. A first suggestion includes assessing the degree of development of intercellular Ca^{2+} storages, a parameter strongly associated with CM maturation (Robertson et al., 2013). The following pharmacological agents are of particular interest for this case: i) caffeine, a agonist of the ryanodine receptor (RyR) which mediates release of Ca^{2+} from the sarcoplasmic reticulum (SR) (Dolnikov et al., 2006, Itzhaki et al., 2011), ii) ryanodine, a RyR antagonist; iii) thapsigargin, inhibitor of Ca^{2+}-ATPase (SERCA), the mediator of Ca^{2+} reuptake to the SR (Liu et al., 2002, Itzhaki et al., 2011, Dolnikov et al., 2006). The information obtained from these tests can be complemented by dose-response analysis with L-type Ca^{2+} channel blockers, such as nifedipine (Itzhaki et al., 2011, Escobar et al., 2004) or verapamil (Dolnikov et al., 2006). Furthermore, measuring the twitch force generated in the presence of inotropic agents can provide more information regarding the development of the mechanisms of contraction (Dolnikov et al., 2006).

Future studies should also evaluate in more detail the metabolic profile of the engineered cardiac tissue against specific cardiotoxic drugs. The use of Seahorse XF Analyzer may increase the throughput of these analyses. The effect of the drug on CM contraction can be also evaluated with voltage sensitive dyes.

Future studies should also evaluate the effect of MNF+PIEZO scaffold in the maturation of human CMs derived from iPSCs. For practical reasons, all the experimental results described in this thesis were performed with rat-derived cardiac cells, however, rat cardiac cells might not reflect all the biology of human cells. Therefore, we have already initiated the culture of iPSC-derived human CMs in MNF+PIEZO scaffolds. In addition, we have initiated the co-culture of CMs with endothelial cells (EC) to further enhance CM maturation (Caspi et al., 2007, Tulloch et al., 2011). The first set of experiments aimed at observing the effects of co-culturing

EC and CM over 12 days of culture. Cell were plated on tissue culture poly(styrene) (PS) with a ratio of 1:3 (EC/CM) and the control condition was a mono-culture of CMs. Immunofluorescence results showed no significant variations in the numbers of each cell population over the course of 12 days, for both the co- and mono-culture conditions (Figure 1A). Confocal analyses showed higher degree of ultrastructure organization on CMs cultured with ECs. This was particularly evident when analysing fluorescence intensity levels for troponin I, a CM structural marker. At the 3rd and 12th day of culture, a nearly two-fold increase was seen in the co-culture condition, when comparing to the mono-culture (Figure 1B). The EC population was analysed with the cell marker CD31 and a significant drop was seen in the expression levels of this protein (Figure 1C). Since the cell population shows no significant indications of decreasing over time, this reduced marker expression might be due to trans-differentiation.

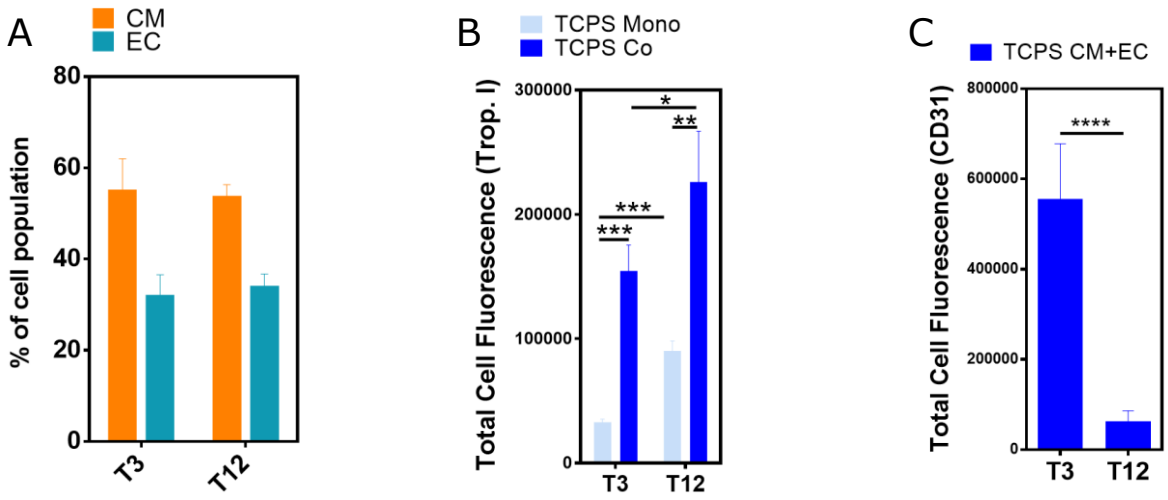

Figure 1 - **Cell population analysis and assessment of lineage markers. A**) Quantification of CM and EC total population per culture area (0.8 cm^2) by confocal microscopy. Quantifications were performed in immunostained samples (63x). The independent experiment shown has three technical replicas. **B-C**) Quantification of troponin I and CD31 from confocal microscope images. Results are Average ± SEM (n=1, 3 technical replicates). *Denotes statistical significance: *P<0,05, **P<0,01, ***P<0,001, ****P<0,0001.

Quantification of cardiac α-actin and skeletal α-actin transcripts by qRT-PCR showed higher levels of expression of the skeletal form than the cardiac one, in both co- and mono-culture conditions. This leads to a relative lower ratio of cardiac/skeletal forms of actin, when comparing with CMs before seeding (T0) (Figure 2A). Regarding the maturation markers α- and β-myosin heavy chain (MHC), transcript levels showed significantly higher expression for the alpha isoform in the co-culture condition at day 12. Consequently, the ratio of α/β-MHC is nearly 6 times higher than T0, and 4 times higher than the mono-culture condition (Figure 2B).

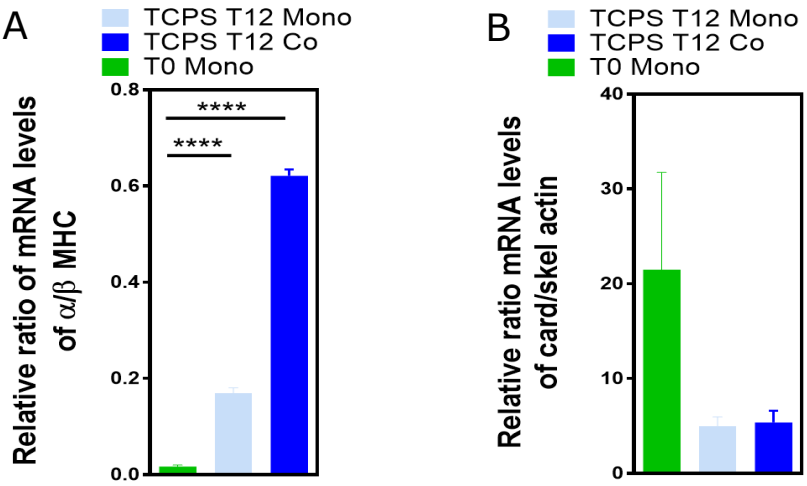

Figure 2 – **Assessment of CM maturation markers. A-B**) Cells were cultured on TCPS scaffolds for 12 days (T12). CMs prior seeding were used as control. Expression ratio of α-MHC/β-MHC (A), and α-cardiac/α-skeletal actin (B). The expression of genes was normalised by the expression of CSQ2 gene. Results are Average ± SEM (n=1, 3 technical replicates). *Denotes statistical significance: ****P<0,0001.

To evaluate whether the co-culture of CMs and ECs maintains CM function, the number of synchronous beatings was registered over 12 days after cell seeding (Figure 3). CMs cultured with ECs maintained a stable beating rate for the first 8 days (17 beats/min), after which increased until the 12th day of culture (maximum value: 70 beats/min), resulting in a total average of 30 beats/min. In contrast, CMs cultured alone showed a fluctuating beating rate with 12 beats/min at day 12.

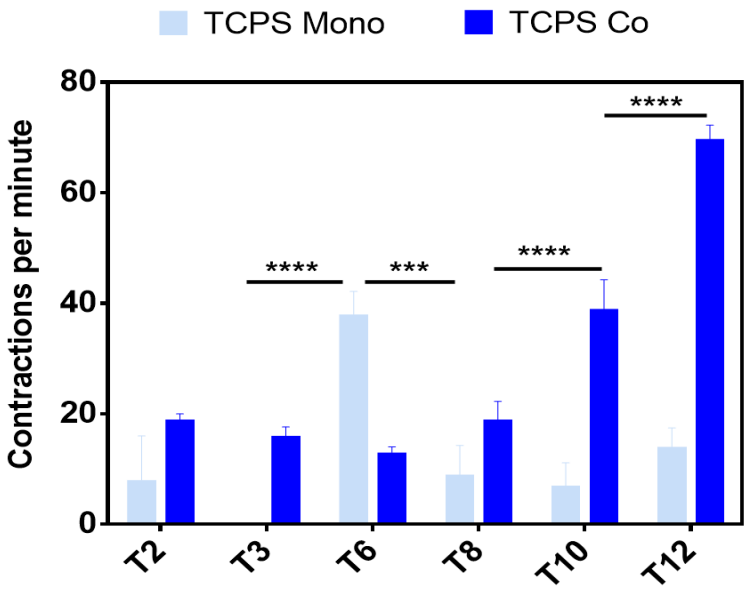

Figure 3 – **Beating rate of iPSC-derived CMs cultured alone or with ECs in polystyrene**. Average of spontaneous cardiac tissue beatings per minute. Results are Average ± SEM, n=1 (3 technical replicates). *Denotes statistical significance: *P<0,05, **P<0,01, ***P<0,001, ****P<0,0001.

To assess the impact of this co-culture strategy in the development of intracellular ion dynamics, the transcript levels of five ion channels subunits (KCNH2, KCNQ1, SCN5A, CACNA1D, CACNA1C) were evaluated by qRT-PCR. Among these, three showed significantly higher levels on the co-culture conditions than in the control (Fig. 4). These transcripts encode for the L-type Ca^{2+} channel, subunit α-1D (Cav.1.3) and voltage-gated K^{+} channels (including the hERG subunit), which have relevant roles in the ionic homeostasis of CMs (Zhang et al., 2013, Su et al., 2011).

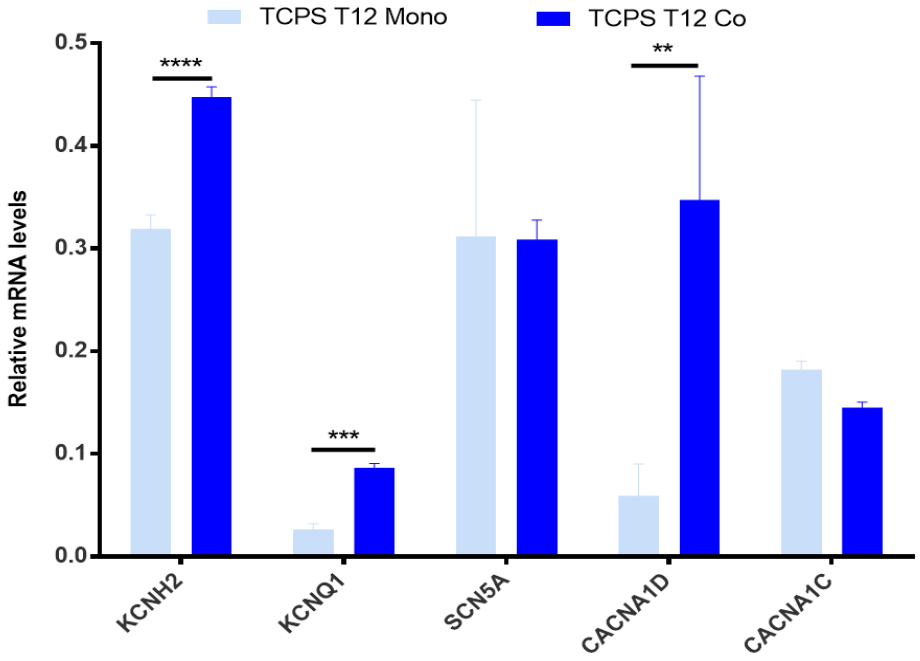

Figure 4 - **Quantification of ion channel mRNA transcripts by qRT-PCR**. Cells were cultured on TCPS for 12 days. Target genes include: voltage gated K channel subunits Kv7.1 (KCNQ1), Kv11.1 (KCNH2; a.k.a. hERG), voltage gated Na channel subunits Nav1.5 (SCN5A), and voltage gated L-type Ca channel subunits Cav1.2 (CACNA1C), Cav1.3 (CACNA1D). Target genes were normalized against TBP gene expression. Results are Average ± SEM, n=1 (3 technical replicates). *Denotes statistical significance: *P<0,05, **P<0,01, ***P<0,001.

Our preliminary results show that iPSC-derived CMs co-cultured with iPSC-derived endothelial cells have enhanced contraction and signs of maturation. Experiments are in progress to study the proteome of CMs cultured alone or in co-culture with ECs. In addition, we will evaluate the effect of MNF+PIEZO scaffold in the maturation process of CMs.

As was previously discussed, the degree of maturation of the CMs achieved in the MNF+PIEZO scaffold is still relatively low, when compared to the adult rat tissue. Therefore, the enhancement of cardiac cell maturation might require the addition of more factors or features to the culture system. For example, the addition of soluble factors, such as T3 thyroid hormone (Chattergoon et al., 2012) and insulin-like growth

factor-1 (Montessuit et al., 2006, Ruvinov et al., 2011), might help the maturation of CMs. Likewise, the substitution of glucose with other carbon sources, such as galactose or fatty acids, might induce CM maturation (Rana et al., 2012). Other strategies include the addition of natural biochemical cues to the scaffold (e.g. collagen epitopes), prolonged duration in culture (Lundy et al., 2013), and stretch stimulation (Dhein et al., 2014).

The presence of a piezoelectric material in a scaffold for growth of muscle cells brings a unique feature to the tissue construct. As referred previously, the possibility of inducing electric stimulation *in situ* without the need of a complex apparatus (Nunes et al., 2013, Miklas et al., 2014) is a great advantage. This piezoelectric feature can be greatly enhanced with the introduction of stretch stimulation. On one hand, the external application of mechanical strain would further stimulate the maturation of CMs, has seen in other studies (Eschenhagen et al., 1997, Zimmermann et al., 2000, Kreutzer et al.). On the other hand, it would guarantee the deformation of the piezo material and subsequent generation of electric charge.

The integration of MNF+PIEZO scaffold into an actuator system requires further developments. MNF+PIEZO scaffolds are not elastic enough to support cyclic deformations in an actuator system already developed in the context of this thesis. In addition, MNF scaffolds (E=0.06 MPa) do not show adequate elastic properties to sustain dynamic strain over long periods of time. For this purpose, elastomeric polymers may offer the perfect combination of deformation compliance and physical resistance. The polymer of choice was PDMS, since it is well characterized and has been widely used (Hirt et al., 2014b, Buikema et al., 2013, Miklas et al., 2014, Rao et al., 2013). Preliminary characterization has been performed for PDMS nanofilms produced with different ratios of cure agent and polymer. The results show lower elastic moduli values (Figure 5A), when compared to PCL nanofilms (Figure 5B), therefore, PDMS films offer higher compliance to deformation. Next, to verify the physical resistance of the PDMS film towards cyclic phases of stretching, two tools had to be created: a force actuator system and a scaffold holder. The purpose of the force actuator is to allow the application of a deformation force over the surface of the scaffold (Figure 5C). Several requirements had to be taken in consideration for this actuator: the design had to be simple, allow automatization, and be compatible with a high-throughput context. With these aims in mind, an electromechanical force actuator was created to fit in a cell incubator. Furthermore, it allows the simultaneous growth of at least 40 isolated tissue

constructs on common cell culture plates. Regarding the scaffold holder, it will substitute the currently used CellCrown® holder (Scaffdex). The creation of this tool was necessary to meet the design requirements of the force actuation system. Besides holding the scaffold platform in suspension, it also enables a proper flow of the medium inside the plate well, consequently maximizing scaffold deformation. Experiments are in progress to test the maturation of cardiac cells under dynamic conditions.

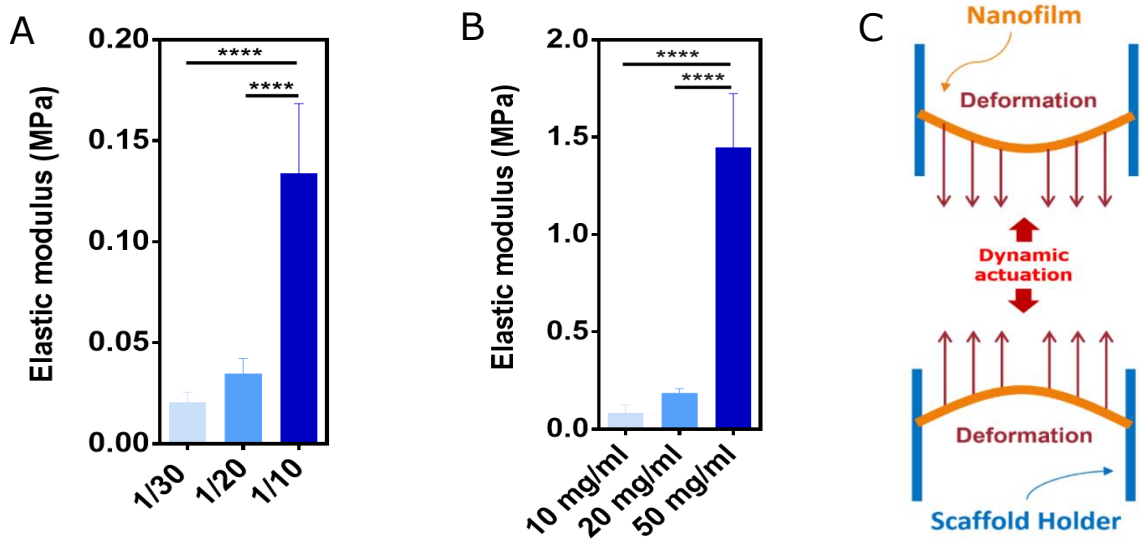

Figure 5 - **Mechanical properties of nanofilms and design for dynamic mechanical actuation**. **A**) Elastic moduli values measured for PDMS nanofilms prepared with different ratios of polymer and curing agent (CA/P); **B**) Elastic moduli values measured for PCL nanofilms with different concentrations of the polymer (w/v). Results are Average ± SEM, n=6. * Denotes statistical significance: *P<0,05, **P<0,01, ***P<0,001, ****P<0,0001. **C**) Schematic of the basic design for force actuation on elastic nanofilms.

Chapter 6

References

ADAO, R., DE KEULENAER, G., LEITE-MOREIRA, A. & BRAS-SILVA, C. 2013. Cardiotoxicity associated with cancer therapy: pathophysiology and prevention strategies. *Rev Port Cardiol,* 32**,** 395-409.

AKHYARI, P., FEDAK, P. W., WEISEL, R. D., LEE, T. Y., VERMA, S., MICKLE, D. A. & LI, R. K. 2002. Mechanical stretch regimen enhances the formation of bioengineered autologous cardiac muscle grafts. *Circulation,* 106**,** I137-42.

ALFORD, P. W., FEINBERG, A. W., SHEEHY, S. P. & PARKER, K. K. 2010. Biohybrid thin films for measuring contractility in engineered cardiovascular muscle. *Biomaterials,* 31**,** 3613-3621.

ANDERSSON, H., STEEL, D., ASP, J., DAHLENBORG, K., JONSSON, M., JEPPSSON, A., LINDAHL, A., KÅGEDAL, B., SARTIPY, P. & MANDENIUS, C.-F. 2010. Assaying cardiac biomarkers for toxicity testing using biosensing and cardiomyocytes derived from human embryonic stem cells. *Journal of Biotechnology,* 150**,** 175-181.

ANDO, M., KATARE, R. G., KAKINUMA, Y., ZHANG, D., YAMASAKI, F., MURAMOTO, K. & SATO, T. 2005. Efferent vagal nerve stimulation protects heart against ischemia-induced arrhythmias by preserving connexin43 protein. *Circulation,* 112**,** 164-70.

ANGST, B. D., KHAN, L. U. R., SEVERS, N. J., WHITELY, K., ROTHERY, S., THOMPSON, R. P., MAGEE, A. I. & GOURDIE, R. G. 1997. Dissociated Spatial Patterning of Gap Junctions and Cell Adhesion Junctions During Postnatal Differentiation of Ventricular Myocardium. *Circulation Research,* 80**,** 88-94.

ANNABI, N., TSANG, K., MITHIEUX, S. M., NIKKHAH, M., AMERI, A., KHADEMHOSSEINI, A. & WEISS, A. S. 2013. Highly Elastic Micropatterned Hydrogel for Engineering Functional Cardiac Tissue. *Adv Funct Mater,* 23.

ARONSEN, J. M., SWIFT, F. & SEJERSTED, O. M. 2013. Cardiac sodium transport and excitation-contraction coupling. *J Mol Cell Cardiol,* 61**,** 11-9.

AU, H. T., CHENG, I., CHOWDHURY, M. F. & RADISIC, M. 2007. Interactive effects of surface topography and pulsatile electrical field stimulation on orientation and elongation of fibroblasts and cardiomyocytes. *Biomaterials,* 28**,** 4277-93.

AUBIN, H., NICHOL, J. W., HUTSON, C. B., BAE, H., SIEMINSKI, A. L., CROPEK, D. M., AKHYARI, P. & KHADEMHOSSEINI, A. 2010. Directed 3D cell alignment and elongation in microengineered hydrogels. *Biomaterials,* 31**,** 6941-6951.

AUMAILLEY, M. 2012. The laminin family. *Cell Adhesion & Migration,* 7**,** 48-55.

BAAR, K., BIRLA, R., BOLUYT, M. O., BORSCHEL, G. H., ARRUDA, E. M. & DENNIS, R. G. 2005. Self-organization of rat cardiac cells into contractile 3-D cardiac tissue. *Faseb j,* 19**,** 275-7.

BANERJEE, I., FUSELER, J. W., PRICE, R. L., BORG, T. K. & BAUDINO, T. A. 2007. Determination of cell types and numbers during cardiac development in the neonatal and adult rat and mouse. *Am J Physiol Heart Circ Physiol,* 293**,** H1883-91.

BARUSCOTTI, M., BARBUTI, A. & BUCCHI, A. 2010. The cardiac pacemaker current. *J Mol Cell Cardiol,* 48**,** 55-64.

BATALOV, I. & FEINBERG, A. W. 2015. Differentiation of Cardiomyocytes from Human Pluripotent Stem Cells Using Monolayer Culture. *Biomark Insights,* 10**,** 71-6.

BAUMGARTNER, S., HALBACH, M., KRAUSGRILL, B., MAASS, M., SRINIVASAN, S. P., SAHITO, R. G. A., PEINKOFER, G., NGUEMO, F., MÜLLER-EHMSEN, J. & HESCHELER, J. 2015. Electrophysiological and Morphological Maturation of Murine Fetal Cardiomyocytes During Electrical Stimulation In Vitro. *Journal of Cardiovascular Pharmacology and Therapeutics,* 20**,** 104-112.

BECKERS, S., NOOR, F., MÜLLER-VIEIRA, U., MAYER, M., STRIGUN, A. & HEINZLE, E. 2010. High throughput, non-invasive and dynamic toxicity screening on adherent cells using respiratory measurements. *Toxicology in Vitro,* 24**,** 686-694.

BELTRAMI, C. A., FINATO, N., ROCCO, M., FERUGLIO, G. A., PURICELLI, C., CIGOLA, E., QUAINI, F., SONNENBLICK, E. H., OLIVETTI, G. & ANVERSA, P. 1994. Structural basis of end-stage failure in ischemic cardiomyopathy in humans. *Circulation,* 89**,** 151-63.

BERGER, H. J., PRASAD, S. K., DAVIDOFF, A. J., PIMENTAL, D., ELLINGSEN, O., MARSH, J. D., SMITH, T. W. & KELLY, R. A. 1994. Continual electric field stimulation preserves contractile function of adult ventricular myocytes in primary culture. *American Journal of Physiology - Heart and Circulatory Physiology,* 266**,** H341-H349.

BERINGER, L. T., XU, X., SHIH, W., SHIH, W.-H., HABAS, R. & SCHAUER, C. L. 2014. An electrospun PVDF-TrFe fiber sensor platform for biological applications. *Sensors and Actuators A: Physical,* 222**,** 293-300.

BERK, B. C., FUJIWARA, K. & LEHOUX, S. 2007. ECM remodeling in hypertensive heart disease. *Journal of Clinical Investigation,* 117**,** 568-575.

BHANA, B., IYER, R. K., CHEN, W. L., ZHAO, R., SIDER, K. L., LIKHITPANICHKUL, M., SIMMONS, C. A. & RADISIC, M. 2010. Influence of substrate stiffness on the phenotype of heart cells. *Biotechnol Bioeng,* 105**,** 1148-60.

BIELA, S. A., SU, Y., SPATZ, J. P. & KEMKEMER, R. 2009. Different sensitivity of human endothelial cells, smooth muscle cells and fibroblasts to topography in the nano-micro range. *Acta Biomater,* 5**,** 2460-6.

BIRD, S. D., DOEVENDANS, P. A., VAN ROOIJEN, M. A., BRUTEL DE LA RIVIERE, A., HASSINK, R. J., PASSIER, R. & MUMMERY, C. L. 2003. The human adult cardiomyocyte phenotype. *Cardiovascular Research,* 58**,** 423-434.

BIRLA, R. K., HUANG, Y. C. & DENNIS, R. G. 2007. Development of a novel bioreactor for the mechanical loading of tissue-engineered heart muscle. *Tissue Eng,* 13**,** 2239-48.

BLACK, L. D., 3RD, MEYERS, J. D., WEINBAUM, J. S., SHVELIDZE, Y. A. & TRANQUILLO, R. T. 2009. Cell-induced alignment augments twitch force in fibrin gel-based engineered myocardium via gap junction modification. *Tissue Eng Part A,* 15**,** 3099-108.

BOHELER, K. R., CARRIER, L., CHASSAGNE, C., DE LA BASTIE, D., MERCADIER, J. J. & SCHWARTZ, K. 1991. Regulation of myosin heavy chain and actin isogenes expression during cardiac growth. *Molecular and Cellular Biochemistry,* 104**,** 101-107.

BOUDAOUD, A., BURIAN, A., BOROWSKA-WYKRET, D., UYTTEWAAL, M., WRZALIK, R., KWIATKOWSKA, D. & HAMANT, O. 2014a. FibrilTool, an ImageJ plug-in to quantify fibrillar structures in raw microscopy images. *Nature Protocols,* 9**,** 457-63.

BOUDAOUD, A., BURIAN, A., BOROWSKA-WYKRET, D., UYTTEWAAL, M., WRZALIK, R., KWIATKOWSKA, D. & HAMANT, O. 2014b. FibrilTool, an ImageJ plug-in to quantify fibrillar structures in raw microscopy images. 9**,** 457-63.

BOUTEN, C. V. C., DANKERS, P. Y. W., DRIESSEN-MOL, A., PEDRON, S., BRIZARD, A. M. A. & BAAIJENS, F. P. T. 2011. Substrates for cardiovascular tissue engineering. *Advanced Drug Delivery Reviews,* 63**,** 221-241.

BOYETT, M. R., HONJO, H. & KODAMA, I. 2000. The sinoatrial node, a heterogeneous pacemaker structure. *Cardiovasc Res,* 47**,** 658-87.

BRAAM, S. R., TERTOOLEN, L., VAN DE STOLPE, A., MEYER, T., PASSIER, R. & MUMMERY, C. L. 2010. Prediction of drug-induced cardiotoxicity using human embryonic stem cell-derived cardiomyocytes. *Stem Cell Research,* 4**,** 107-116.

BRODSKY, V. Y., CHERNYAEV, A. L. & VASILYEVA, I. A. 1992. Variability of the cardiomyocyte ploidy in normal human hearts. *Virchows Archiv B,* 61**,** 289-294.
BROWN, R. D., AMBLER, S. K., MITCHELL, M. D. & LONG, C. S. 2005. The cardiac fibroblast: therapeutic target in myocardial remodeling and failure. *Annu Rev Pharmacol Toxicol,* 45**,** 657-87.
BUIKEMA, J. W., VAN DER MEER, P., SLUIJTER, J. P. G. & DOMIAN, I. J. 2013. Engineering Myocardial Tissue: The Convergence of Stem Cells Biology and Tissue Engineering Technology. *Stem cells (Dayton, Ohio),* 31**,** 2587-2598.
BUKAUSKAS, F. F. 2014. 8 - Molecular Organization, Gating, and Function of Gap Junction Channels. *In:* JALIFE, D. P. Z. (ed.) *Cardiac Electrophysiology: From Cell to Bedside (Sixth Edition).* Philadelphia: W.B. Saunders.
BURRIDGE, P. W., KELLER, G., GOLD, J. D. & WU, J. C. 2012. Production of de novo cardiomyocytes: human pluripotent stem cell differentiation and direct reprogramming. *Cell Stem Cell,* 10**,** 16-28.
BURSAC, N., PARKER, K. K., IRAVANIAN, S. & TUNG, L. 2002. Cardiomyocyte cultures with controlled macroscopic anisotropy: a model for functional electrophysiological studies of cardiac muscle. *Circ Res,* 91**,** e45-54.
CALLISTER 2003. *Materials Science and Engineering: An Introduction* New York: Wiley.
CARRIER, R. L., RUPNICK, M., LANGER, R., SCHOEN, F. J., FREED, L. E. & VUNJAK-NOVAKOVIC, G. 2002a. Effects of oxygen on engineered cardiac muscle. *Biotechnol Bioeng,* 78**,** 617-25.
CARRIER, R. L., RUPNICK, M., LANGER, R., SCHOEN, F. J., FREED, L. E. & VUNJAK-NOVAKOVIC, G. 2002b. Perfusion improves tissue architecture of engineered cardiac muscle. *Tissue Eng,* 8**,** 175-88.
CARVALHO, R. A., SOUSA, R. P. B., CADETE, V. J. J., LOPASCHUK, G. D., PALMEIRA, C. M. M., BJORK, J. A. & WALLACE, K. B. 2010. Metabolic remodeling associated with subchronic doxorubicin cardiomyopathy. *Toxicology,* 270**,** 92-98.
CASPI, O. & GEPSTEIN, L. 2004. Potential applications of human embryonic stem cell-derived cardiomyocytes. *Ann N Y Acad Sci,* 1015**,** 285-98.
CASPI, O., ITZHAKI, I., KEHAT, I., GEPSTEIN, A., ARBEL, G., HUBER, I., SATIN, J. & GEPSTEIN, L. 2009. In Vitro Electrophysiological Drug Testing Using Human Embryonic Stem Cell Derived Cardiomyocytes. *Stem Cells and Development,* 18**,** 161-172.
CASPI, O., LESMAN, A., BASEVITCH, Y., GEPSTEIN, A., ARBEL, G., HABIB, I. H., GEPSTEIN, L. & LEVENBERG, S. 2007. Tissue engineering of vascularized cardiac muscle from human embryonic stem cells. *Circ Res,* 100**,** 263-72.
CHAN, Y.-C., TING, S., LEE, Y.-K., NG, K.-M., ZHANG, J., CHEN, Z., SIU, C.-W., OH, S. W. & TSE, H.-F. 2013. Electrical Stimulation Promotes Maturation of Cardiomyocytes Derived from Human Embryonic Stem Cells. *Journal of Cardiovascular Translational Research,* 6**,** 989-999.
CHATTERGOON, N. N., GIRAUD, G. D., LOUEY, S., STORK, P., FOWDEN, A. L. & THORNBURG, K. L. 2012. Thyroid hormone drives fetal cardiomyocyte maturation. *The FASEB Journal,* 26**,** 397-408.
CHEN, Q. Z., BISMARCK, A., HANSEN, U., JUNAID, S., TRAN, M. Q., HARDING, S. E., ALI, N. N. & BOCCACCINI, A. R. 2008. Characterisation of a soft elastomer poly(glycerol sebacate) designed to match the mechanical properties of myocardial tissue. *Biomaterials,* 29**,** 47-57.
CHOPRA, I. 2002. Review of State of Art of Smart Structures and Integrated Systems. *AIAA Journal,* 40**,** 2145-2187.
CHUNG, C.-Y., BIEN, H. & ENTCHEVA, E. 2007. The Role of Cardiac Tissue Alignment in Modulating Electrical Function. *Journal of Cardiovascular Electrophysiology,* 18**,** 1323-1329.

CLUBB, F. J. & BISHOP, S. P. 1984. Formation of binucleated myocardial cells in the neonatal rat. An index for growth hypertrophy. *Laboratory investigation; a journal of technical methods and pathology,* 50**,** 571-577.
CORDA, S., SAMUEL, J.-L. & RAPPAPORT, L. 2000. Extracellular Matrix and Growth Factors During Heart Growth. *Heart Failure Reviews,* 5**,** 119-130.
COURTNEY, T., SACKS, M. S., STANKUS, J., GUAN, J. & WAGNER, W. R. 2006. Design and analysis of tissue engineering scaffolds that mimic soft tissue mechanical anisotropy. *Biomaterials,* 27**,** 3631-3638.
CURTIS, M. W. & RUSSELL, B. 2011. Micromechanical regulation in cardiac myocytes and fibroblasts: implications for tissue remodeling. *Pflugers Arch*.
DAMARAJU, S. M., WU, S., JAFFE, M. & ARINZEH, T. L. 2013. Structural changes in PVDF fibers due to electrospinning and its effect on biological function. *Biomed Mater,* 8**,** 045007.
DE LANGE, W. J., HEGGE, L. F., GRIMES, A. C., TONG, C. W., BROST, T. M., MOSS, R. L. & RALPHE, J. C. 2011. Neonatal mouse-derived engineered cardiac tissue: a novel model system for studying genetic heart disease. *Circ Res,* 109**,** 8-19.
DE SOUZA, R. R. 2002. Aging of myocardial collagen. *Biogerontology,* 3**,** 325-335.
DEBESSA, C., MAIFRINO, L. & DE SOUZA, R. 2001. Age related changes of the collagen network of the human heart. *Mechanisms of Ageing and Development,* 122**,** 1049-1058.
DESHPANDE, R. R., WITTMANN, C. & HEINZLE, E. 2004. Microplates with integrated oxygen sensing for medium optimization in animal cell culture. *Cytotechnology,* 46**,** 1-8.
DHEIN, S., SCHREIBER, A., STEINBACH, S., APEL, D., SALAMEH, A., SCHLEGEL, F., KOSTELKA, M., DOHMEN, P. M. & MOHR, F. W. 2014. Mechanical control of cell biology. Effects of cyclic mechanical stretch on cardiomyocyte cellular organization. *Progress in Biophysics and Molecular Biology,* 115**,** 93-102.
DISCHER, D. E., JANMEY, P. & WANG, Y. L. 2005. Tissue cells feel and respond to the stiffness of their substrate. *Science,* 310**,** 1139-43.
DOGGRELL, S. A. & BROWN, L. 1998. Rat models of hypertension, cardiac hypertrophy and failure. *Cardiovascular Research,* 39**,** 89-105.
DOLNIKOV, K., SHILKRUT, M., ZEEVI-LEVIN, N., GERECHT-NIR, S., AMIT, M., DANON, A., ITSKOVITZ-ELDOR, J. & BINAH, O. 2006. Functional Properties of Human Embryonic Stem Cell–Derived Cardiomyocytes: Intracellular Ca2+ Handling and the Role of Sarcoplasmic Reticulum in the Contraction. *STEM CELLS,* 24**,** 236-245.
DONG, Z., KENNEDY, S. J. & WU, Y. 2011. Electrospinning materials for energy-related applications and devices. *Journal of Power Sources,* 196**,** 4886-4904.
DROUIN, E., CHARPENTIER, F., GAUTHIER, C., LAURENT, K. & LE MAREC, H. 1995. Electrophysiologic characteristics of cells spanning the left ventricular wall of human heart: Evidence for presence of M cells. *Journal of the American College of Cardiology,* 26**,** 185-192.
DVIR, T., TIMKO, B. P., BRIGHAM, M. D., NAIK, S. R., KARAJANAGI, S. S., LEVY, O., JIN, H., PARKER, K. K., LANGER, R. & KOHANE, D. S. 2011. Nanowired three-dimensional cardiac patches. *Nat Nanotechnol,* 6**,** 720-5.
EBERLE, G., SCHMIDT, H. & EISENMENGER, W. 1996. Piezoelectric polymer electrets. *Dielectrics and Electrical Insulation, IEEE Transactions on,* 3**,** 624-646.
ENGELMAYR, G. C., JR., CHENG, M., BETTINGER, C. J., BORENSTEIN, J. T., LANGER, R. & FREED, L. E. 2008. Accordion-like honeycombs for tissue engineering of cardiac anisotropy. *Nat Mater,* 7**,** 1003-10.
ENGLER, A. J., CARAG-KRIEGER, C., JOHNSON, C. P., RAAB, M., TANG, H. Y., SPEICHER, D. W., SANGER, J. W., SANGER, J. M. & DISCHER, D. E. 2008.

Embryonic cardiomyocytes beat best on a matrix with heart-like elasticity: scar-like rigidity inhibits beating. *J Cell Sci,* 121**,** 3794-802.
ENGLER, A. J., SEN, S., SWEENEY, H. L. & DISCHER, D. E. 2006. Matrix Elasticity Directs Stem Cell Lineage Specification. *Cell,* 126**,** 677-689.
ESCHENHAGEN, T., FINK, C., REMMERS, U., SCHOLZ, H., WATTCHOW, J., WEIL, J., ZIMMERMANN, W., DOHMEN, H. H., SCHAFER, H., BISHOPRIC, N., WAKATSUKI, T. & ELSON, E. L. 1997. Three-dimensional reconstitution of embryonic cardiomyocytes in a collagen matrix: a new heart muscle model system. *Faseb j,* 11**,** 683-94.
ESCHENHAGEN, T. & ZIMMERMANN, W. H. 2005. Engineering myocardial tissue. *Circ Res,* 97**,** 1220-31.
ESCOBAR, A. L., RIBEIRO-COSTA, R., VILLALBA-GALEA, C., ZOGHBI, M. E., PÉREZ, C. G. & MEJÍA-ALVAREZ, R. 2004. Developmental changes of intracellular Ca2+ transients in beating rat hearts. *American Journal of Physiology - Heart and Circulatory Physiology,* 286**,** H971-H978.
FAST, V. G. & KLÉBER, A. G. 1995. Cardiac tissue geometry as a determinant of unidirectional conduction block: assessment of microscopic excitation spread by optical mapping in patterned cell cultures and in a computer model. *Cardiovascular Research,* 29**,** 697-707.
FEINBERG, A. W., FEIGEL, A., SHEVKOPLYAS, S. S., SHEEHY, S., WHITESIDES, G. M. & PARKER, K. K. 2007. Muscular Thin Films for Building Actuators and Powering Devices. *Science,* 317**,** 1366-1370.
FENG, Z., MATSUMOTO, T., NOMURA, Y. & NAKAMURA, T. 2005. An electro-tensile bioreactor for 3-D culturing of cardiomyocytes. A bioreactor system that simulates the myocardium's electrical and mechanical response in vivo. *IEEE Eng Med Biol Mag,* 24**,** 73-9.
FINE, E. G., VALENTINI, R. F., BELLAMKONDA, R. & AEBISCHER, P. 1991. Improved Nerve Regeneration through Piezoelectric Vinylidenefluoride-Trifluoroethylene Copolymer Guidance Channels. *Biomaterials,* 12**,** 775-780.
FINK, C., ERGUN, S., KRALISCH, D., REMMERS, U., WEIL, J. & ESCHENHAGEN, T. 2000. Chronic stretch of engineered heart tissue induces hypertrophy and functional improvement. *FASEB J,* 14**,** 669-79.
FOLMES, C. D. L., NELSON, T. J., DZEJA, P. P. & TERZIC, A. 2012. Energy metabolism plasticity enables stemness programs. *Annals of the New York Academy of Sciences,* 1254**,** 82-89.
FREEDMAN, B. R., BADE, N. D., RIGGIN, C. N., ZHANG, S., HAINES, P. G., ONG, K. L. & JANMEY, P. A. 2015. The (dys)functional extracellular matrix. *Biochimica et Biophysica Acta (BBA) - Molecular Cell Research*.
FRIAS, C., REIS, J., CAPELA E SILVA, F., POTES, J., SIMÕES, J. & MARQUES, A. T. 2010. Polymeric piezoelectric actuator substrate for osteoblast mechanical stimulation. *Journal of Biomechanics,* 43**,** 1061-1066.
FRITZSCHE, M., FREDRIKSSON, J. M., CARLSSON, M. & MANDENIUS, C.-F. 2009. A cell-based sensor system for toxicity testing using multiwavelength fluorescence spectroscopy. *Analytical Biochemistry,* 387**,** 271-275.
FROST, B. M., EKSBORG, S., BJORK, O., ABRAHAMSSON, J., BEHRENDTZ, M., CASTOR, A., FORESTIER, E. & LONNERHOLM, G. 2002. Pharmacokinetics of doxorubicin in children with acute lymphoblastic leukemia: multi-institutional collaborative study. *Med Pediatr Oncol,* 38**,** 329-37.
FUJIE, T., AHADIAN, S., LIU, H., CHANG, H., OSTROVIDOV, S., WU, H., BAE, H., NAKAJIMA, K., KAJI, H. & KHADEMHOSSEINI, A. 2013. Engineered nanomembranes for directing cellular organization toward flexible biodevices. *Nano Lett,* 13**,** 3185-92.

FUJIMOTO, K. L., MA, Z., NELSON, D. M., HASHIZUME, R., GUAN, J., TOBITA, K. & WAGNER, W. R. 2009. Synthesis, characterization and therapeutic efficacy of a biodegradable, thermoresponsive hydrogel designed for application in chronic infarcted myocardium. *Biomaterials,* 30**,** 4357-68.

FUKADA, E. & YASUDA, L. 1957. On the Piezoelectric Effect of Bone. *J. Phys. Soc. Japan,* 12.

FURUKAWA, T. 1989. Piezoelectricity and pyroelectricity in polymers. *Electrical Insulation, IEEE Transactions on,* 24**,** 375-394.

GABRIELSON, K., BEDJA, D., PIN, S., TSAO, A., GAMA, L., YUAN, B. & MURATORE, N. 2007. Heat Shock Protein 90 and ErbB2 in the Cardiac Response to Doxorubicin Injury. *Cancer Research,* 67**,** 1436-1441.

GALIE, P. A., BYFIELD, F. J., CHEN, C. S., KRESH, J. Y. & JANMEY, P. A. 2015. Mechanically Stimulated Contraction of Engineered Cardiac Constructs Using a Microcantilever. *Biomedical Engineering, IEEE Transactions on,* 62**,** 438-442.

GASPAR, J. A., DOSS, M. X., HENGSTLER, J. G., CADENAS, C., HESCHELER, J. & SACHINIDIS, A. 2014. Unique Metabolic Features of Stem Cells, Cardiomyocytes, and Their Progenitors. *Circulation Research,* 114**,** 1346-1360.

GERDES, A. M., KELLERMAN, S. E., MOORE, J. A., MUFFLY, K. E., CLARK, L. C., REAVES, P. Y., MALEC, K. B., MCKEOWN, P. P. & SCHOCKEN, D. D. 1992. Structural remodeling of cardiac myocytes in patients with ischemic cardiomyopathy. *Circulation,* 86**,** 426-30.

GERECHT-NIR, S., RADISIC, M., PARK, H., CANNIZZARO, C., BOUBLIK, J., LANGER, R. & VUNJAK-NOVAKOVIC, G. 2006. Biophysical regulation during cardiac development and application to tissue engineering. *Int J Dev Biol,* 50**,** 233-43.

GERSHLAK, J. R., RESNIKOFF, J. I. N., SULLIVAN, K. E., WILLIAMS, C., WANG, R. M. & BLACK III, L. D. 2013. Mesenchymal stem cells ability to generate traction stress in response to substrate stiffness is modulated by the changing extracellular matrix composition of the heart during development. *Biochemical and Biophysical Research Communications,* 439**,** 161-166.

GIANNI, L., HERMAN, E. H., LIPSHULTZ, S. E., MINOTTI, G., SARVAZYAN, N. & SAWYER, D. B. 2008. Anthracycline Cardiotoxicity: From Bench to Bedside. *Journal of clinical oncology : official journal of the American Society of Clinical Oncology,* 26**,** 3777-3784.

GIRAUD, M. N., ARMBRUSTER, C., CARREL, T. & TEVAEARAI, H. T. 2007. Current state of the art in myocardial tissue engineering. *Tissue Eng,* 13**,** 1825-36.

GOLDSMITH, E. C., BRADSHAW, A. D., ZILE, M. R. & SPINALE, F. G. 2014. Myocardial Fibroblast-Matrix Interactions and Potential Therapeutic Targets. *Journal of molecular and cellular cardiology,* 0**,** 92-99.

GOORMAGHTIGH, E., CHATELAIN, P., CASPERS, J. & RUYSSCHAERT, J. M. 1980. Evidence of a complex between adriamycin derivatives and cardiolipin: Possible role in cardiotoxicity. *Biochemical Pharmacology,* 29**,** 3003-3010.

GOURDIE, R., GREEN, C., SEVERS, N. & THOMPSON, R. 1992. Immunolabelling patterns of gap junction connexins in the developing and mature rat heart. *Anatomy and Embryology,* 185**,** 363-378.

GRECO, F., ZUCCA, A., TACCOLA, S., MENCIASSI, A., FUJIE, T., HANIUDA, H., TAKEOKA, S., DARIO, P. & MATTOLI, V. 2011. Ultra-thin conductive free-standing PEDOT/PSS nanofilms. *Soft Matter,* 7**,** 10642-10650.

GUNATILLAKE, P., MAYADUNNE, R. & ADHIKARI, R. 2006. Recent developments in biodegradable synthetic polymers. *Biotechnol Annu Rev,* 12**,** 301-47.

GUO, H.-F., LI, Z.-S., DONG, S.-W., CHEN, W.-J., DENG, L., WANG, Y.-F. & YING, D.-J. 2012. Piezoelectric PU/PVDF electrospun scaffolds for wound healing applications. *Colloids and Surfaces B: Biointerfaces,* 96**,** 29-36.

GUO, W., KAMIYA, K. & TOYAMA, J. 1996. Modulated expression of transient outward current in cultured neonatal rat ventricular myocytes: comparison with development in situ. *Cardiovascular Research,* 32**,** 524-533.
GWATHMEY, J. K., TSAIOUN, K. & HAJJAR, R. J. 2009. Cardionomics: a new integrative approach for screening cardiotoxicity of drug candidates. *Expert Opin Drug Metab Toxicol,* 5**,** 647-60.
HANSEN, A., EDER, A., BONSTRUP, M., FLATO, M., MEWE, M., SCHAAF, S., AKSEHIRLIOGLU, B., SCHWOERER, A. P., UEBELER, J. & ESCHENHAGEN, T. 2010. Development of a drug screening platform based on engineered heart tissue. *Circ Res,* 107**,** 35-44.
HASENFUSS, G., MULIERI, L. A., BLANCHARD, E. M., HOLUBARSCH, C., LEAVITT, B. J., ITTLEMAN, F. & ALPERT, N. R. 1991. Energetics of isometric force development in control and volume-overload human myocardium. Comparison with animal species. *Circulation Research,* 68**,** 836-46.
HIRT, M. N., BOEDDINGHAUS, J., MITCHELL, A., SCHAAF, S., BÖRNCHEN, C., MÜLLER, C., SCHULZ, H., HUBNER, N., STENZIG, J., STOEHR, A., NEUBER, C., EDER, A., LUTHER, P. K., HANSEN, A. & ESCHENHAGEN, T. 2014a. Functional improvement and maturation of rat and human engineered heart tissue by chronic electrical stimulation. *Journal of Molecular and Cellular Cardiology,* 74**,** 151-161.
HIRT, M. N., HANSEN, A. & ESCHENHAGEN, T. 2014b. Cardiac tissue engineering: state of the art. *Circ Res,* 114**,** 354-67.
HIRT, M. N., SÖRENSEN, N. A., BARTHOLDT, L. M., BOEDDINGHAUS, J., SCHAAF, S., EDER, A., VOLLERT, I., STÖHR, A., SCHULZE, T., WITTEN, A., STOLL, M., HANSEN, A. & ESCHENHAGEN, T. 2012. Increased afterload induces pathological cardiac hypertrophy: a new in vitro model. *Basic Research in Cardiology,* 107**,** 307.
HOWARD, C. M. & BAUDINO, T. A. 2014. Dynamic cell–cell and cell–ECM interactions in the heart. *Journal of Molecular and Cellular Cardiology,* 70**,** 19-26.
HOYT, R. H., COHEN, M. L. & SAFFITZ, J. E. 1989. Distribution and three-dimensional structure of intercellular junctions in canine myocardium. *Circulation Research,* 64**,** 563-74.
HSUEH, W. A., LAW, R. E. & DO, Y. S. 1998. Integrins, Adhesion, and Cardiac Remodeling. *Hypertension,* 31**,** 176-180.
ICHIKAWA, Y., GHANEFAR, M., BAYEVA, M., WU, R. X., KHECHADURI, A., PRASAD, S. V. N., MUTHARASAN, R. K., NAIK, T. J. & ARDEHALI, H. 2014. Cardiotoxicity of doxorubicin is mediated through mitochondrial iron accumulation. *Journal of Clinical Investigation,* 124**,** 617-630.
ISHII, O., SHIN, M., SUEDA, T. & VACANTI, J. P. 2005. In vitro tissue engineering of a cardiac graft using a degradable scaffold with an extracellular matrix–like topography. *The Journal of Thoracic and Cardiovascular Surgery,* 130**,** 1358-1363.
ISHISAKA, T., SATO, H., AKIYAMA, Y., FURUKAWA, Y. & MORISHIMA, K. Muscle-actuated power generator using cultured cardiomyocytes and pzt fiber. Engineering in Medicine and Biology Society, 2006. EMBS '06. 28th Annual International Conference of the IEEE, Aug. 30 2006-Sept. 3 2006 2006. 6685-6688.
ISKRATSCH, T., WOLFENSON, H. & SHEETZ, M. P. 2014. Appreciating force and shape [mdash] the rise of mechanotransduction in cell biology. *Nat Rev Mol Cell Biol,* 15**,** 825-833.
ITZHAKI, I., RAPOPORT, S., HUBER, I., MIZRAHI, I., ZWI-DANTSIS, L., ARBEL, G., SCHILLER, J. & GEPSTEIN, L. 2011. Calcium Handling in Human Induced Pluripotent Stem Cell Derived Cardiomyocytes. *PLoS ONE,* 6**,** e18037.

IVASHCHENKO, C. Y., PIPES, G. C., LOZINSKAYA, I. M., LIN, Z., XIAOPING, X., NEEDLE, S., GRYGIELKO, E. T., HU, E., TOOMEY, J. R., LEPORE, J. J. & WILLETTE, R. N. 2013. Human-induced pluripotent stem cell-derived cardiomyocytes exhibit temporal changes in phenotype. *American Journal of Physiology - Heart and Circulatory Physiology,* 305**,** H913-H922.

IYER, R. K., CHIU, L. L. & RADISIC, M. 2009. Microfabricated poly(ethylene glycol) templates enable rapid screening of triculture conditions for cardiac tissue engineering. *J Biomed Mater Res A,* 89**,** 616-31.

JACOT, J. G., KITA-MATSUO, H., WEI, K. A., CHEN, H. S., OMENS, J. H., MERCOLA, M. & MCCULLOCH, A. D. 2010. Cardiac myocyte force development during differentiation and maturation. *Ann N Y Acad Sci,* 1188**,** 121-7.

JAWAD, H., LYON, A. R., HARDING, S. E., ALI, N. N. & BOCCACCINI, A. R. 2008. Myocardial tissue engineering. *Br Med Bull,* 87**,** 31-47.

JIANG, X. J., WANG, T., LI, X. Y., WU, D. Q., ZHENG, Z. B., ZHANG, J. F., CHEN, J. L., PENG, B., JIANG, H., HUANG, C. & ZHANG, X. Z. 2009. Injection of a novel synthetic hydrogel preserves left ventricle function after myocardial infarction. *J Biomed Mater Res A,* 90**,** 472-7.

JUGDUTT, B. I. 2003. Ventricular remodeling after infarction and the extracellular collagen matrix: when is enough enough? *Circulation,* 108**,** 1395-403.

JUN, I., JEONG, S. & SHIN, H. 2009. The stimulation of myoblast differentiation by electrically conductive sub-micron fibers. *Biomaterials,* 30**,** 2038-2047.

KAI, D., PRABHAKARAN, M. P., JIN, G. & RAMAKRISHNA, S. 2011. Guided orientation of cardiomyocytes on electrospun aligned nanofibers for cardiac tissue engineering. *Journal of Biomedical Materials Research Part B: Applied Biomaterials,* 98B**,** 379-386.

KAMAKURA, T., MAKIYAMA, T., SASAKI, K., YOSHIDA, Y., WURIYANGHAI, Y., CHEN, J., HATTORI, T., OHNO, S., KITA, T., HORIE, M., YAMANAKA, S. & KIMURA, T. 2013. Ultrastructural maturation of human-induced pluripotent stem cell-derived cardiomyocytes in a long-term culture. *Circ J,* 77**,** 1307-14.

KAMKIN, A., KISELEVA, I., LOZINSKY, I. & SCHOLZ, H. 2005. Electrical interaction of mechanosensitive fibroblasts and myocytes in the heart. *Basic Research in Cardiology,* 100**,** 337-345.

KANNANKERIL, P. J. & RODEN, D. M. 2007. Drug-induced long QT and torsade de pointes: recent advances. *Curr Opin Cardiol,* 22**,** 39-43.

KASHFI, K., ISRAEL, M., SWEATMAN, T. W., SESHADRI, R. & COOK, G. A. 1990. Inhibition of mitochondrial carnitine palmitoyltransferases by adriamycin and adriamycin analogues. *Biochemical Pharmacology,* 40**,** 1441-1448.

KENSAH, G., ROA LARA, A., DAHLMANN, J., ZWEIGERDT, R., SCHWANKE, K., HEGERMANN, J., SKVORC, D., GAWOL, A., AZIZIAN, A., WAGNER, S., MAIER, L. S., KRAUSE, A., DRAGER, G., OCHS, M., HAVERICH, A., GRUH, I. & MARTIN, U. 2013. Murine and human pluripotent stem cell-derived cardiac bodies form contractile myocardial tissue in vitro. *Eur Heart J,* 34**,** 1134-46.

KEUNG, W., BOHELER, K. R. & LI, R. A. 2014. Developmental cues for the maturation of metabolic, electrophysiological and calcium handling properties of human pluripotent stem cell-derived cardiomyocytes. *Stem Cell Res Ther,* 5**,** 17.

KHADEMHOSSEINI, A., ENG, G., YEH, J., KUCHARCZYK, P. A., LANGER, R., VUNJAK-NOVAKOVIC, G. & RADISIC, M. 2007. Microfluidic patterning for fabrication of contractile cardiac organoids. *Biomed Microdevices,* 9**,** 149-57.

KHOLKIN, A., AMDURSKY, N., BDIKIN, I., GAZIT, E. & ROSENMAN, G. 2010. Strong piezoelectricity in bioinspired peptide nanotubes. *ACS Nano,* 4**,** 610-4.

KHOLKIN, A. L., PERTSEV, N. A. & GOLTSEV, A. V. 2008. Piezoelectricity and Crystal Symmetry. *In:* SAFARI, A. & AKDOĞAN, E. K. (eds.) *Piezoelectric and Acoustic Materials for Transducer Applications.* Springer US.

KIM, D. H., LIPKE, E. A., KIM, P., CHEONG, R., THOMPSON, S., DELANNOY, M., SUH, K. Y., TUNG, L. & LEVCHENKO, A. 2010. Nanoscale cues regulate the structure and function of macroscopic cardiac tissue constructs. *Proc Natl Acad Sci U S A,* 107**,** 565-70.

KIM, H. N., JIAO, A., HWANG, N. S., KIM, M. S., KANG, D. H., KIM, D.-H. & SUH, K.-Y. 2013. Nanotopography-guided tissue engineering and regenerative medicine. *Advanced Drug Delivery Reviews,* 65**,** 536-558.

KIM, M., PARK, S. R. & CHOI, B. H. 2014. Biomaterial scaffolds used for the regeneration of spinal cord injury (SCI). *Histol Histopathol,* 29**,** 1395-408.

KLÉBER, A. G. 2014. 27 - Intercellular Communication and Impulse Propagation. *In:* JALIFE, D. P. Z. (ed.) *Cardiac Electrophysiology: From Cell to Bedside (Sixth Edition).* Philadelphia: W.B. Saunders.

KLÉBER, A. G. & RUDY, Y. 2004. Basic Mechanisms of Cardiac Impulse Propagation and Associated Arrhythmias. *Physiological Reviews,* 84**,** 431-488.

KLUGE, J., LEISK, G., CARDWELL, R., FERNANDES, A., HOUSE, M., WARD, A., DORFMANN, A. L. & KAPLAN, D. 2011. Bioreactor System Using Noninvasive Imaging and Mechanical Stretch for Biomaterial Screening. *Annals of Biomedical Engineering,* 39**,** 1390-1402.

KOCHERVINSKII, V. V. 2003. Piezoelectricity in crystallizing ferroelectric polymers: Poly(vinylidene fluoride) and its copolymers (A review). *Crystallography Reports,* 48**,** 649-675.

KOHL, P., CAMELLITI, P., BURTON, F. L. & SMITH, G. L. 2005. Electrical coupling of fibroblasts and myocytes: relevance for cardiac propagation. *Journal of Electrocardiology,* 38**,** 45-50.

KOLA, I. & LANDIS, J. 2004. Can the pharmaceutical industry reduce attrition rates? *Nat Rev Drug Discov,* 3**,** 711-716.

KOLWICZ, S. C., PUROHIT, S. & TIAN, R. 2013. Cardiac Metabolism and its Interactions With Contraction, Growth, and Survival of Cardiomyocytes. *Circulation Research,* 113**,** 603-616.

KOMURO, I., KUDO, S., YAMAZAKI, T., ZOU, Y., SHIOJIMA, I. & YAZAKI, Y. 1996. Mechanical stretch activates the stress-activated protein kinases in cardiac myocytes. *The FASEB Journal,* 10**,** 631-6.

KOSTIN, S., RIEGER, M., DAMMER, S., HEIN, S., RICHTER, M., KLÖVEKORN, W.-P., BAUER, E. & SCHAPER, J. 2003. Gap junction remodeling and altered connexin43 expression in the failing human heart. *Molecular and Cellular Biochemistry,* 242**,** 135-144.

KRAEHENBUEHL, T. P., FERREIRA, L. S., HAYWARD, A. M., NAHRENDORF, M., VAN DER VLIES, A. J., VASILE, E., WEISSLEDER, R., LANGER, R. & HUBBELL, J. A. 2011. Human embryonic stem cell-derived microvascular grafts for cardiac tissue preservation after myocardial infarction. *Biomaterials,* 32**,** 1102-9.

KREUTZER, J., IKONEN, L., HIRVONEN, J., PEKKANEN-MATTILA, M., AALTO-SETÄLÄ, K. & KALLIO, P. Pneumatic cell stretching system for cardiac differentiation and culture. *Medical Engineering and Physics,* 36**,** 496-501.

KWAK, H.-B. 2013. Aging, exercise, and extracellular matrix in the heart. *Journal of exercise rehabilitation,* 9**,** 338-347.

LAFLAMME, M. A. & MURRY, C. E. 2011. Heart regeneration. *Nature,* 473**,** 326-35.

LEE, H., RHO, J. & MESSERSMITH, P. B. 2009. Facile Conjugation of Biomolecules onto Surfaces via Mussel Adhesive Protein Inspired Coatings. *Adv Mater,* 21**,** 431-434.

LEE, J., CUDDIHY, M. J. & KOTOV, N. A. 2008. Three-Dimensional Cell Culture Matrices: State of the Art. *Tissue Engineering Part B: Reviews,* 14**,** 61-86.
LEE, Y.-S., COLLINS, G. & LIVINGSTON ARINZEH, T. 2011. Neurite extension of primary neurons on electrospun piezoelectric scaffolds. *Acta Biomaterialia,* 7**,** 3877-3886.
LEE, Y.-S. & LIVINGSTON ARINZEH, T. 2011. Electrospun Nanofibrous Materials for Neural Tissue Engineering. *Polymers,* 3**,** 413-426.
LEGANT, W. R., PATHAK, A., YANG, M. T., DESHPANDE, V. S., MCMEEKING, R. M. & CHEN, C. S. 2009. Microfabricated tissue gauges to measure and manipulate forces from 3D microtissues. *Proceedings of the National Academy of Sciences,* 106**,** 10097-10102.
LEYCHENKO, A., KONOREV, E., JIJIWA, M. & MATTER, M. L. 2011. Stretch-induced hypertrophy activates NFkB-mediated VEGF secretion in adult cardiomyocytes. *PLoS ONE,* 6**,** e29055.
LI, F., WANG, X., CAPASSO, J. M. & GERDES, A. M. 1996a. Rapid Transition of Cardiac Myocytes from Hyperplasia to Hypertrophy During Postnatal Development. *Journal of Molecular and Cellular Cardiology,* 28**,** 1737-1746.
LI, F., WANG, X., CAPASSO, J. M. & GERDES, A. M. 1996b. Rapid transition of cardiac myocytes from hyperplasia to hypertrophy during postnatal development. *J Mol Cell Cardiol,* 28**,** 1737-46.
LI, M., MONDRINOS, M. J., GANDHI, M. R., KO, F. K., WEISS, A. S. & LELKES, P. I. 2005. Electrospun protein fibers as matrices for tissue engineering. *Biomaterials,* 26**,** 5999-6008.
LI, R. K., YAU, T. M., WEISEL, R. D., MICKLE, D. A., SAKAI, T., CHOI, A. & JIA, Z. Q. 2000. Construction of a bioengineered cardiac graft. *J Thorac Cardiovasc Surg,* 119**,** 368-75.
LI, S. C., WANG, L., JIANG, H., ACEVEDO, J., CHANG, A. C. & LOUDON, W. G. 2009. Stem cell engineering for treatment of heart diseases: potentials and challenges. *Cell Biol Int,* 33**,** 255-67.
LIAN, L. & SOTTOS, N. R. 2000. Effects of thickness on the piezoelectric and dielectric properties of lead zirconate titanate thin films. *Journal of Applied Physics,* 87**,** 3941-3949.
LIAU, B., ZHANG, D. & BURSAC, N. 2012. Functional cardiac tissue engineering. *Regen Med,* 7**,** 187-206.
LIN, F. & WORMAN, H. J. 1993. Structural organization of the human gene encoding nuclear lamin A and nuclear lamin C. *J Biol Chem,* 268**,** 16321-6.
LIU, J., SUN, N., BRUCE, M. A., WU, J. C. & BUTTE, M. J. 2012a. Atomic Force Mechanobiology of Pluripotent Stem Cell-Derived Cardiomyocytes. *PLoS ONE,* 7**,** e37559.
LIU, W., YASUI, K., OPTHOF, T., ISHIKI, R., LEE, J.-K., KAMIYA, K., YOKOTA, M. & KODAMA, I. 2002. Developmental changes of Ca2+ handling in mouse ventricular cells from early embryo to adulthood. *Life Sciences,* 71**,** 1279-1292.
LIU, X., HOLZWARTH, J. M. & MA, P. X. 2012b. Functionalized synthetic biodegradable polymer scaffolds for tissue engineering. *Macromol Biosci,* 12**,** 911-9.
LIU, X., WANG, X., ZHAO, H. & DU, Y. 2014. Myocardial Cell Pattern on Piezoelectric Nanofiber Mats for Energy Harvesting. *Journal of Physics: Conference Series,* 557**,** 012057.
LOCKHART, M., WIRRIG, E., PHELPS, A. & WESSELS, A. 2011. Extracellular matrix and heart development. *Birth Defects Research Part A: Clinical and Molecular Teratology,* 91**,** 535-550.
LOE, M. J. & EDWARDS, W. D. 2004. A light-hearted look at a lion-hearted organ (or, a perspective from three standard deviations beyond the norm). Part 1 (of two parts). *Cardiovasc Pathol,* 13**,** 282-92.

LOPASCHUK, G. D. & JASWAL, J. S. 2010. Energy metabolic phenotype of the cardiomyocyte during development, differentiation, and postnatal maturation. *J Cardiovasc Pharmacol,* 56**,** 130-40.
LOUCH, W. E., SHEEHAN, K. A. & WOLSKA, B. M. 2011. Methods in Cardiomyocyte Isolation, Culture, and Gene Transfer. *Journal of molecular and cellular cardiology,* 51**,** 288-298.
LU, T., LI, Y. & CHEN, T. 2013. Techniques for fabrication and construction of three-dimensional scaffolds for tissue engineering. *International Journal of Nanomedicine,* 8**,** 337-350.
LUNDY, S. D., ZHU, W. Z., REGNIER, M. & LAFLAMME, M. A. 2013. Structural and functional maturation of cardiomyocytes derived from human pluripotent stem cells. *Stem Cells Dev,* 22**,** 1991-2002.
LUSIOLA, T., HUSSAIN, A., KIM, M., GRAULE, T. & CLEMENS, F. 2015. Ferroelectric KNNT Fibers by Thermoplastic Extrusion Process: Microstructure and Electromechanical Characterization. *Actuators,* 4**,** 99.
MACKENNA, D. A., DOLFI, F., VUORI, K. & RUOSLAHTI, E. 1998. Extracellular signal-regulated kinase and c-Jun NH2-terminal kinase activation by mechanical stretch is integrin-dependent and matrix-specific in rat cardiac fibroblasts. *Journal of Clinical Investigation,* 101**,** 301-310.
MAIDHOF, R., TANDON, N., LEE, E. J., LUO, J., DUAN, Y., YEAGER, K., KONOFAGOU, E. & VUNJAK-NOVAKOVIC, G. 2012. Biomimetic perfusion and electrical stimulation applied in concert improved the assembly of engineered cardiac tissue. *Journal of tissue engineering and regenerative medicine,* 6**,** e12-e23.
MALHOTRA, R., D'SOUZA, K. M., STARON, M. L., BIRUKOV, K. G., BODI, I. & AKHTER, S. A. 2010. Gαq-mediated Activation of GRK2 by Mechanical Stretch in Cardiac Myocytes: THE ROLE OF PROTEIN KINASE C. *Journal of Biological Chemistry,* 285**,** 13748-13760.
MANDAL, D., YOON, S. & KIM, K. J. 2011a. Origin of piezoelectricity in an electrospun poly(vinylidene fluoride-trifluoroethylene) nanofiber web-based nanogenerator and nano-pressure sensor. *Macromol Rapid Commun,* 32**,** 831-7.
MANDAL, D., YOON, S. & KIM, K. J. 2011b. Origin of Piezoelectricity in an Electrospun Poly(vinylidene fluoride-trifluoroethylene) Nanofiber Web-Based Nanogenerator and Nano-Pressure Sensor. *Macromolecular Rapid Communications,* 32**,** 831-837.
MANDENIUS, C. F., STEEL, D., NOOR, F., MEYER, T., HEINZLE, E., ASP, J., ARAIN, S., KRAUSHAAR, U., BREMER, S., CLASS, R. & SARTIPY, P. 2011. Cardiotoxicity testing using pluripotent stem cell-derived human cardiomyocytes and state-of-the-art bioanalytics: a review. *J Appl Toxicol,* 31**,** 191-205.
MANSO, A. M., ELSHERIF, L., KANG, S.-M. & ROSS, R. S. 2006. Integrins, membrane-type matrix metalloproteinases and ADAMs: Potential implications for cardiac remodeling. *Cardiovascular Research,* 69**,** 574-584.
MARINO, A. & BECKER, R. O. 1970. Piezoelectric effect and growth control in bone. *Nature,* 228**,** 473-4.
MARQUEZ-ROSADO, L., SOLAN, J. L., DUNN, C. A., NORRIS, R. P. & LAMPE, P. D. 2012. Connexin43 phosphorylation in brain, cardiac, endothelial and epithelial tissues. *Biochim Biophys Acta,* 1818**,** 1985-92.
MARSANO, A., MAIDHOF, R., WAN, L. Q., WANG, Y., GAO, J., TANDON, N. & VUNJAK-NOVAKOVIC, G. 2010. Scaffold stiffness affects the contractile function of three-dimensional engineered cardiac constructs. *Biotechnol Prog,* 26**,** 1382-90.
MARTINS, A. M., ENG, G., CARIDADE, S. G., MANO, J. F., REIS, R. L. & VUNJAK-NOVAKOVIC, G. 2014. Electrically Conductive Chitosan/Carbon Scaffolds for Cardiac Tissue Engineering. *Biomacromolecules,* 15**,** 635-643.

MARTINS, P. M., RIBEIRO, S., RIBEIRO, C., SENCADAS, V., GOMES, A. C., GAMA, F. M. & LANCEROS-MENDEZ, S. 2013. Effect of poling state and morphology of piezoelectric poly(vinylidene fluoride) membranes for skeletal muscle tissue engineering. *RSC Advances,* 3**,** 17938-17944.

MATHUR, A., LOSKILL, P., SHAO, K., HUEBSCH, N., HONG, S., MARCUS, S. G., MARKS, N., MANDEGAR, M., CONKLIN, B. R., LEE, L. P. & HEALY, K. E. 2015. Human iPSC-based cardiac microphysiological system for drug screening applications. *Sci Rep,* 5**,** 8883.

MCCAIN, M. L., LEE, H., ARATYN-SCHAUS, Y., KLÉBER, A. G. & PARKER, K. K. 2012. Cooperative coupling of cell-matrix and cell–cell adhesions in cardiac muscle. *Proceedings of the National Academy of Sciences,* 109**,** 9881-9886.

MCDEVITT, T. C., WOODHOUSE, K. A., HAUSCHKA, S. D., MURRY, C. E. & STAYTON, P. S. 2003. Spatially organized layers of cardiomyocytes on biodegradable polyurethane films for myocardial repair. *J Biomed Mater Res A,* 66**,** 586-95.

MCDONALD, T. F., SACHS, H. G. & DEHAAN, R. L. 1972. Development of sensitivity to tetrodotoxin in beating chick embryo hearts, single cells, and aggregates. *Science,* 176**,** 1248-50.

MCDONOUGH, P. M. & GLEMBOTSKI, C. C. 1992. Induction of atrial natriuretic factor and myosin light chain-2 gene expression in cultured ventricular myocytes by electrical stimulation of contraction. *Journal of Biological Chemistry,* 267**,** 11665-11668.

MIKLAS, J. W., NUNES, S. S., SOFLA, A., REIS, L. A., PAHNKE, A., XIAO, Y., LASCHINGER, C. & RADISIC, M. 2014. Bioreactor for modulation of cardiac microtissue phenotype by combined static stretch and electrical stimulation. *Biofabrication,* 6**,** 024113-024113.

MONTESSUIT, C., PALMA, T., VIGLINO, C., PELLIEUX, C. & LERCH, R. 2006. Effects of insulin-like growth factor-I on the maturation of metabolism in neonatal rat cardiomyocytes. *Pflügers Archiv,* 452**,** 380-386.

MORAES, C., SUN, Y. & SIMMONS, C. A. 2011. (Micro)managing the mechanical microenvironment. *Integr Biol (Camb),* 3**,** 959-71.

MORDWINKIN, N. M., BURRIDGE, P. W. & WU, J. C. 2013. A review of human pluripotent stem cell-derived cardiomyocytes for high-throughput drug discovery, cardiotoxicity screening, and publication standards. *J Cardiovasc Transl Res,* 6**,** 22-30.

MORENO, A. P. 2004. Biophysical properties of homomeric and heteromultimeric channels formed by cardiac connexins. *Cardiovascular Research,* 62**,** 276-286.

MORGAN, K. Y. & BLACK, L. D. 2014. Mimicking Isovolumic Contraction with Combined Electromechanical Stimulation Improves the Development of Engineered Cardiac Constructs. *Tissue Engineering. Part A,* 20**,** 1654-1667.

MOSCONA, A. A. 1959. Tissues from dissociated cells. *Sci Am,* 200**,** 132-4 passim.

MOTLAGH, D., HARTMAN, T. J., DESAI, T. A. & RUSSELL, B. 2003. Microfabricated grooves recapitulate neonatal myocyte connexin43 and N-cadherin expression and localization. *J Biomed Mater Res A,* 67**,** 148-57.

MURPHY, C. M., MATSIKO, A., HAUGH, M. G., GLEESON, J. P. & O'BRIEN, F. J. 2012. Mesenchymal stem cell fate is regulated by the composition and mechanical properties of collagen–glycosaminoglycan scaffolds. *Journal of the Mechanical Behavior of Biomedical Materials,* 11**,** 53-62.

NADAL-GINARD, B. & MAHDAVI, V. 1989. Molecular basis of cardiac performance. Plasticity of the myocardium generated through protein isoform switches. *Journal of Clinical Investigation,* 84**,** 1693-1700.

NAIR, L. S. & LAURENCIN, C. T. 2006. Polymers as biomaterials for tissue engineering and controlled drug delivery. *Adv Biochem Eng Biotechnol,* 102**,** 47-90.

NAITO, H., MELNYCHENKO, I., DIDIE, M., SCHNEIDERBANGER, K., SCHUBERT, P., ROSENKRANZ, S., ESCHENHAGEN, T. & ZIMMERMANN, W. H. 2006. Optimizing engineered heart tissue for therapeutic applications as surrogate heart muscle. *Circulation,* 114**,** I72-8.

NAKAYAMA, K. H., HOU, L. & HUANG, N. F. 2014. Role of Extracellular Matrix Signaling Cues in Modulating Cell Fate Commitment for Cardiovascular Tissue Engineering. *Advanced healthcare materials,* 3**,** 628-641.

NALWA, H. 1995. *Ferroelectric Polymers: Chemistry: Physics, and Applications,* New York, Marcel Dekker.

NAWROTH, J. C., LEE, H., FEINBERG, A. W., RIPPLINGER, C. M., MCCAIN, M. L., GROSBERG, A., DABIRI, J. O. & PARKER, K. K. 2012. A tissue-engineered jellyfish with biomimetic propulsion. *Nat Biotech,* 30**,** 792-797.

NIKLAS, J., SCHNEIDER, K. & HEINZLE, E. 2010. Metabolic flux analysis in eukaryotes. *Current Opinion in Biotechnology,* 21**,** 63-69.

NUNES, S. S., MIKLAS, J. W., LIU, J., ASCHAR-SOBBI, R., XIAO, Y., ZHANG, B., JIANG, J., MASSE, S., GAGLIARDI, M., HSIEH, A., THAVANDIRAN, N., LAFLAMME, M. A., NANTHAKUMAR, K., GROSS, G. J., BACKX, P. H., KELLER, G. & RADISIC, M. 2013. Biowire: a platform for maturation of human pluripotent stem cell-derived cardiomyocytes. *Nat Methods,* 10**,** 781-7.

OBREZTCHIKOVA, M. N. M. N., SOSUNOV, E. A. E. A., PLOTNIKOV, A., ANYUKHOVSKY, E. P. E. P., GAINULLIN, R. Z., DANILO, P., YEOM, Z.-H., ROBINSON, R. B. & ROSEN, M. R. 2003. Developmental changes in IKr and IKs contribute to age-related expression of dofetilide effects on repolarization and proarrhythmia. *Cardiovascular Research,* 59**,** 339-350.

OCTAVIA, Y., TOCCHETTI, C. G., GABRIELSON, K. L., JANSSENS, S., CRIJNS, H. J. & MOENS, A. L. 2012. Doxorubicin-induced cardiomyopathy: from molecular mechanisms to therapeutic strategies. *J Mol Cell Cardiol,* 52**,** 1213-25.

OLIVETTI, G., CIGOLA, E., MAESTRI, R., CORRADI, D., LAGRASTA, C., GAMBERT, S. R. & ANVERSA, P. 1996. Aging, Cardiac Hypertrophy and Ischemic Cardiomyopathy Do Not Affect the Proportion of Mononucleated and Multinucleated Myocytes in the Human Heart. *Journal of Molecular and Cellular Cardiology,* 28**,** 1463-1477.

OLSON, E. N. 2004. A decade of discoveries in cardiac biology. *Nat Med,* 10**,** 467-74.

ORLOVA, Y., MAGOME, N., LIU, L., CHEN, Y. & AGLADZE, K. 2011. Electrospun nanofibers as a tool for architecture control in engineered cardiac tissue. *Biomaterials,* 32**,** 5615-5624.

OTT, H. C., MATTHIESEN, T. S., GOH, S.-K., BLACK, L. D., KREN, S. M., NETOFF, T. I. & TAYLOR, D. A. 2008. Perfusion-decellularized matrix: using nature's platform to engineer a bioartificial heart. *Nat Med,* 14**,** 213-221.

PANKOV, R. & YAMADA, K. M. 2002. Fibronectin at a glance. *Journal of Cell Science,* 115**,** 3861-3863.

PAPKOVSKY, D. B. 2004. Methods in Optical Oxygen Sensing: Protocols and Critical Analyses. *Methods in Enzymology.* Academic Press.

PAPKOVSKY, D. B., HYNES, J. & WILL, Y. 2006. Respirometric Screening Technology for ADME-Tox studies. *Expert Opinion on Drug Metabolism & Toxicology,* 2**,** 313-323.

PARK, G.-T., PARK, C.-S., CHOI, J.-J., LEE, J.-W. & KIM, H.-E. 2006. Effects of Thickness on Piezoelectric Properties of Highly Oriented Lead Zirconate Titanate Films. *Journal of the American Ceramic Society,* 89**,** 2314-2316.

PASSIER, R., ZENG, H., FREY, N., NAYA, F. J., NICOL, R. L., MCKINSEY, T. A., OVERBEEK, P., RICHARDSON, J. A., GRANT, S. R. & OLSON, E. N. 2000. CaM kinase signaling induces cardiac hypertrophy and activates the MEF2 transcription factor in vivo. *Journal of Clinical Investigation,* 105**,** 1395-1406.

PEGO, A. P., VAN LUYN, M. J., BROUWER, L. A., VAN WACHEM, P. B., POOT, A. A., GRIJPMA, D. W. & FEIJEN, J. 2003. In vivo behavior of poly(1,3-trimethylene carbonate) and copolymers of 1,3-trimethylene carbonate with D,L-lactide or epsilon-caprolactone: Degradation and tissue response. *J Biomed Mater Res A,* 67**,** 1044-54.

PERUMAL, S., ANTIPOVA, O. & ORGEL, J. P. R. O. 2008. Collagen fibril architecture, domain organization, and triple-helical conformation govern its proteolysis. *Proceedings of the National Academy of Sciences,* 105**,** 2824-2829.

PHAM, Q. P., SHARMA, U. & MIKOS, A. G. 2006. Electrospinning of polymeric nanofibers for tissue engineering applications: a review. *Tissue Eng,* 12**,** 1197-211.

PIETRONAVE, S., ZAMPERONE, A., OLTOLINA, F., COLANGELO, D., FOLLENZI, A., NOVELLI, E., DIENA, M., PAVESI, A., CONSOLO, F., FIORE, G. B., SONCINI, M. & PRAT, M. 2014. Monophasic and Biphasic Electrical Stimulation Induces a Precardiac Differentiation in Progenitor Cells Isolated from Human Heart. *Stem Cells and Development,* 23**,** 888-898.

PILLEKAMP, F., HAUSTEIN, M., KHALIL, M., EMMELHEINZ, M., NAZZAL, R., ADELMANN, R., NGUEMO, F., RUBENCHYK, O., PFANNKUCHE, K., MATZKIES, M., REPPEL, M., BLOCH, W., BROCKMEIER, K. & HESCHELER, J. 2012. Contractile Properties of Early Human Embryonic Stem Cell-Derived Cardiomyocytes: Beta-Adrenergic Stimulation Induces Positive Chronotropy and Lusitropy but Not Inotropy. *Stem Cells and Development,* 21**,** 2111-2121.

PIQUEREAU, J., CAFFIN, F., NOVOTOVA, M., LEMAIRE, C., VEKSLER, V., GARNIER, A., VENTURA-CLAPIER, R. & JOUBERT, F. 2013. Mitochondrial dynamics in the adult cardiomyocytes: which roles for a highly specialized cell? *Frontiers in Physiology,* 4**,** 102.

POK, S. & JACOT, J. G. 2011. Biomaterials advances in patches for congenital heart defect repair. *J Cardiovasc Transl Res,* 4**,** 646-54.

PORTER, G., HOM, J., HOFFMAN, D., QUINTANILLA, R., DE MESY BENTLEY, K. & SHEU, S. 2011. Bioenergetics, mitochondria, and cardiac myocyte differentiation. *Progress in pediatric cardiology,* 31**,** 75-81.

PORTER, K. E. & TURNER, N. A. 2009. Cardiac fibroblasts: at the heart of myocardial remodeling. *Pharmacol Ther,* 123**,** 255-78.

RADISIC, M. & CHRISTMAN, K. L. 2013. Materials science and tissue engineering: repairing the heart. *Mayo Clin Proc,* 88**,** 884-98.

RADISIC, M., DEEN, W., LANGER, R. & VUNJAK-NOVAKOVIC, G. 2005. Mathematical model of oxygen distribution in engineered cardiac tissue with parallel channel array perfused with culture medium containing oxygen carriers. *Am J Physiol Heart Circ Physiol,* 288**,** H1278-89.

RADISIC, M., EULOTH, M., YANG, L., LANGER, R., FREED, L. E. & VUNJAK-NOVAKOVIC, G. 2003. High-density seeding of myocyte cells for cardiac tissue engineering. *Biotechnol Bioeng,* 82**,** 403-14.

RADISIC, M., PARK, H., MARTENS, T. P., SALAZAR-LAZARO, J. E., GENG, W., WANG, Y., LANGER, R., FREED, L. E. & VUNJAK-NOVAKOVIC, G. 2008. Pre-treatment of synthetic elastomeric scaffolds by cardiac fibroblasts improves engineered heart tissue. *J Biomed Mater Res A,* 86**,** 713-24.

RADISIC, M., PARK, H., SHING, H., CONSI, T., SCHOEN, F. J., LANGER, R., FREED, L. E. & VUNJAK-NOVAKOVIC, G. 2004a. Functional assembly of engineered myocardium by electrical stimulation of cardiac myocytes cultured on scaffolds. *Proc Natl Acad Sci U S A,* 101**,** 18129-34.

RADISIC, M., YANG, L., BOUBLIK, J., COHEN, R. J., LANGER, R., FREED, L. E. & VUNJAK-NOVAKOVIC, G. 2004b. Medium perfusion enables engineering of compact and contractile cardiac tissue. *Am J Physiol Heart Circ Physiol,* 286**,** H507-16.

RAKUSAN, K., FLANAGAN, M. F., GEVA, T., SOUTHERN, J. & VAN PRAAGH, R. 1992. Morphometry of human coronary capillaries during normal growth and the effect of age in left ventricular pressure-overload hypertrophy. *Circulation,* 86**,** 38-46.

RAKUSAN, K. & KORECKY, B. 1982. The effect of growth and aging on functional capillary supply of the rat heart. *Growth,* 46**,** 275-81.

RANA, P., ANSON, B., ENGLE, S. & WILL, Y. 2012. Characterization of Human-Induced Pluripotent Stem Cell–Derived Cardiomyocytes: Bioenergetics and Utilization in Safety Screening. *Toxicological Sciences,* 130**,** 117-131.

RAO, C., PRODROMAKIS, T., KOLKER, L., CHAUDHRY, U. A. R., TRANTIDOU, T., SRIDHAR, A., WEEKES, C., CAMELLITI, P., HARDING, S. E., DARZI, A., YACOUB, M. H., ATHANASIOU, T. & TERRACCIANO, C. M. 2013. The effect of microgrooved culture substrates on calcium cycling of cardiac myocytes derived from human induced pluripotent stem cells. *Biomaterials,* 34**,** 2399-2411.

RAVICHANDRAN, R., VENUGOPAL, J. R., SUNDARRAJAN, S., MUKHERJEE, S. & RAMAKRISHNA, S. 2011. Poly(Glycerol sebacate)/gelatin core/shell fibrous structure for regeneration of myocardial infarction. *Tissue Eng Part A,* 17**,** 1363-73.

RIBEIRO, C., MOREIRA, S., CORREIA, V., SENCADAS, V., ROCHA, J. G., GAMA, F. M., GOMEZ RIBELLES, J. L. & LANCEROS-MENDEZ, S. 2012. Enhanced proliferation of pre-osteoblastic cells by dynamic piezoelectric stimulation. *RSC Advances,* 2**,** 11504-11509.

RIBEIRO, C., SENCADAS, V., CORREIA, D. M. & LANCEROS-MÉNDEZ, S. 2015. Piezoelectric polymers as biomaterials for tissue engineering applications. *Colloids and Surfaces B: Biointerfaces,* 136**,** 46-55.

RICOTTI, L., TACCOLA, S., BERNARDESCHI, I., PENSABENE, V., DARIO, P. & MENCIASSI, A. 2011. Quantification of growth and differentiation of C2C12 skeletal muscle cells on PSS-PAH-based polyelectrolyte layer-by-layer nanofilms. *Biomed Mater,* 6**,** 031001.

RICOTTI, L., TACCOLA, S., PENSABENE, V., MATTOLI, V., FUJIE, T., TAKEOKA, S., MENCIASSI, A. & DARIO, P. 2010. Adhesion and proliferation of skeletal muscle cells on single layer poly(lactic acid) ultra-thin films. *Biomed Microdevices,* 12**,** 809-19.

ROBERTSON, C., TRAN, D. D. & GEORGE, S. C. 2013. Concise review: maturation phases of human pluripotent stem cell-derived cardiomyocytes. *Stem Cells,* 31**,** 829-37.

ROCKWOOD, D. N., AKINS, R. E., JR., PARRAG, I. C., WOODHOUSE, K. A. & RABOLT, J. F. 2008. Culture on electrospun polyurethane scaffolds decreases atrial natriuretic peptide expression by cardiomyocytes in vitro. *Biomaterials,* 29**,** 4783-91.

ROHR, S., KUCERA, J. P. & KLÉBER, A. G. 1998. Slow Conduction in Cardiac Tissue, I: Effects of a Reduction of Excitability Versus a Reduction of Electrical Coupling on Microconduction. *Circulation Research,* 83**,** 781-794.

RUOSLAHTI, E. & YAMAGUCHI, Y. 1991. Proteoglycans as modulators of growth factor activities. *Cell,* 64**,** 867-869.

RUVINOV, E., LEOR, J. & COHEN, S. 2011. The promotion of myocardial repair by the sequential delivery of IGF-1 and HGF from an injectable alginate biomaterial in a model of acute myocardial infarction. *Biomaterials,* 32**,** 565-78.

SALAMEH, A., KARL, S., DJILALI, H., DHEIN, S., JANOUSEK, J. & DAEHNERT, I. 2010a. Opposing and synergistic effects of cyclic mechanical stretch and α- or β-adrenergic stimulation on the cardiac gap junction protein Cx43. *Pharmacological Research,* 62**,** 506-513.

SALAMEH, A., WUSTMANN, A., KARL, S., BLANKE, K., APEL, D., ROJAS-GOMEZ, D., FRANKE, H., MOHR, F. W., JANOUSEK, J. & DHEIN, S. 2010b. Cyclic mechanical stretch induces cardiomyocyte orientation and polarization of the gap junction protein connexin43. *Circ Res,* 106**,** 1592-602.

SALICK, M. R., NAPIWOCKI, B. N., SHA, J., KNIGHT, G. T., CHINDHY, S. A., KAMP, T. J., ASHTON, R. S. & CRONE, W. C. 2014. Micropattern width dependent sarcomere development in human ESC-derived cardiomyocytes. *Biomaterials,* 35**,** 4454-4464.

SARTIANI, L., BETTIOL, E., STILLITANO, F., MUGELLI, A., CERBAI, E. & JACONI, M. E. 2007. Developmental Changes in Cardiomyocytes Differentiated from Human Embryonic Stem Cells: A Molecular and Electrophysiological Approach. *STEM CELLS,* 25**,** 1136-1144.

SATIN, J., ITZHAKI, I., RAPOPORT, S., SCHRODER, E. A., IZU, L., ARBEL, G., BEYAR, R., BALKE, C. W., SCHILLER, J. & GEPSTEIN, L. 2008. Calcium Handling in Human Embryonic Stem Cell-Derived Cardiomyocytes. *STEM CELLS,* 26**,** 1961-1972.

SCHAAF, S., SHIBAMIYA, A., MEWE, M., EDER, A., STÖHR, A., HIRT, M. N., RAU, T., ZIMMERMANN, W.-H., CONRADI, L., ESCHENHAGEN, T. & HANSEN, A. 2011. Human Engineered Heart Tissue as a Versatile Tool in Basic Research and Preclinical Toxicology. *PLoS ONE,* 6**,** e26397.

SCHLAME, M., RUA, D. & GREENBERG, M. L. 2000. The biosynthesis and functional role of cardiolipin. *Progress in Lipid Research,* 39**,** 257-288.

SCHWARZBAUER, J. E. 1991. Fibronectin: from gene to protein. *Current Opinion in Cell Biology,* 3**,** 786-791.

SERRADO NUNES, J., WU, A., GOMES, J., SENCADAS, V., VILARINHO, P. M. & LANCEROS-MÉNDEZ, S. 2009. Relationship between the microstructure and the microscopic piezoelectric response of the α- and β-phases of poly(vinylidene fluoride). *Applied Physics A,* 95**,** 875-880.

SEVERS, N. J. 2000. The cardiac muscle cell. *BioEssays,* 22**,** 188-199.

SHAH, U., BIEN, H. & ENTCHEVA, E. 2010. Microtopographical effects of natural scaffolding on cardiomyocyte function and arrhythmogenesis. *Acta Biomater,* 6**,** 3029-34.

SHAMOS, M. H. & LAVINE, L. S. 1967. Piezoelectricity as a Fundamental Property of Biological Tissues. *Nature,* 213**,** 267-269.

SHARP, W. W., SIMPSON, D. G., BORG, T. K., SAMAREL, A. M. & TERRACIO, L. 1997. Mechanical forces regulate focal adhesion and costamere assembly in cardiac myocytes. *American Journal of Physiology - Heart and Circulatory Physiology,* 273**,** H546-H556.

SHAW, R. M. & RUDY, Y. 1997. Ionic Mechanisms of Propagation in Cardiac Tissue: Roles of the Sodium and L-type Calcium Currents During Reduced Excitability and Decreased Gap Junction Coupling. *Circulation Research,* 81**,** 727-741.

SHEPARD, T. H., MUFFLEY, L. A. & SMITH, L. T. 1998. Ultrastructural study of mitochondria and their cristae in embryonic rats and primate (N. nemistrina). *Anat Rec,* 252**,** 383-92.

SHI, X. T., FUJIE, T., SAITO, A., TAKEOKA, S., HOU, Y., SHU, Y. W., CHEN, M. W., WU, H. K. & KHADEMHOSSEINI, A. 2014. Periosteum-Mimetic Structures Made from Freestanding Microgrooved Nanosheets. *Advanced Materials,* 26**,** 3290-+.

SHIM, J., GROSBERG, A., NAWROTH, J. C., PARKER, K. K. & BERTOLDI, K. 2012. Modeling of cardiac muscle thin films: pre-stretch, passive and active behavior. *J Biomech,* 45**,** 832-41.

SHIMIZU, T., YAMATO, M., ISOI, Y., AKUTSU, T., SETOMARU, T., ABE, K., KIKUCHI, A., UMEZU, M. & OKANO, T. 2002. Fabrication of pulsatile cardiac tissue grafts using

a novel 3-dimensional cell sheet manipulation technique and temperature-responsive cell culture surfaces. *Circ Res,* 90**,** e40.
SHIN, M., ISHII, O., SUEDA, T. & VACANTI, J. P. 2004. Contractile cardiac grafts using a novel nanofibrous mesh. *Biomaterials,* 25**,** 3717-23.
SHIN, S. R., JUNG, S. M., ZALABANY, M., KIM, K., ZORLUTUNA, P., KIM, S. B., NIKKHAH, M., KHABIRY, M., AZIZE, M., KONG, J., WAN, K. T., PALACIOS, T., DOKMECI, M. R., BAE, H., TANG, X. S. & KHADEMHOSSEINI, A. 2013. Carbon-nanotube-embedded hydrogel sheets for engineering cardiac constructs and bioactuators. *ACS Nano,* 7**,** 2369-80.
SHINOZAWA, T., IMAHASHI, K., SAWADA, H., FURUKAWA, H. & TAKAMI, K. 2012. Determination of appropriate stage of human-induced pluripotent stem cell-derived cardiomyocytes for drug screening and pharmacological evaluation in vitro. *J Biomol Screen,* 17**,** 1192-203.
SIGURDSON, W., RUKNUDIN, A. & SACHS, F. 1992. Calcium imaging of mechanically induced fluxes in tissue-cultured chick heart: role of stretch-activated ion channels. *American Journal of Physiology - Heart and Circulatory Physiology,* 262**,** H1110-H1115.
SIMPSON, D. G., SHARP, W. W., BORG, T. K., PRICE, R. L., TERRACIO, L. & SAMAREL, A. M. 1996. Mechanical regulation of cardiac myocyte protein turnover and myofibrillar structure. *American Journal of Physiology - Cell Physiology,* 270**,** C1075-C1087.
SPACH, M. S., HEIDLAGE, J. F., BARR, R. C. & DOLBER, P. C. 2004a. Cell size and communication: role in structural and electrical development and remodeling of the heart. *Heart Rhythm,* 1**,** 500-15.
SPACH, M. S., HEIDLAGE, J. F., BARR, R. C. & DOLBER, P. C. 2004b. Cell size and communication: Role in structural and electrical development and remodeling of the heart. *Heart Rhythm,* 1**,** 500-515.
SPACH, M. S. & KOOTSEY, J. M. 1985. Relating the Sodium Current and Conductance to the Shape of Transmembrane and Extracellular Potentials by Simulation: Effects of Propagation Boundaries. *Biomedical Engineering, IEEE Transactions on,* BME-32**,** 743-755.
STEVEN, R. A. & HENRY, A. S. 2007. A review of power harvesting using piezoelectric materials (2003–2006). *Smart Materials and Structures,* 16**,** R1.
STEVENS, K. R., KREUTZIGER, K. L., DUPRAS, S. K., KORTE, F. S., REGNIER, M., MUSKHELI, V., NOURSE, M. B., BENDIXEN, K., REINECKE, H. & MURRY, C. E. 2009. Physiological function and transplantation of scaffold-free and vascularized human cardiac muscle tissue. *Proceedings of the National Academy of Sciences,* 106**,** 16568-16573.
STOPPEL, W. L., HU, D., DOMIAN, I. J., KAPLAN, D. L. & BLACK, L. D. 2015a. Anisotropic silk biomaterials containing cardiac extracellular matrix for cardiac tissue engineering. *Biomedical Materials,* 10**,** 034105.
STOPPEL, W. L., KAPLAN, D. L. & BLACK III, L. D. 2015b. Electrical and mechanical stimulation of cardiac cells and tissue constructs. *Advanced Drug Delivery Reviews*.
SU, X., YOUNG, E. W., UNDERKOFLER, H. A., KAMP, T. J., JANUARY, C. T. & BEEBE, D. J. 2011. Microfluidic cell culture and its application in high-throughput drug screening: cardiotoxicity assay for hERG channels. *J Biomol Screen,* 16**,** 101-11.
TACCOLA, S., DESII, A., PENSABENE, V., FUJIE, T., SAITO, A., TAKEOKA, S., DARIO, P., MENCIASSI, A. & MATTOLI, V. 2011. Free-Standing Poly(l-lactic acid) Nanofilms Loaded with Superparamagnetic Nanoparticles. *Langmuir*.
TAKAHASHI, K. & YAMANAKA, S. 2006. Induction of pluripotent stem cells from mouse embryonic and adult fibroblast cultures by defined factors. *Cell,* 126**,** 663-76.

TANDON, N., CANNIZZARO, C., CHAO, P. H., MAIDHOF, R., MARSANO, A., AU, H. T., RADISIC, M. & VUNJAK-NOVAKOVIC, G. 2009. Electrical stimulation systems for cardiac tissue engineering. *Nat Protoc,* 4**,** 155-73.

TANK, A. & WONG, D. 2011. Peripheral and Central Effects of Circulating Catecholamines. *Comprehensive Physiology.* John Wiley & Sons, Inc.

TCHAO, J., HAN, L., LIN, B., YANG, L. & TOBITA, K. 2014. Combined biophysical and soluble factor modulation induces cardiomyocyte differentiation from human muscle derived stem cells. *Sci. Rep.,* 4.

TERRACIO, L., RUBIN, K., GULLBERG, D., BALOG, E., CARVER, W., JYRING, R. & BORG, T. K. 1991. Expression of collagen binding integrins during cardiac development and hypertrophy. *Circulation Research,* 68**,** 734-44.

THAVANDIRAN, N., DUBOIS, N., MIKRYUKOV, A., MASSE, S., BECA, B., SIMMONS, C. A., DESHPANDE, V. S., MCGARRY, J. P., CHEN, C. S., NANTHAKUMAR, K., KELLER, G. M., RADISIC, M. & ZANDSTRA, P. W. 2013. Design and formulation of functional pluripotent stem cell-derived cardiac microtissues. *Proc Natl Acad Sci U S A,* 110**,** E4698-707.

THOMAS, S. P., BIRCHER-LEHMANN, L., THOMAS, S. A., ZHUANG, J., SAFFITZ, J. E. & KLEBER, A. G. 2000. Synthetic strands of neonatal mouse cardiac myocytes: structural and electrophysiological properties. *Circ Res,* 87**,** 467-73.

THOMSON, J. A., ITSKOVITZ-ELDOR, J., SHAPIRO, S. S., WAKNITZ, M. A., SWIERGIEL, J. J., MARSHALL, V. S. & JONES, J. M. 1998. Embryonic Stem Cell Lines Derived from Human Blastocysts. *Science,* 282**,** 1145-1147.

TIAN, B., LIU, J., DVIR, T., JIN, L., TSUI, J. H., QING, Q., SUO, Z., LANGER, R., KOHANE, D. S. & LIEBER, C. M. 2012. Macroporous nanowire nanoelectronic scaffolds for synthetic tissues. *Nat Mater,* 11**,** 986-94.

TIBURCY, M., DIDIE, M., BOY, O., CHRISTALLA, P., DOKER, S., NAITO, H., KARIKKINETH, B. C., EL-ARMOUCHE, A., GRIMM, M., NOSE, M., ESCHENHAGEN, T., ZIESENISS, A., KATSCHINKSI, D. M., HAMDANI, N., LINKE, W. A., YIN, X., MAYR, M. & ZIMMERMANN, W. H. 2011. Terminal differentiation, advanced organotypic maturation, and modeling of hypertrophic growth in engineered heart tissue. *Circ Res,* 109**,** 1105-14.

TRESSLER, J., ALKOY, S. & NEWNHAM, R. 1998. Piezoelectric Sensors and Sensor Materials. *Journal of Electroceramics,* 2**,** 257-272.

TULLOCH, N. L., MUSKHELI, V., RAZUMOVA, M. V., KORTE, F. S., REGNIER, M., HAUCH, K. D., PABON, L., REINECKE, H. & MURRY, C. E. 2011. Growth of engineered human myocardium with mechanical loading and vascular coculture. *Circ Res,* 109**,** 47-59.

VAN TASSEL, P. R. 2013. Nanotechnology in Medicine: Nanofilm Biomaterials. *The Yale Journal of Biology and Medicine,* 86**,** 527-536.

VAN VEEN, T. A. B., VAN RIJEN, H. V. M. & OPTHOF, T. 2001. Cardiac gap junction channels: modulation of expression and channel properties. *Cardiovascular Research,* 51**,** 217-229.

VAN VEEN, T. A. B., VAN RIJEN, H. V. M., VAN KEMPEN, M. J. A., MIQUEROL, L., OPTHOF, T., GROS, D., VOS, M. A., JONGSMA, H. J. & DE BAKKER, J. M. T. 2005. Discontinuous Conduction in Mouse Bundle Branches Is Caused by Bundle-Branch Architecture. *Circulation,* 112**,** 2235-2244.

VAN WAMEL, J. E. T., RUWHOF, C., VAN DER VALK-KOKSHOORN, E. J. M., SCHRIER, P. I. & VAN DER LAARSE, A. 2000. Rapid gene transcription induced by stretch in cardiac myocytes and fibroblasts and their paracrine influence on stationary myocytes and fibroblasts. *Pflügers Archiv,* 439**,** 781-788.

VANDENBURGH, H. H., SOLERSSI, R., SHANSKY, J., ADAMS, J. W. & HENDERSON, S. A. 1996. Mechanical stimulation of organogenic cardiomyocyte growth in vitro. *American Journal of Physiology - Cell Physiology,* 270**,** C1284-C1292.
VANPUTTE, C., REGAN, J. & RUSSO, A. 2015. *Seeley's Essentials of Anatomy and Physiology*, McGraw-Hill Science/Engineering/Math.
VEERMAN, C. C., KOSMIDIS, G., MUMMERY, C. L., CASINI, S., VERKERK, A. O. & BELLIN, M. 2015. Immaturity of Human Stem-Cell-Derived Cardiomyocytes in Culture: Fatal Flaw or Soluble Problem? *Stem Cells and Development,* 24**,** 1035-1052.
VEGA, R. B., HORTON, J. L. & KELLY, D. P. 2015. Maintaining ancient organelles: mitochondrial biogenesis and maturation. *Circ Res,* 116**,** 1820-34.
VELAGAPUDI, V. R., WITTMANN, C., SCHNEIDER, K. & HEINZLE, E. 2007. Metabolic flux screening of Saccharomyces cerevisiae single knockout strains on glucose and galactose supports elucidation of gene function. *Journal of Biotechnology,* 132**,** 395-404.
VENTURA-CLAPIER, R., GARNIER, A. & VEKSLER, V. 2004. Energy metabolism in heart failure. *The Journal of Physiology,* 555**,** 1-13.
VIKHANSKAYA, F., D'INCALCI, M. & BROGGINI, M. 1995. Decreased cytotoxic effects of doxorubicin in a human ovarian cancer-cell line expressing wild-type p53 and WAF1/CIP1 genes. *Int J Cancer,* 61**,** 397-401.
VO, T. D. & PALSSON, B. O. 2006. Isotopomer analysis of myocardial substrate metabolism: A systems biology approach. *Biotechnology and Bioengineering,* 95**,** 972-983.
VUNJAK-NOVAKOVIC, G., TANDON, N., GODIER, A., MAIDHOF, R., MARSANO, A., MARTENS, T. P. & RADISIC, M. 2010. Challenges in Cardiac Tissue Engineering. *Tissue Engineering Part B-Reviews,* 16**,** 169-187.
WALL, S. T., YEH, C. C., TU, R. Y., MANN, M. J. & HEALY, K. E. 2010. Biomimetic matrices for myocardial stabilization and stem cell transplantation. *J Biomed Mater Res A,* 95**,** 1055-66.
WANG, B., WANG, G., TO, F., BUTLER, J. R., CLAUDE, A., MCLAUGHLIN, R. M., WILLIAMS, L. N., DE JONGH CURRY, A. L. & LIAO, J. 2013. Myocardial Scaffold-Based Cardiac Tissue Engineering: Application of Coordinated Mechanical and Electrical Stimulations. *Langmuir,* 29**,** 11109-11117.
WANG, H. B., MULLINS, M. E., CREGG, J. M., HURTADO, A., OUDEGA, M., TROMBLEY, M. T. & GILBERT, R. J. 2009a. Creation of highly aligned electrospun poly-L-lactic acid fibers for nerve regeneration applications. *J Neural Eng,* 6**,** 016001.
WANG, T., WU, D. Q., JIANG, X. J., ZHANG, X. Z., LI, X. Y., ZHANG, J. F., ZHENG, Z. B., ZHUO, R., JIANG, H. & HUANG, C. 2009b. Novel thermosensitive hydrogel injection inhibits post-infarct ventricle remodelling. *Eur J Heart Fail,* 11**,** 14-9.
WEBER, K. T., JANICKI, J. S., SHROFF, S. G., PICK, R., CHEN, R. M. & BASHEY, R. I. 1988. Collagen remodeling of the pressure-overloaded, hypertrophied nonhuman primate myocardium. *Circulation Research,* 62**,** 757-65.
WEBER, N., LEE, Y. S., SHANMUGASUNDARAM, S., JAFFE, M. & ARINZEH, T. L. 2010a. Characterization and in vitro cytocompatibility of piezoelectric electrospun scaffolds. *Acta Biomater,* 6**,** 3550-6.
WEBER, N., LEE, Y. S., SHANMUGASUNDARAM, S., JAFFE, M. & ARINZEH, T. L. 2010b. Characterization and in vitro cytocompatibility of piezoelectric electrospun scaffolds. *Acta Biomaterialia,* 6**,** 3550-3556.
WIECHERT, W. & DE GRAAF, A. A. 1997. Bidirectional reaction steps in metabolic networks: I. Modeling and simulation of carbon isotope labeling experiments. *Biotechnol Bioeng,* 55**,** 101-17.

WILLIAMS, C. & BLACK, L., III 2015. The Role of Extracellular Matrix in Cardiac Development. *In:* SUURONEN, E. J. & RUEL, M. (eds.) *Biomaterials for Cardiac Regeneration.* Springer International Publishing.

WITTMANN, C. & HEINZLE, E. 1999. Mass spectrometry for metabolic flux analysis. *Biotechnology and Bioengineering,* 62**,** 739-750.

WU, J., ZENG, F., HUANG, X. P., CHUNG, J. C., KONECNY, F., WEISEL, R. D. & LI, R. K. 2011. Infarct stabilization and cardiac repair with a VEGF-conjugated, injectable hydrogel. *Biomaterials,* 32**,** 579-86.

XIA, L., XIAOHONG, W., SONG, L. & LIWEI, L. Energy harvesting using uniaxially aligned cardiomyocytes. Micro Electro Mechanical Systems (MEMS), 2014 IEEE 27th International Conference on, 26-30 Jan. 2014 2014. 159-162.

XIA, Y., BUJA, L. M. & MCMILLIN, J. B. 1998. Activation of the Cytochrome c Gene by Electrical Stimulation in Neonatal Rat Cardiac Myocytes: ROLE OF NRF-1 AND c-Jun. *Journal of Biological Chemistry,* 273**,** 12593-12598.

XIA, Y., MCMILLIN, J. B., LEWIS, A., MOORE, M., ZHU, W. G., WILLIAMS, R. S. & KELLEMS, R. E. 2000. Electrical Stimulation of Neonatal Cardiac Myocytes Activates the NFAT3 and GATA4 Pathways and Up-regulates the Adenylosuccinate Synthetase 1 Gene. *Journal of Biological Chemistry,* 275**,** 1855-1863.

XIAO, Y., ZHANG, B., LIU, H., MIKLAS, J. W., GAGLIARDI, M., PAHNKE, A., THAVANDIRAN, N., SUN, Y., SIMMONS, C., KELLER, G. & RADISIC, M. 2014. Microfabricated perfusable cardiac biowire: a platform that mimics native cardiac bundle. *Lab on a chip,* 14**,** 869-882.

XU, X. Q., SOO, S. Y., SUN, W. & ZWEIGERDT, R. 2009. Global Expression Profile of Highly Enriched Cardiomyocytes Derived from Human Embryonic Stem Cells. *STEM CELLS,* 27**,** 2163-2174.

YAMASHITA, J. K. 2010. ES and iPS cell research for cardiovascular regeneration. *Exp Cell Res,* 316**,** 2555-9.

YANG, K.-C., BONINI, M. G. & DUDLEY, S. C. 2014a. Mitochondria and Arrhythmias. *Free radical biology & medicine,* 71**,** 351-361.

YANG, X., PABON, L. & MURRY, C. E. 2014b. Engineering adolescence: maturation of human pluripotent stem cell-derived cardiomyocytes. *Circ Res,* 114**,** 511-23.

YASUDA, N., BANNO, T., FUJITA, K., OHWA, H., MATUSHITA, M., YAMASHITA, Y., IWATA, M. & ISHIBASHI, Y. 2006. Pressure dependence of piezoelectric properties of a Pb(Mg(1/3)Nb(2/3))O(3)-PbTiO(3) binary system single crystal near a morphotropic phase boundary. *J Phys Condens Matter,* 18**,** 7659-68.

YOKOO, N., BABA, S., KAICHI, S., NIWA, A., MIMA, T., DOI, H., YAMANAKA, S., NAKAHATA, T. & HEIKE, T. 2009. The effects of cardioactive drugs on cardiomyocytes derived from human induced pluripotent stem cells. *Biochemical and Biophysical Research Communications,* 387**,** 482-488.

YOU, J. O., RAFAT, M., YE, G. J. & AUGUSTE, D. T. 2011. Nanoengineering the heart: conductive scaffolds enhance connexin 43 expression. *Nano Lett,* 11**,** 3643-8.

YOUNG, J. L. & ENGLER, A. J. 2011. Hydrogels with time-dependent material properties enhance cardiomyocyte differentiation in vitro. *Biomaterials,* 32**,** 1002-9.

ZHANG, D., SHADRIN, I. Y., LAM, J., XIAN, H. Q., SNODGRASS, H. R. & BURSAC, N. 2013. Tissue-engineered cardiac patch for advanced functional maturation of human ESC-derived cardiomyocytes. *Biomaterials,* 34**,** 5813-20.

ZHANG, J., WILSON, G. F., SOERENS, A. G., KOONCE, C. H., YU, J., PALECEK, S. P., THOMSON, J. A. & KAMP, T. J. 2009a. Functional cardiomyocytes derived from human induced pluripotent stem cells. *Circ Res,* 104**,** e30-41.

ZHANG, Y. W., SHI, J., LI, Y. J. & WEI, L. 2009b. Cardiomyocyte death in doxorubicin-induced cardiotoxicity. *Arch Immunol Ther Exp (Warsz),* 57**,** 435-45.

ZHU, W.-Z., XIE, Y., MOYES, K. W., GOLD, J. D., ASKARI, B. & LAFLAMME, M. A. 2010. Neuregulin/ErbB Signaling Regulates Cardiac Subtype Specification in Differentiating Human Embryonic Stem Cells. *Circulation research,* 107**,** 776-786.

ZIMMERMANN, W. H., DIDIE, M., DOKER, S., MELNYCHENKO, I., NAITO, H., ROGGE, C., TIBURCY, M. & ESCHENHAGEN, T. 2006a. Heart muscle engineering: an update on cardiac muscle replacement therapy. *Cardiovasc Res,* 71**,** 419-29.

ZIMMERMANN, W. H., FINK, C., KRALISCH, D., REMMERS, U., WEIL, J. & ESCHENHAGEN, T. 2000. Three-dimensional engineered heart tissue from neonatal rat cardiac myocytes. *Biotechnol Bioeng,* 68**,** 106-14.

ZIMMERMANN, W. H., MELNYCHENKO, I., WASMEIER, G., DIDIE, M., NAITO, H., NIXDORFF, U., HESS, A., BUDINSKY, L., BRUNE, K., MICHAELIS, B., DHEIN, S., SCHWOERER, A., EHMKE, H. & ESCHENHAGEN, T. 2006b. Engineered heart tissue grafts improve systolic and diastolic function in infarcted rat hearts. *Nat Med,* 12**,** 452-8.

ZIMMERMANN, W. H., SCHNEIDERBANGER, K., SCHUBERT, P., DIDIE, M., MUNZEL, F., HEUBACH, J. F., KOSTIN, S., NEUHUBER, W. L. & ESCHENHAGEN, T. 2002. Tissue engineering of a differentiated cardiac muscle construct. *Circ Res,* 90**,** 223-30.

ZONG, X., BIEN, H., CHUNG, C. Y., YIN, L., FANG, D., HSIAO, B. S., CHU, B. & ENTCHEVA, E. 2005. Electrospun fine-textured scaffolds for heart tissue constructs. *Biomaterials,* 26**,** 5330-8.

ZWI, L., CASPI, O., ARBEL, G., HUBER, I., GEPSTEIN, A., PARK, I. H. & GEPSTEIN, L. 2009. Cardiomyocyte differentiation of human induced pluripotent stem cells. *Circulation,* 120**,** 1513-23.